ABSTRACT

The increased usage of titanium and its alloys in the aerospace industry and for biomedical applications has been attributed to its good strength to weight ratio, exceptional corrosion resistance and high melting point. In this research the titanium alloy that was focused on is the Ti-6Al-4V (by weight) alloy. With these good properties the alloys are also susceptible to poor tribological property behaviour. Surface engineering processes help improve these poor properties and one such process is known as Oxygen Boost Diffusion Hardening (OBDH). The OBDH process is a two-step process. The first step involves oxidation of the samples in air at elevated temperatures and the second step is carried out in order to diffusion treat the pre-oxidised specimens in a vacuum or argon environment. This was done using different oxygen and diffusion step temperatures and times. A comparison of the different fatigue lives after the treatments was made using the untreated specimen as the yardstick.

The specimens were heat treated, in an oxidation furnace for the first stage and a contpolled atmosphere furnace for the second stage. Thereaftdr, a rotational bending machine was used for the fatigue teqting where fatigue failure data was obtaaned. For assistance in fully analysing the fatigue data; hardness tests, microstructural analysis and fracture morphology were undertaken and quantified.

The results revealed that the fatigue life of the heat treated samples was inferior to that of the as received sp%cimen. The values of fatigue life cycle span were relatively low for the treated specimens and this is undesirable considering that the treated alloy products could be used in the aerospace industry. Microhardness, grain size, heat treatment time and diffusion environment all play a role in determining the fatigue behaviour of the Ti-6Al-4V alloy. The reduction in fatigue life is caused by a combination of embrittlement at the surface and accelerated fatigue crack growth rate due to larger grain size that arises as a result of the prolonged heating at diffusion treatment process temperature.

The grain growth in treated specimens results in a reduction of their fracture toughness and critical crack length. These specimens fail due to brittle fracture initiated in the hardened layer whereas the as received specimen, that has smaller grains, fails in a ductile manner.

DECLARATION

I know that plagiarism is use of another person's work and pretend that it is your own which wrong. Hence, I do, hereby declare that this dissertation contains my original work, except where reference is made. I have used the convention for citation and referencing and each contribution for this document by other people has been cited and referenced. Finally I also declare that this material has not been submitted for any purpose or examination to any other Department or University.

Lester Tinashe Chihoro (CHHLES001)

Date:

ACKNOWLEDGEMENTS

I would like to acknowledge the following people for their helpful comments, suggestions and assistance whilst I undertook this research.

Firstly, I would like to express my sincere gratitude to my supervisor Prof. Rob Knutsen for his invaluable assistance regarding advice, corrections and discussing all aspects of the research and seeing it to its completion.

I would also like to thank Prof. R. B. Tait for the provision of key advice when I was carrying out the core work in the project.

I wish to also acknowledge Penny Park-Ross and my colleagues in the Mechanical/Materials Engineering Department for assistance with my laboratory work and machinery usage.

I am also indebted to Glen Newins, Jules Mayer and fellow technical staff from workshop for the machining of the test pieces and modification and repair of my test rig.

I would also like to thank Mrs Noma Africa for all the administrative assistance.

I wish to thank Mrs F. D. Young and the cleaning staff in the department for making the department a pleasant space to carry out the research.

Special thanks go to AMTS in conjunction with UCT for supporting me financially throughout my study.

Lastly, I would like to thank my Dad, Mum, family and friends across the globe whose constructive words of encouragement were invaluable and truly inspiring in helping me succeed with the project.

Dedicated to my loving parents and family –

Peter and Francesca Chihoro (Parents)

Petros, Elizabeth and Bertram Chihoro (Family)

Table of Contents

Glossary

OBDH – Oxygen Boost Diffusion Hardening

% - Percent

Ti-6Al-4V – Titanium containing 6% Aluminium and 4% Vanadium (weight percentage)

α – Alpha

β – Beta

°C – Degrees Celsius

g – Grams

cm – Centimetres

J – Joules

kg – Kilograms

W – Watts

mm - Millimetres

m – Metres

K – Kelvin

MPa – Mega Pascals

GPa – Giga Pascals

hcp – Hexagonally Close-Packed

bcc – Body-Centred Cubic

PMC – Polymer Matrix Composite

APU - Auxiliary Power Unit

H_v – Vickers Hardness

ppm – Parts Per Million

HCF – High Cycle Fatigue

LCF – Low Cycle Fatigue

FOD – Foreign Object Damage

K_t – Stress Concentration Factor

S-N – Stress-Number of Cycles

PSB – Persistent Slip Band

UHCF - Ultra-High Cycle Fatigue

Glossary

CLD - Crack-Like Discontinuity

FCG – Fatigue Crack Growth

rpm – revolutions per minute

N – Newtons

ml – millilitres

μm – microns

HCP – Hexagonally Closely Packed

BCC – Body Centred Cubic

SEM – Scanning Electron Microscopy

LEFM – Linear Elastic Fracture Mechanics

Mins - Minutes

List of Figures

List of Tables

1. INTRODUCTION

1.1. BACKGROUND TO THE PROJECT

The ever-increasing demands for higher performance and more challenging application conditions have been the stimulant to replace steel components with those designed and manufactured from titanium alloys[1]. In a relatively short period, these alloys have become the fundamental materials in aerospace, chemical and energy industries. Titanium alloys possess desirable mechanical properties, but these advantages are counteracted by poor tribological properties. Surface engineering of titanium alloys, however, provides a suitable way to improve the tribological performance of these alloys. It is a well established fact that oxygen, like nitrogen and carbon, can significantly harden titanium alloys[1]**.** These elements, along with oxygen boost diffusion hardening (OBDH) treatments on the titanium alloy, improve the wear resistance and corrosion behaviour of tested samples. The OBDH treatments involve two steps namely oxidation and diffusion, occurring at elevated temperatures. The oxidation results in an oxide layer being formed on the samples in the initial step. This sample with its oxide layer is then subjected to a diffusion treatment in a heated environment where the oxygen is then diffused into the bulk of the sample thereby creating an oxygen-rich hardened layer below the surface.

Titanium implants in biomedical applications are often surface modified by surface roughening, oxidation or coating techniques[2]. These surface-treated alloys are used as joint replacements in orthopaedics. The same surface treatment techniques may also be used for structural and engine parts of airplanes. Although, work executed by Dong and Li[1] has been completed on the oxidation and surface hardening of titanium alloys, the fatigue behaviour of these oxidised alloys has not been investigated. Consequently, the purpose of this project is to examine the influence of surface hardening by oxidation and oxygen diffusion hardening on fatigue performance.

The aerospace industry is the single largest market for titanium products primarily due to the favourable strength to weight ratio, elevated temperature performance and

corrosion resistance mentioned earlier[3]. The application of titanium is most significant in the jet engine and aircraft components on the airframe that are subject to temperatures up to 590°C. Usage is wide in most commercial and military aircrafts and also spacecrafts where the many benefits of titanium are utilised.

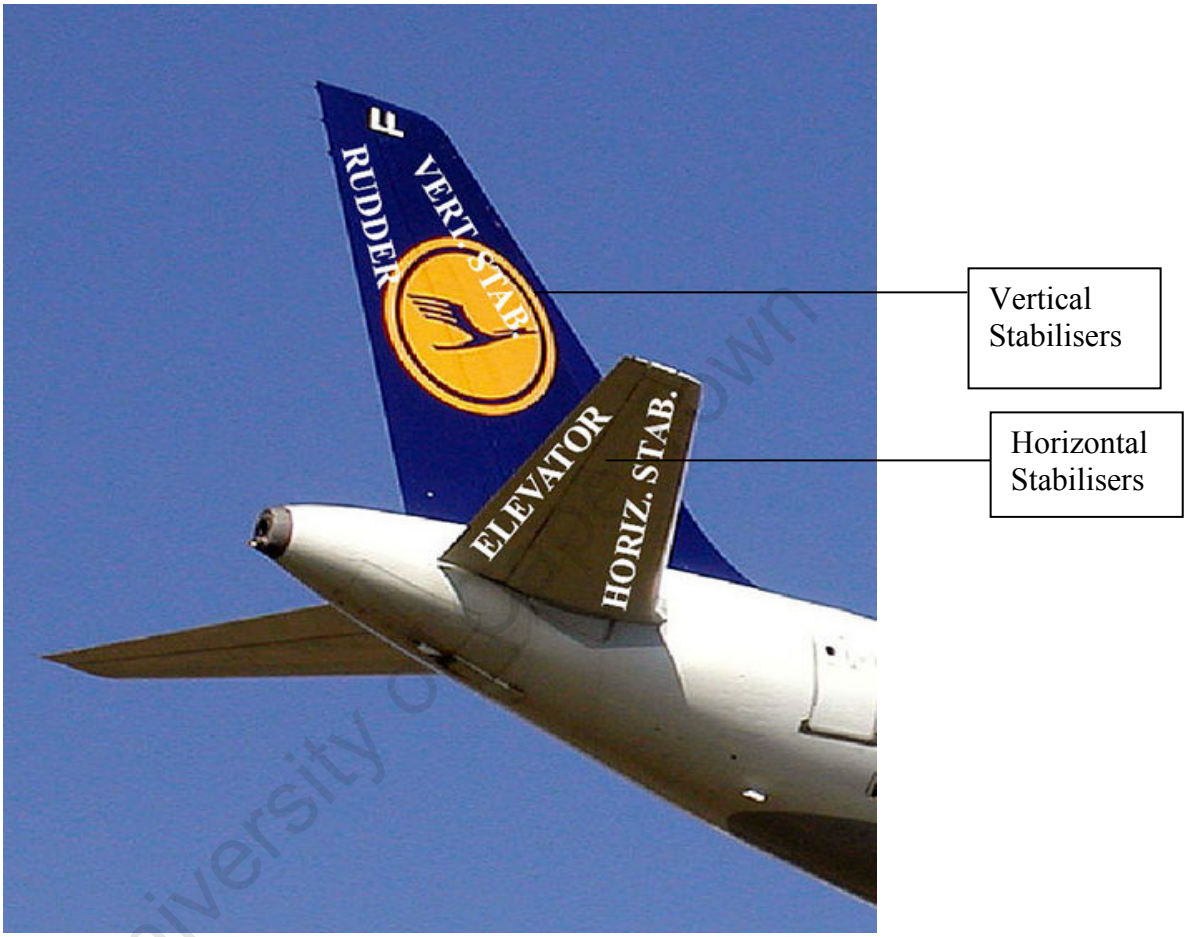

Figure 1.1: Aircraft stabilisers made from titanium alloy[4]

The horizontal stabiliser shown in figure 1.1 is a fixed or adjustable surface from which an elevator maybe hinged. In some aircraft models the entire horizontal stabiliser rotates and functions as an elevator. The vertical stabiliser or fin is fixed to the aircraft and supports the rudder. These stabilisers provide stability whilst the aircraft is flying straight and the airfoil of the horizontal stabiliser balances the forces acting on the aircraft[4]. Cost limits the use of titanium relative to other competing materials like aluminium and steel. Hence the advantages of using titanium must be balanced against the cost[2, 5, 6, 7, 8, 9].

1.2. RESEARCH MOTIVATION

Improving the surface hardness of the titanium alloy under investigation for better wear resistance is a major motivation for this project being undertaken. With this put in place there is need to know how this improved surface hardness and wear resistance may affect the fatigue resistance. This effect on fatigue is to be analysed with regards to different properties that include microstructure, grain size and fracture surfaces. The outcome of the research should help in mechanical property considerations of the aircraft components that may in future undergo manufacturing that encompasses the OBDH process.

Success may be achieved in manufacturing and providing OBDH structures for airplanes and biomedical implants. However, reliability of these products is imperative given the high cost of the raw titanium alloy. Since the OBDH process is complex and costly, it is essential to understand how it may affect the structural integrity of the titanium alloy under investigation. This basically helps minimise the occurrence of life-threatening accidents or engineering-related catastrophes whilst the airplanes are in operation.

The detection and characterisation of mechanically induced surface damages such as fatigue cracks in their original location is of major interest to satisfactorily predict the long term in vivo behaviour of implant materials[2]. This study should help scientists decide how profitable it is to use surface-treated titanium alloys using OBDH in different loading conditions and environment.

1.3. OBJECTIVES

Fatigue failures commonly continue to plague many materials, for instance those materials used in aeroengines. Since fatigue crack initiation is the root of fatigue failure, it is very important to study the fatigue crack initiation in the titanium containing 6% aluminium and 4% vanadium by weight percentage (Ti-6Al-4V) alloy[10]. Fatigue testing on heat treated Ti-6Al-4V specimens, taking note of the

number of cycles reached before crack initiation, propagation and subsequent failure, is of paramount significance and is to be investigated. With the cantilever rotating bending machine used for fatigue testing it is envisaged that investigation of the point of failure of the specimens with respect to number of cycles can be obtained producing reliable values. The data obtained should help to conclude the fatigue endurance analysis of the various specimens used in this study. This is enhanced by the repeatability tests to be performed for reliability purposes.

The effect of OBDH on mechanical and tribological properties of titanium alloys have been studied and quantified producing satisfactory results justifying the use of the end products in industry[11]. OBDH is a process which results in an oxygen-rich diffusion zone being formed up to a depth of approximately 300 μm below the surface of the specimens and this zone tends to be brittle and harder than the as received alloy, depending on the parameters used in the surface modification. These parameters include time, temperature and the environment in which the OBDH is taking place. The diffusion step may occur in an argon or vacuum environment.

Fatigue performance significantly drops in specimens that undergo the OBDH process[1]. The objective of this project is to determine which of the possible and available routes of the OBDH process leads to optimum fatigue performance of Ti-6Al-4V alloy without sacrificing important mechanical properties such as tensile strength, surface hardness, corrosion and elongation. Therefore, the aim is to obtain and explore OBDH routes that result in performances that have highest number of cycles to failure or minimum loss of fatigue endurance. These routes can then be of use to metallurgists and manufacturers in the aerospace industry and the biomedical industry that are in dire need to utilize the OBDH technique for increased wear resistance.

1.4. RESEARCH APPROACH

The research approach to this study involved planning the OBDH routes to be investigated with the intended goal of obtaining the most desirable routes in terms of fatigue performance. There were nine different routes selected in which seven of these

routes involved both steps of the OBDH process which are the oxidation step and the diffusion step. Two routes involved either the oxidation step only or the diffusion step only as this provided a basis to compare which of the two steps had more effect on the fatigue performance of the specimens. In addition, the as-received condition of the specimen also underwent testing to determine by how much the OBDH treatments affected the properties being studied relative to samples in the untreated condition.

1.5. PLAN OF DEVELOPMENT

The thesis layout contains various chapters. The first chapter introduces the topic and explains the relevancy of undertaking the research. The next chapter covers the literature review carried out in this research topic in order to design the experimental work and assist in the interpretation of the results.

Following the literature review the next chapter consists of the experimental methods and techniques used to perform the experiments involved in the study. This section also outlines some difficulties experienced in the experimental procedure.

The proceeding chapter presents the results obtained from the experimental work that was conducted and the results are analysed and interpreted in this section. These results are summarised in the subsequent chapter after which some justifiable conclusions to the study are drawn.

Finally there is a chapter for recommendations for further areas of study to be explored.

2. LITERATURE REVIEW

2.1. TITANIUM AND ITS ALLOYS

Titanium is a light, strong and lustrous metal which has been used extensively in the manufacturing industry. It is a transition metal with a special electron configuration whereby it adds its extra electrons to the third shell and not its outermost fourth shell. The configuration of electrons in the four shells would be sequentially 2-8-10-2, and is therefore ready to bond with other elements. It makes many natural compounds with halogens and oxygen. Since titanium has four valence electrons, it is quite flexible which enables it to form solid solutions with most substitutional elements having a size factor within 20%[10,12]. Titanium can be alloyed with iron, aluminium, vanadium and molybdenum among other elements to produce strong lightweight alloys for use in the aerospace, military, automotive and biomedical applications. There are good attributes and advantages of using titanium in industry but a major drawback is that titanium surfaces and its commercially produced alloys have poor wear resistance. Most notably, titanium surfaces in contact with each other or with other metals readily gall under conditions of sliding contact or fretting.

The major interest in titanium and its development is owed to the following characteristics;

- has a melting point of approximately 1678 °C
- possesses a high strength to weight ratio at elevated temperatures
- exceptional corrosion resistance
- low thermal conductivity
- low density relative to steel

2.1.1. Allotropy of Titanium

The crystal structure of pure titanium is hexagonal close-packed (hcp) alpha (α) phase at ambient temperature and pressure. This structure is maintained up to a temperature of 882°C where it undergoes allotropic transformation to body-centred cubic (bcc) beta (β) phase and this phase transformation temperature is known as the β-

transus[10,13]. The crystal structures with their respective hcp and bcc structures are shown in figures 2.1a and 2.1b. Above the β-transus the pure titanium exists as the bcc β phase till it reaches the melting point. This phenomenon is shown on the extreme left of figure 2.2 when the x-axis shows 0% of aluminium added. This offers the prospect of having α, β and α-β microstructures. The titanium transforms from α to α + β and finally β phase with the temperature rise. The α phase is much harder than the β phase, so the drop in strength as temperature rises is due to easier dislocation movement at elevated temperature. Conversely, formability increases as the phase transforms from α to β [10].

Titanium reacts with several interstitial elements including oxygen, nitrogen, carbon and hydrogen[10, 12]. Oxygen, nitrogen and carbon stabilise the α phase whilst hydrogen stabilises the β phase. The strength of titanium increases gradually as alloy content is added to it. The increase is as a result of dislocation movement being impeded by the solid solution strengthening.

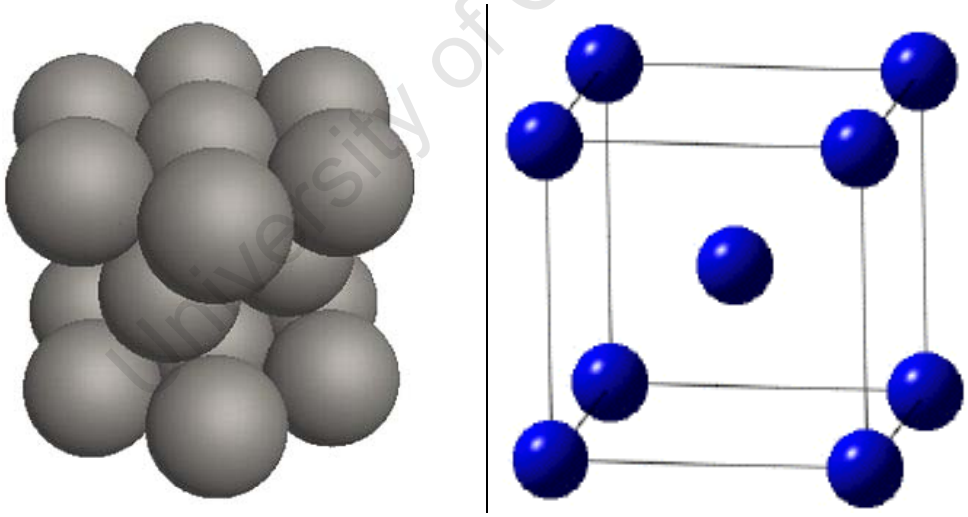

(a) **(b)**

Figure 2.1: Crystal structure of (a) α-titanium and (b) β-titanium[13]

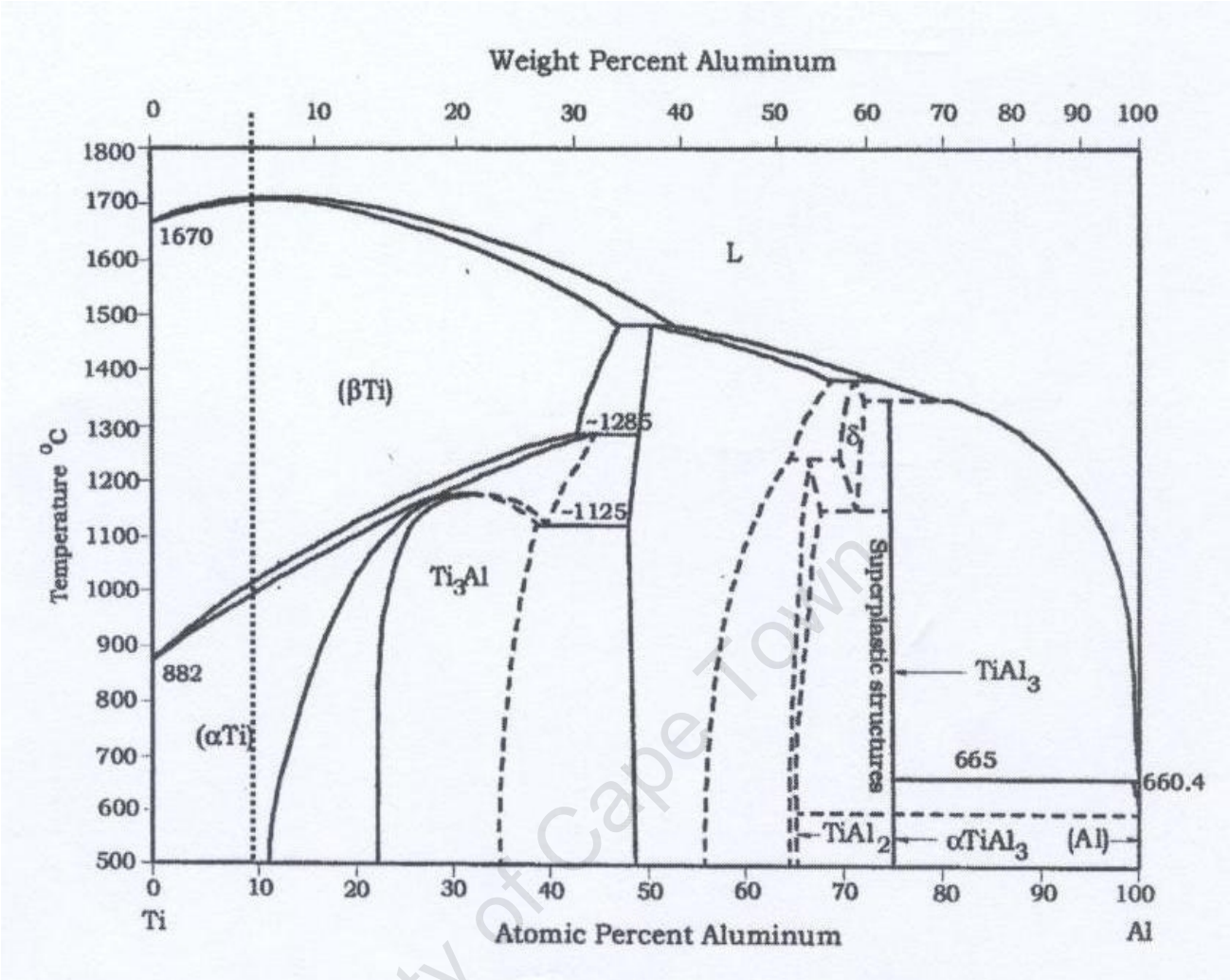

Figure 2.2: Ti-Al binary phase system[11]

2.1.2. Titanium Alloys

There are three titanium alloy types based on the composition of the alloy and the temperature constituent phases, and each of these families of alloys serves a specific role. The alloy types include α and near α-alloys, α-β alloys and the β-alloys. Alpha is the low temperature allotrope of titanium and the microstructure of α and near-α alloys consists predominantly of the α phase. The α-β alloys are mostly α at room temperature, but they do have more of the β phase, the high temperature allotrope, than the α and near-α alloys. β-alloys are capable of retaining 100% β when quenched from the β phase field to room temperature[10, 13,14].

Alloying of titanium is dominated by the ability of elements to stabilise either of the α or the β phases. This behaviour is related to the number of bonding electrons, that is the group number, of the element concerned. Alloying elements with less than 4 electrons in the outermost shell of the atom favourably stabilise the α phase, for instance aluminium; elements with 4 electrons are neutral; and elements with more than 4 electrons stabilise β, for example vanadium.

In comparison to β phase, the α phase is characterised by the following properties;

- lower ductility
- significant anisotropy of physical and mechanical properties
- diffusion rates that are lower by at least two orders of magnitude
- higher creep resistance[10]

There are several heat treatments that are used for titanium alloys. When an α-β titanium alloy such as Ti-6Al-4V is slowly cooled from the fully β region, the α phase emerges in the shape of plates below the β transus temperature with the crystallographic morphology that is related to the parent β phase to form the Widmansttäten structure[11]. Different cooling rates from various temperatures result in distinct microstructures and mechanical properties. The α and the β phases are observed in various volume fractions and combinations owing to annealing temperatures and cooling rates. The martenstitic α' phase is formed by quenching from above the β transus temperature. As the alloy crosses the Ms (start of martensite) line, the β microstructure transforms into titanium martensite as shown in figure 2.3a composition line 1[14].

When titanium martensite is reheated tempering will take place as β precipitates from the supersaturated α' and this is illustrated in figure 2.3b. When highly alloyed α-β alloys are quenched from the β field, β' which is supersaturated in solute is formed as shown in figure 2.3a composition line 2. When this supersaturated structure is aged α will start to precipitate in a Widmanstätten structure and it is illustrated in figure 2.3b.

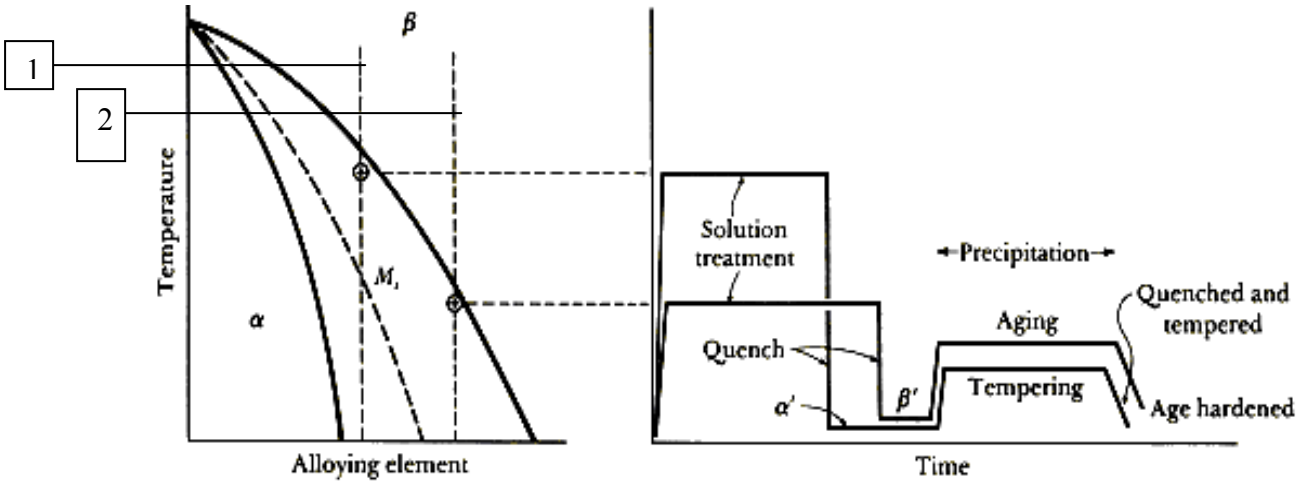

Figure 2.3: Heat treatment of the alpha-beta titanium alloys[11]

It is common for the α-phase to form as Widmansttäten laths in a β matrix, although β may itself transform to martensitic ά[10]. Lath sizes depend on cooling rate and the basket weave structure is obtained when cooling rate is slow as depicted in figure 2.4a. When annealing within the α + β fields, the process is usually carried out at about 700°C, and in addition to providing stress-relief, this treatment results in formation of equi-axed structure composed of α grains and grains of transformed β shown in figure 2.4b.

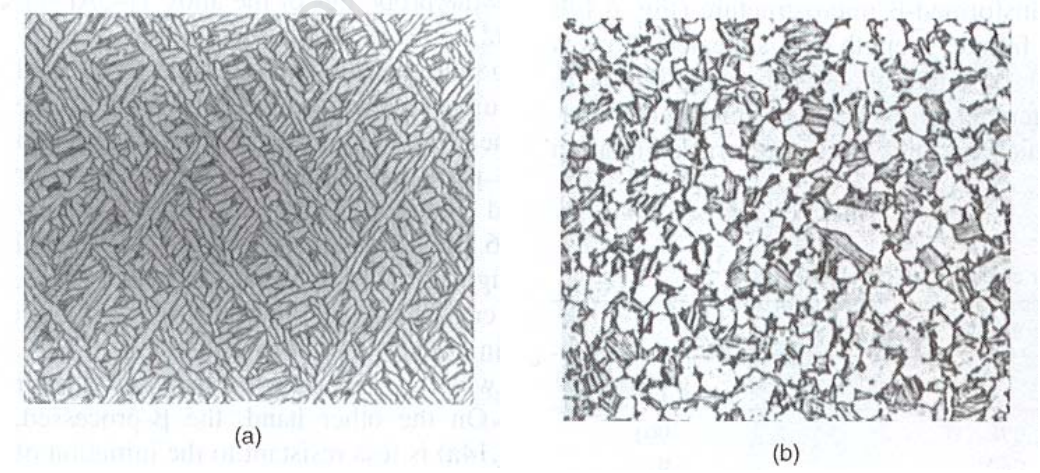

Figure 2.4: Ti-6Al-4V Alloy (a) slowly cooled from β-phase field showing basket weave structure of Widmanstätten α-matrix; (b) annealed at 700°C in α + β phase field. Equi-axed grains of α (white) and transformed β (Widmanstätten α)[10]

2.1.2.1. Ti-6Al-4V Alloy

Ti-6Al-4V is the workhorse of the titanium industry; it accounts for about 60% of the total titanium production. It is a ductile alloy that is normally used at a minimum tensile strength of approximately 900MPa, has good fatigue and fracture properties and is used in all product forms including forgings, bar, castings, foil, sheet, plate, extrusions, tubing and fasteners. Ti-6Al-4V especially offers the prospect of relatively high strength and improved formability[10,15,16]. In order to further improve the operating efficiency of light-weight machines and structures, Ti-6Al-4V alloy is immensely expected to be used in a wide range of applications at both ambient and elevated temperatures[17].

Most α-β alloys contain elements to stabilise and strengthen the α phase, together with 4-6% of β stabilising elements which allow substantial amounts of this phase to be retained on quenching from β to α + β fields[10]. In Ti-6Al-4V alloy aluminium is an α phase stabiliser while vanadium is a β phase stabiliser. The effects of aluminium and vanadium on the phase transformation of the titanium metal are depicted by the phase diagrams in figures 2.2 and 2.5. In the Ti-Al binary system it is shown that titanium dissolves between 6 and 7 %(by weight(wt)) of aluminium at approximately 1700°C which in turn is the highest temperature for the alloy in its β phase. The maximum aluminium that can be dissolved is approximately 34wt% at 1450°C also in the β phase. With the addition of aluminium to pure titanium, the β transus increases and melting point slightly increases up to approximately 6-7wt% aluminium. This contrasts the Ti-V binary system where the titanium completely dissolves the vanadium as shown in figure 2.5.

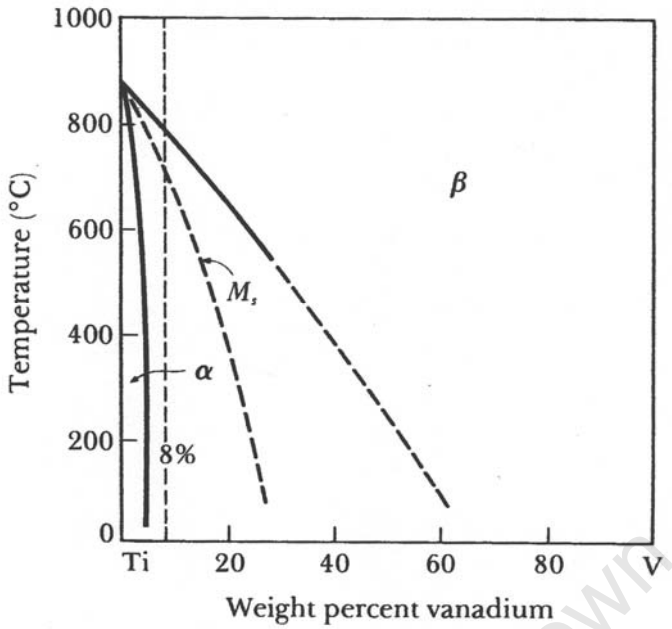

Figure 2.5: Ti-V binary phase diagram[11]

α-β titanium alloys are mostly used in the annealed condition and both the microstructure and mechanical properties differ slightly depending upon whether or not the forming process was performed below or above the β transus. The table 2.1 shows the range in mechanical properties of the Ti-6Al-4V alloy.

The mechanical properties of Ti-6Al-4V alloys are heavily influenced by impurities and heat treatment, making it imperative that the alloys behaviour is linked to microstructure, phase constituents and processing theory[7]. Therefore, there are some characteristic trends observed in Ti-6Al-4V alloys and their mechanical properties in relation to the different environmental conditions they are exposed to during processing or in service. Hardness and tensile strength increase with increasing annealing temperature and cooling rate. In contrast, higher annealing temperature and cooling rate result in lower elongation. Heat treatment produces the different combinations of strength and elongation, but a compromise may be achieved with the annealing temperature just below the β transus and applying air-cooling at a moderate cooling rate[14].

Table 2.1: Mechanical Properties of Ti-6Al-4V alloy[18]

Property	Value
Ultimate Tensile strength	897 – 1000 MPa
Yield Stress	828 – 910 MPa
Elongation over 50 mm	10 – 18 %
Elastic Modulus	114 GPa
Rockwell Hardness C	36

Table 2.2 shows properties of Ti-6Al-4V forgings processed in the α + β phase field and the β phase field. The specimens have been air-cooled after forging as well as annealed for 2 hours at 705°C. The β transus temperature for the alloy is 1005°C and for the fatigue property tests the smooth specimens were axially loaded having a stress concentration factor (K_t) of 1. Tensile properties and yield strength properties are relatively in the same range for both fields whilst the samples forged in the α + β phase field (equi-axed grains) are more ductile. Fracture toughness and more importantly fatigue strength are higher in β forged and annealed material (acicular Widmanstätten).

Table 2.2: Properties of annealed Ti-6Al-4V forgings[10]

	Forging Treatment	
	α + β phase field	β phase field
Ultimate tensile strength (MPa)	978	991
Yield strength (MPa)	940	912
Elongation (%)	16	12
Reduction in area (%)	45	22
Fracture toughness (MPa $m^{1/2}$)	52	79
10^7 fatigue limit(MPa)	+/- 494	+/- 744

Annealed 2 h at 705°C, air-cooled after forging
α/β transus 1005°C
Axial loading: smooth specimens, K_t = 1.0

Uniform properties can be obtained in thick sections by slow cooling from either β or α + β fields known as the β annealed and mill-annealed conditions respectively[10]. The Widmanstätten α microstructure in figure 2.4a that is produced by slow continuous cooling from the β phase field is less resistant to fatigue crack initiation than the equi-axed α + β microstructure shown in figure 2.4b. Therefore, the low-cycle fatigue strength of β annealed alloys is inferior to that of mill-annealed (α + β) condition as shown in figure 2.6.

This phenomenon is enhanced at elevated temperatures because increased oxidation occurs along phase boundaries which permits premature crack initiation along surface-connected, acicular α interfaces. Thus it has been noted that to achieve a good balance of fatigue properties in α-β alloys, a duplex structure consisting of about 30 % volume of equi-axed α combined with Widmanstätten α is favoured for rotating components, for instance compressor discs that operate at high temperatures[10].

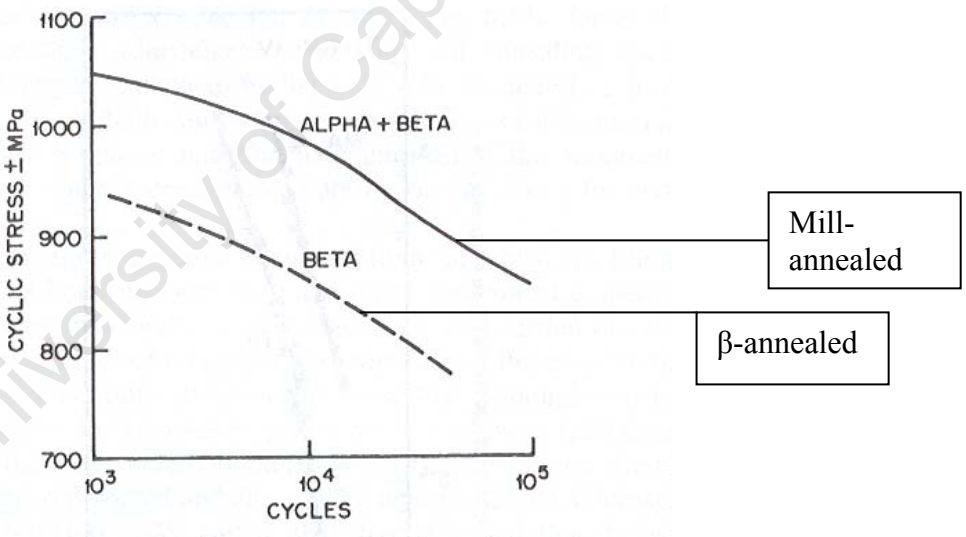

Figure 2.6: Comparison of low-cycle fatigue lives of Ti-6Al-4V in mill-annealed and β-annealed condition[10]

2.2. TITANIUM USAGE ON AIRCRAFT

The primary justifications for using titanium in the aerospace industry are;

- weight savings

The lower density of titanium compared with steel permits weight savings replacing steels even though they may be higher strength.

- space limitation

Space can also be increased within the aircraft as the strength of the titanium alloys is significantly higher than aluminium alloys. Volume component of the titanium would then be less and hence allow greater space.

- operating temperature

Titanium could also replace aluminium when the operating temperature exceeds about 130°C, which is the normal maximum operating temperature for conventional aluminium

- corrosion resistance

This is a very important issue. The corrosion resistance of titanium is such that corrosion protective coatings or paint are not required. Much of the floor support structure under the galleys and lavatories is in a very corrosive environment which dictates the use of titanium to provide high structural durability.

- composite compatibility

Polymer matrix composite (PMC) compatibility is a big issue with higher utilisation of composite structure on aircraft. Titanium is galvanically compatible with the carbon fibres in the composites. Furthermore, titanium has also been used with PMC structure due to its compatible coefficient of thermal expansion[6, 8].

2.2.1. Aircraft Component Use of Ti-6Al-4V Alloys

Ti-6Al-4V has been the workhorse of the titanium industry as mentioned earlier, and probably 80%-90% of the titanium used on airframes has been this alloy. It is used on all sections of the aircraft – fuselage, nacelles (housing to the jet engine), landing gear, wing and empennage (vertical and horizontal stabilisers, rudder and elevator). Figure 2.7 illustrates the various sections and components of the superstructure of an aircraft.

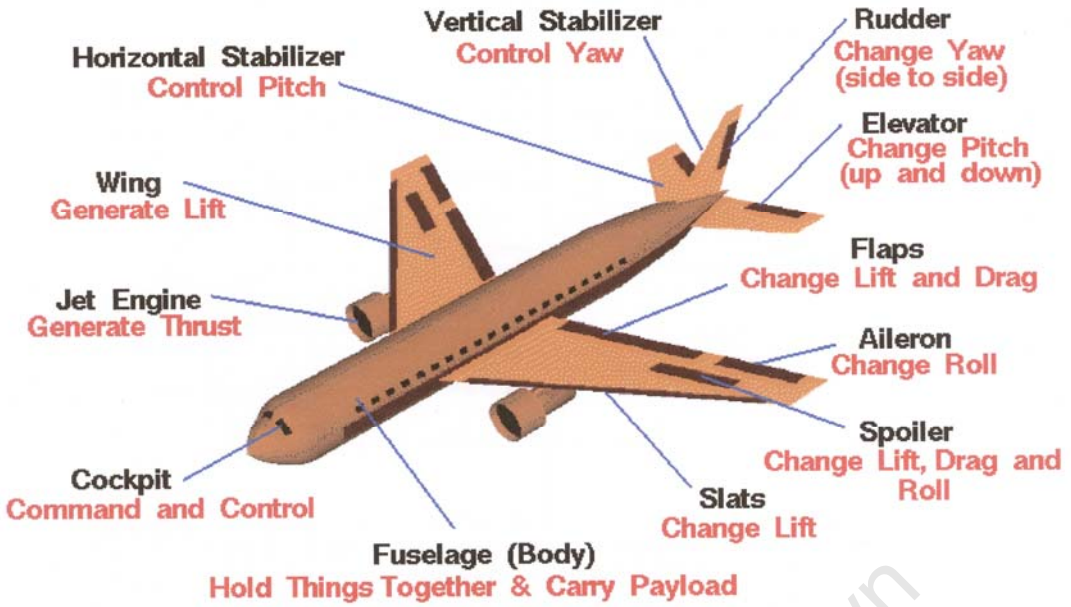

Figure 2.7: Superstructure of an aircraft with annotations of component functions[13]

In gas turbines Ti-6Al-4V is used for static and rotating components[6]. Castings are used to manufacture the more complex static components like the intermediate compressor case shown in figure 2.8.

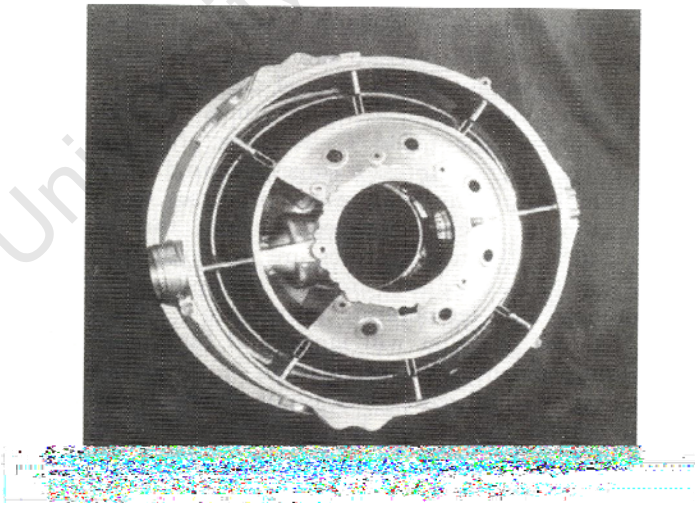

Figure 2.8: Cast Ti-6Al-4V intermediate compressor case for the EJ200 Eurofighter[6]

Rotating components which include fan discs and low pressure compressor discs and blades are found in the jet engine. Ti-6Al-4V is used on the first cooler compressor

stages, up to temperatures of about 315 °C. Forgings are typically used for the manufacturing of rotating components[6].

The Boeing 757 aircraft offers an excellent example of the use of titanium in the landing gear area shown in figure 2.9. The rationale for using titanium for the landing gear beam, which is a massive structure, is its ability to carry the required loads without compromising too much space and lower density as compared to other alternatives such as steel and aluminium. The titanium parts machined from forgings are used because of the alloy's excellent corrosion resistance with the added benefit of reduced weight[6].

Figure 2.9: Titanium forging used in 757 landing gear support structure[6]

The windshield frames on the Boeings 757, 767 and 777 are machined from beta-annealed Ti-6Al-4V forgings, and the crown panel just above them is fabricated from formed Ti-6Al-4V sheet as shown in figure 2.10[6]. These components are titanium owing to its high strength which is needed to withstand the damage incurred during bird strikes.

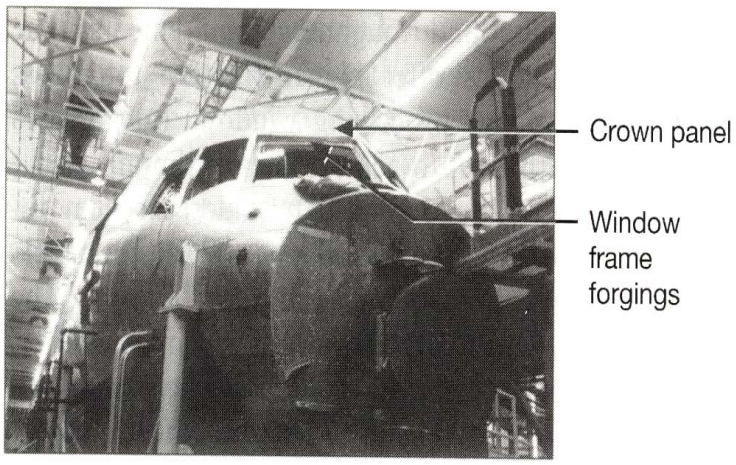

Figure 2.10: Window frame forgings used on the Boeing 757, 767, and 777[6]

The fin deck on the Boeing 777, where composite vertical fin attaches to the fuselage, uses Ti-6Al-4V hot-formed plate[6]. The reason for this application is the coefficient of thermal expansion of the titanium, which more closely matches that of graphite in the PMC better than other structural materials.

Beta annealed Ti-6Al-4V machined forgings are also used for the critical fittings attaching the composite horizontal and vertical fins to the fuselage of the Boeing 777[6]. This is owing to the corrosion compatibility between the titanium and graphite. Ti-6Al-4V formed sheet metal is used in the floor support structure in areas of the galleys and lavatories for the same reasons. But due to the corrosion compatibility with the PMC floor beams, the reliance of a corrosion protection system to prevent galvanic corrosion was precluded.

The Boeing 777 tail cone and the auxiliary power unit (APU) exhaust duct use Ti-6Al-4V owing to the high temperatures associated with the APU[6]. The exhaust duct is fabricated from a casting. Owing to the complexity of the geometry and the difficulty of machining, a casting was the most cost effective means of producing this component. The magnitude of the use of titanium in the industry is immense but future efforts have to be directed toward lower final component costs for the aircraft manufacturer. The cost of titanium components can be reduced and there are two approaches to achieving this; development of lower cost alloys and/or processing

improvements to reduce the fabrication costs, with the latter probably offering the greatest potential.

2.3. SURFACE TREATMENTS ON TITANIUM ALLOYS

As mentioned in the previous chapter, titanium and its alloys show poor tribological properties due to their strong tendency to weld to themselves, or to other metals, under sliding contact conditions. With regards to surface treatments, significant success has been achieved with more costly techniques such as physical vapour deposition (ion plating) and plasma processing, where particular use has been made of surface coatings of titanium nitride (TiN) [10].

- **Physical Vapour Deposition**

This process involves reacting titanium vapour that is obtained from a separate source, with nitrogen ions generated by glow discharge in a nitrogen atmosphere. The operating temperature is normally 500°C and the deposited coatings, which are typically 3 μm thick, provide a hard, smooth and low-friction surface capable of withstanding appreciable loading conditions[10].

- **Plasma Nitriding**

With plasma nitriding, the titanium component is made the cathode in a low-pressure nitrogen glow discharge and the positive nitrogen ions accelerate towards the surface where they react to form TiN. This treatment results in thick coatings of up to 10 μm at higher temperatures of 700-850°C[10].

The rate of diffusion of nitrogen in titanium, which is several orders of magnitude less than iron or steel, is a limiting factor in the depth of the hardening with this technique. In order to obtain deeper layers it would be necessary to carry out the process in the molten state, which is by melting and alloying the surface of a component by means of a high-energy beam source. In such situations laser nitriding or alternatively electron beam melting can be used.

- **Thermal Oxidation Treatment**

A recently developed lower cost method for improving tribological properties of titanium alloys has been explored and developed to an advanced stage[10]. This treatment is analogous to surface carburising of steel components. It involves a thermal oxidation process and treatment that simultaneously produces a thin, hard and adherent surface film of rutile (TiO_2) supported by a thicker oxygen-rich, α-titanium sub-surface zone.

For components made from Ti-6Al-4V, oxygen in concentrations of 100-200 parts per million (ppm) was added to an argon gas carrier and was heated to 900°C for up to 24 hours. The depths of the 2 layers were measured to be approximately 2 μm and 20 μm respectively. Surface hardness was found to be around 1000 H_v which compares with 400 H_v in the interior of the alloy[10].

There are some effects of surface oxide films on degradation of titanium that are experienced during surface treatment. Titanium is an active metal and as mentioned earlier its surface oxide film (TiO_2) provides corrosion resistance and biocompatibility to the metal. During annealing of titanium in ambient air, it is covered with crystalline oxide films such as anatase (another mineral form of titanium oxide) and rutile which in turn improve corrosion resistance. Oxide film thickness rapidly increases at temperatures higher than 1000°C, and flakes fall down as scale[19].

- **OBDH Treatment**

To recap the description in chapter 1, the OBDH treatments involve a two-step process whereby oxidation and diffusion occur at elevated temperatures. The oxidation results in an oxide layer being formed on the samples in the first step. The sample accumulates an oxide layer and is further subjected to a diffusion treatment in a heated environment during the second step where the oxygen is diffused into the bulk of the sample thereby creating an oxygen-rich hardened layer below the surface.

Figure 2.11 shows some changes that can be effected on fatigue properties due to heat treatments[1]. The OBDH treatment resulted in a 27% decrease in the fatigue limit. The concluded cause of such a decrease in the study was the coarsening of the α grains

after heat treatment. However, this reduction in the fatigue limit induced by the heat treatment can be fully restored and increased beyond the as received material by a process known as shot peening as depicted in figure 2.11. Shot peening is a process whereby a compressive residual stress layer is produced thereby modifying the mechanical properties of the titanium.

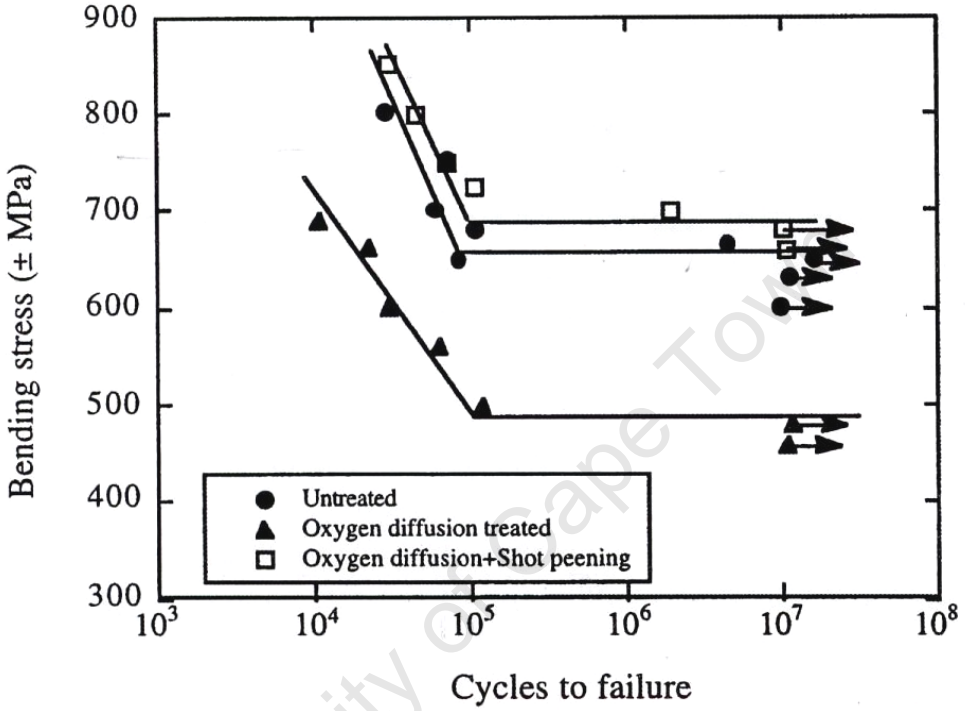

Figure 2.11: Influence of OBDH and shot peening on fatigue properties of Ti-6Al-4V[1]

Figure 2.12 shows that a significant hardening effect is obtained due to the OBDH process, with higher values obtained at the surface. This is obtained from the two-step process whereby surface oxide formed during the oxidation stage serves an oxygen reservoir for the diffusion step. In the diffusion step the oxygen is liberated from the surface oxide layer and diffused into the base metal, forming a deep oxygen diffusion case[1]. This case is strong and hardened by solid solution hardening of oxygen in the titanium lattice. The time variation also plays a major role in showing how much more the alloys get hardened. Figure 2.13 shows the variations more conspicuously. The surface and sub-surface region is hardest when the oxidation time is 30 minutes. This proves to be the optimum time for oxidation as lower and higher oxidation times

yielded lower hardness values at the surface as shown by the results from 15 and 45 minutes.

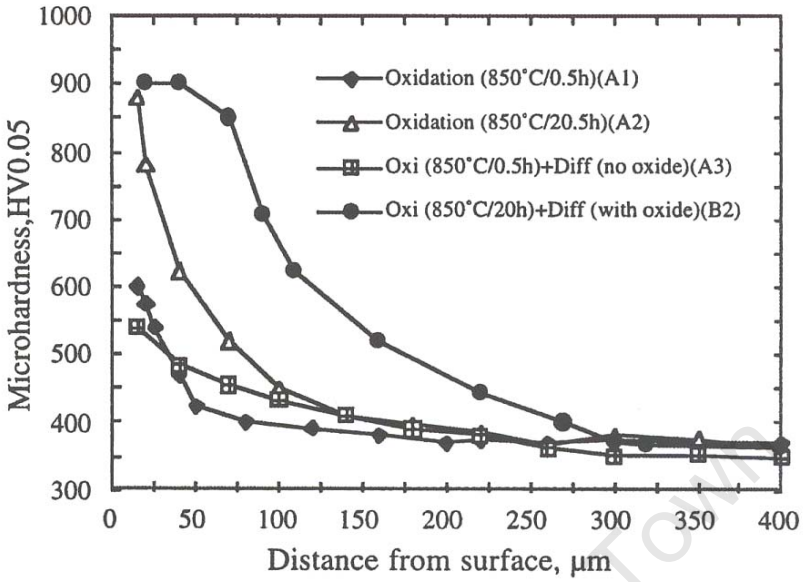

Figure 2.12: Microhardness profiles for oxygen surface engineered Ti-6Al-4V[1]

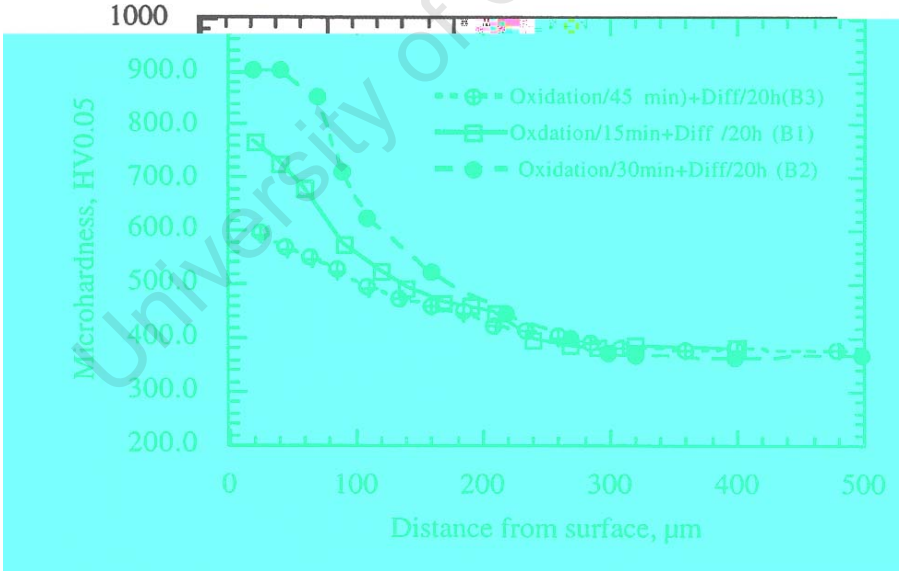

Figure 2.13: Effect of oxidation time on the microhardness distribution of the oxygen boost diffusion treated material[1]

- **Laser Shock Peening**

An alternative surface treatment that can improve fatigue strength is known as laser-shock peening. Relevant to this study is the fact that it is used in certain fields of the

aircraft industry, especially for fan blades of military aircraft. This treatment is actually a process which involves a short high energy pulse that hits a surface of a metallic workpiece which is in most cases coated. The surface of the metal which is usually coated encounters evaporation of this layer due to the high power density of the laser impact and forms and expanding plasma inducing the desired elastic-plastic shockwave for the generation of strain-hardening and compressive residual stresses[20]. This process significantly improves fatigue behaviour. It should be noted that the improvement of fatigue life is independent of the testing temperature and that it takes place in temperature ranges where compressive residual stresses have almost relaxed fully through thermo-mechanical loading. Similar to a less expensive process known as shot peening, laser-shock peening can be used for complicated geometries and specimens and produces thermally and highly stable microstructures which could be favourable effects for high temperature applications.

- **Coating and Plating**

Improvement of desirable mechanical properties like fatigue of titanium alloys by application of surface treatments can be done by about six different kinds of treatments on the Ti-6Al-4V alloy[21]. These include two kinds of plasma flame, three kinds of diamond-like carbon coating and electroless plating method.

Plasma Flame Coating

The plasma flame coating is a process which involves the application of protective coatings on a substrate material by injecting powdered material into a high temperature gas stream[21]. The plasma gas heats the powdered coating material to a molten state and sprays it onto the substrate at high velocity. Plasma satisfies stringent military and commercial aerospace applications and makes it ideal for wear resistant applications.

Diamond-like Carbon Coating

In diamond-like carbon coating the carbon for the diamond-like carbon is deposited under energetic conditions. Carbon is then strongly bonded in all directions as in a diamond, but as an amorphous (having no apparent crystalline) structure, while graphite is strongly bonded in a plane, but weakly between planes[21]. These coatings

are wear and corrosion resistant and are highly applicable in aerospace and biomedical applications.

Electroless Plating Method

Plating describes surface-covering where a metal is deposited on a conductive surface. The electroless plating method is a non-galvanic type of plating method that involves several simultaneous reactions in aqueous solution, which occur without the use of external electrical power[21]. The reaction is accomplished when hydrogen is released by a reducing agent and then oxidised thus producing a negative charge on the surface of the part. This plating method also increases the wear resistance property of the metallic parts plated.

2.3.1. Effects of Surface Treatments on Titanium Alloys

The free surface of a component is a common site for the nucleation of a fatigue crack. Therefore, the manner in which the surface is prepared during manufacturing of the component has a decisive role in dictating the initiation life for fatigue cracks[22]. There exists a variety of surface treatments, such as carburising, nitriding, flame hardening, induction hardening and shot peening which are designed to impart high strength, wear resistance or corrosion resistance locally in the near-surface regions of the material. Along with these treatments OBDH can be incorporated. Furthermore, common machining operations such as grinding, polishing and milling cause different degrees of surface roughness to develop. The valleys on the rough surface serve as stress concentrations, which, in turn, induce different levels of resistance to fatigue crack nucleation.

In addition to the roughness of the surfaces, the residual stresses that are induced by the surface treatments have an important effect on the fatigue life. Residual stresses are generated in a component as a consequence of thermal, chemical or mechanical treatments[5,22]. Residual stresses arising from fabrication or surface and heat treatments, when superimposed with applied fatigue loads, alter the mean level of the fatigue cycle and the fatigue life for crack nucleation. In general, residual stresses affect the fatigue behaviour of materials in the same way as the static mechanical stresses superimposed on cyclic stress amplitude. Therefore, residual stresses are

favourable, if compressive, and detrimental, if tensile; this is especially true for high strength materials. Fatigue strength of titanium alloys undergoing various heat treatments decreases significantly in comparison to plain fatigue strength of untreated specimens in both low and high cycle fatigue life regions. The low cycle fatigue occurs where the stress is high enough for plastic deformation. With this in mind the stress is less useful and the strain in the material offers the simpler description as it is high in magnitude. On the other hand the high cycle fatigue refers to situations that require 10^4 cycles to failure where stress is low and deformation is primarily elastic.

Oxide layers are very easily formed on the surfaces of titanium materials. This is because the total free energy of the system is lowered by such formation and this effect is enhanced at high temperatures. In some cases, an oxide layer maybe protective of the surface, whereas in others it may introduce cracks[17].

2.4. FATIGUE

Fatigue is defined as a term which 'applies to changes in properties which can occur in a metallic material due to the repeated application of stresses and strains, although usually this term applies specially to those changes which lead to cracking or failure'[22].

Fatigue failures occur in many different forms. Mere fluctuations in externally applied stresses or strains result in mechanical fatigue**.** In this study it is this mechanical fatigue that is being analysed. Other types of fatigue would include creep-fatigue, thermomechanical fatigue, corrosion fatigue, sliding contact fatigue, rolling contact fatigue and fretting fatigue.

Fatigue environments may be divided into two distinguished groups namely stress-controlled and strain-controlled. In practice most environments are indeed a combination of the two but the nature of biological materials tends to place them towards the direction of strain-controlled[23]. The fatigue performance of an alloy is a vital mechanical property for confirming the reliability of the alloy. In titanium alloys

it is common knowledge that this property changes according to the microstructures obtained by heat and thermomechanical treatments[24].

2.4.1. Fatigue Loading, Test Machines and Specimens

In order for testing to occur and obtain the fatigue data under study there is need to have the proper essentials to carry out the experimental work. These essentials involve the fatigue loading modes, machinery and the test specimens.

- **Fatigue Loading**

Thin-walled structures in the aerospace industry are normally subjected to cyclic internal pressure, which in turn represents a component subjected to mean tensile stresses[25]. Taking cognisance of this a variety of specimen configurations and test techniques have been devised to generate fatigue data. As suggested by the figure 2.14 the results may depend on;

- the type of specimen (smooth, notched)
- the loading mode (axial, bending, torsion)
- the range of cyclic stresses or strains
- the level of mean stress
- grain direction within the specimen (rolled sheet, plate, bar stock)[25]

An illustrative analysis on an aircraft shows that, on the airfoil section of turbine blades, high cycle fatigue (HCF) cracks can initiate at sites of foreign-object damage (FOD) caused by the ingestion of debris into the engine. After such an occurrence the problem would then involve impact-induced residual stresses, microstructural distortion, incipient microcrack formation, and geometric stress concentration[26]. Crack initiation can also occur in the attachment section of the blade, where contact between the blade dovetail and disk can lead to the formation of fretting fatigue cracks[8, 26].

An example of different bending and axial fatigue data trends for an alloy steel is shown in the figure 2.14. The apparent higher fatigue resistance in bending is due partially to the fact that only the surface of the bending specimen is exposed to the maximum stresses. More importantly, however, the apparent difference in fatigue properties results because the elastic bending relation routinely used to calculate stress is prone to increasing errors at high stresses (due to plasticity effects)[15].

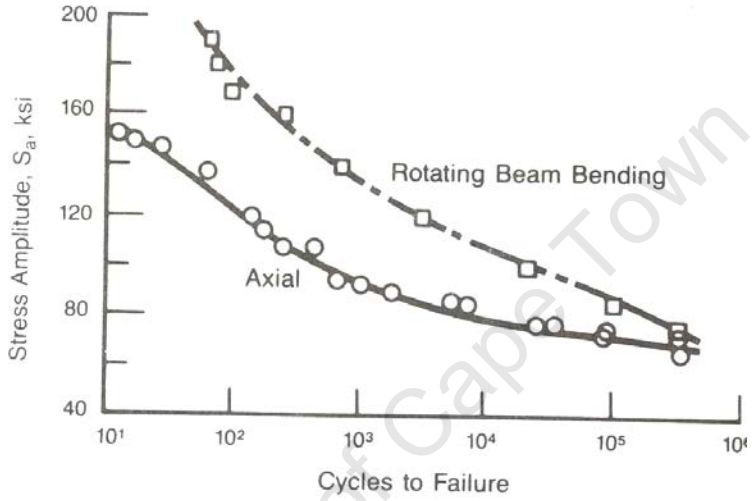

Figure 2.14: Comparison of fatigue data from rotational bending and axial loading tests[15]

- **Fatigue Test Machines**

Rotating bending machines are shown in figures 2.15a and 2.15b. The test machine in (b) produces uniform pure bending moment over the entire test length of the specimen, while the cantilever test machine in (a) has a non-uniform bending moment along the specimen's length. The load amplitudes of these test machines do not change hence they are known as "constant load amplitude machines", despite changes in material properties or crack growth.

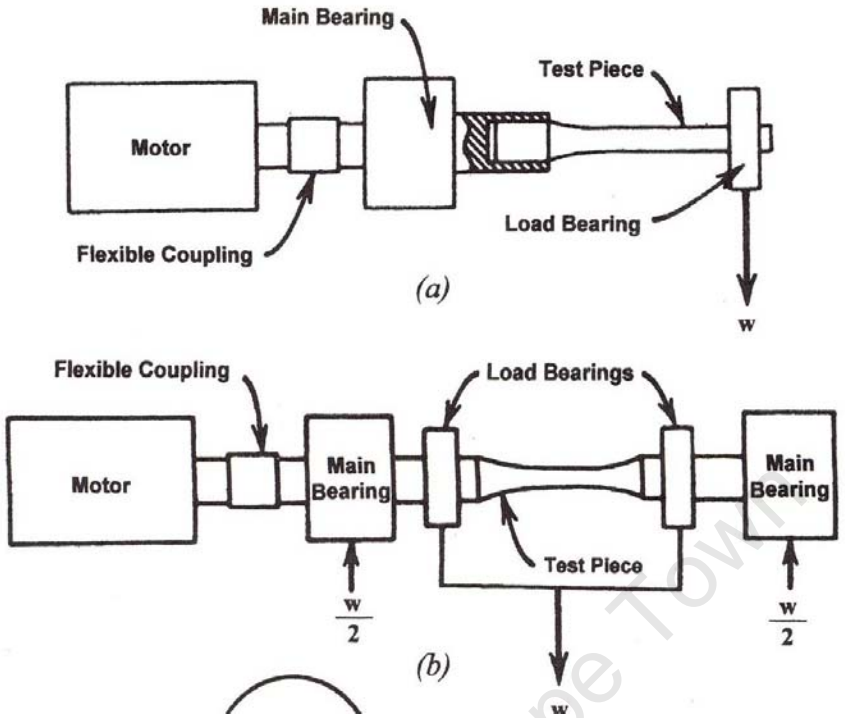

Figure 2.15: (a) Cantilever rotating bending machine and (b) Rotating pure bending machine[25]

- **Fatigue Test Specimens**

Common test specimens for obtaining fatigue data are shown in the figure 2.16. They have been used to obtain total fatigue life, that includes crack nucleation life and crack growth life. These specimens often have finely polished surfaces to minimise surface roughness effects. No distinction between crack nucleation and growth is normally made with these specimens. Bending and axial specimens with solid circular cross sections usually have diameters between about 3 and 10 mm.

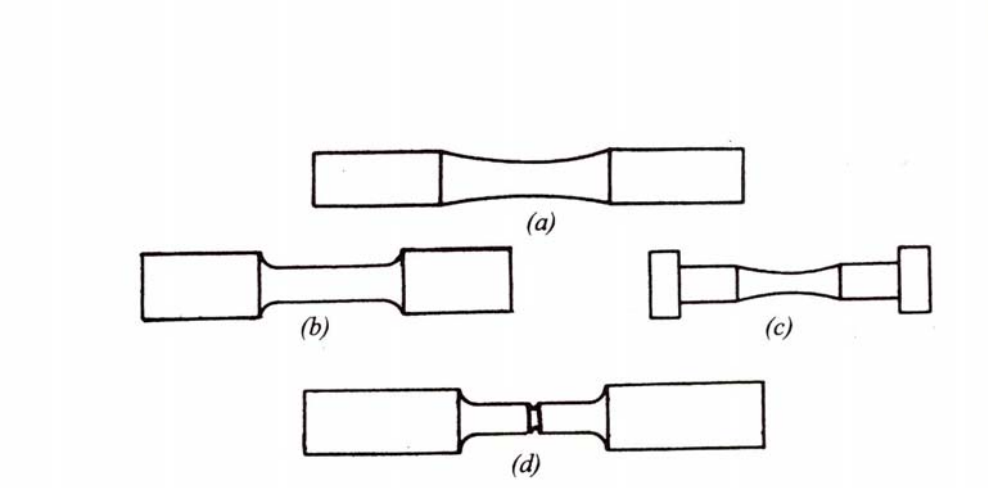

Figure 2.16: (a) Rotating bending, (b) Axial uniform, (c) Axial hourglass and (d) Axial and bending with circumferential groove[25]

Pins, fillets and the irregular shape of the samples all contribute to stress raising and should be dimensioned for calculation of stress concentration[27]. Surface condition of the specimens is also of paramount importance. A rough surface condition plays a major role on a notch or fillet effect during fatigue testing and may lead to deteriorating fatigue limits[21]. Notches can be cracks or metallurgical defects. More severe stress raisers having significant stress concentration factors (K_t) have greater influence on fatigue performance. Stress raisers on the different components made of titanium in industry are present and the magnitude of the stress concentration should be investigated. It should be noted that the magnitude of the effect of a notch is also very material dependent[17,27].

2.4.2. Different Approaches to Fatigue Evaluation

There are different stages of fatigue damage in an engineering component where defects may nucleate in an initially undamaged section and propagate in a stable manner until catastrophic fracture ensues. The conditions for the nucleation of microdefects and the rate of advance of the dominant fatigue crack are strongly influenced by a wide range of mechanical, microstructural and environmental factors. The principal differences among different design philosophies often rest on how crack

initiation and the crack propagation stages of fatigue are quantitatively treated. What constitutes crack initiation and, making clear demarcation between crack initiation and crack propagation can become a critical task[22].

- Total-life Approaches

Classical approaches to fatigue design involve the characterisation of total fatigue life to failure in terms of the cyclic stress range (the S-N curve approach) or the (plastic or total) strain range. The resulting fatigue life incorporates the number of fatigue cycles to initiate a dominant crack (which can be as high as some 90% of the total fatigue life) and to propagate this dominant flaw until catastrophic failure occurs. Since the crack initiation life constitutes a major component of the total fatigue life in smooth specimens, the classical stress-range and strain-range approaches represent, in many cases, design against fatigue crack initiation. Under high-cycle, low stress fatigue situation, the material deforms primarily elastically; the failure time or the number of cycles to failure under such high-cycle has traditionally been characterised in terms of the stress range. However, the stresses associated with low-cycle fatigue are generally high enough to cause appreciable plastic deformation prior to failure. Under these circumstances, the fatigue life is characterised in terms of the strain range[22]. The stress-based and strain-based approaches have found widespread application, most notably in the design of many fatigue-critical components for airplanes, automobiles and other surface vehicles.

- Defect-tolerant Approach

The basic premise of this approach is that all engineering components are inherently flawed. The size of the pre-existing flaw is generally determined from non-destructive flaw detection techniques (such as visual, dye-penetrant or X-ray techniques or the ultrasonic, magnetic or acoustic emission methods). If no cracks are detected by the non-destructive test method and if catastrophic failure does not occur during testing, the largest (undetected) initial crack size is estimated from the linear elastic fracture mechanics (LEFM) also referred to as the defect-tolerant approach. The useful fatigue life is then defined as the number of fatigue cycles or time to propagate the dominant

crack from this initial size to some critical dimension. The choice of the critical size for the fatigue crack may be based on the fracture toughness of the material, the limit load for the particular structural part, the allowable strain or the permissible change in the compliance of the component. The prediction of crack propagation life using the defect-tolerant approach involves empirical crack growth laws based on fracture mechanics[22]. The equations used in the empirical crack growth in order to successfully implement the approach are as follows;

$$\mathbf{K = Y\sigma\sqrt{(\Pi a)}}$$

$$\mathbf{da/dN = C\,(\Delta K)^{m}} \quad \textbf{(Paris Equation)}$$

where K = Stress intensity factor

Y = Constant configuration factor

σ = Stress

a = Crack length

N = Number of cycles

C and m = scaling constants

ΔK = Stress intensity range.

Differentiating a or N, using the Paris equation, depending on whether the parameter being investigated is initial or final crack length, or crack propagation life the approach can be applied.

The different approaches to fatigue also provide apparently different guidelines for the design of microstructural variables for optimum fatigue resistance. These differences are merely a consequence of the varying degrees to which the role of crack initiation and crack growth are incorporated in the calculation of useful fatigue life. For example, in many structural alloys the resistance to the growth of long fatigue cracks generally increases with an increase in grain size (or a decrease in yield strength). On the other hand, the total fatigue life estimated on the basis of stress-life plots generally exhibits the opposite trend; higher strength materials and finer grained microstructures usually lead to longer fatigue life. The apparent contradiction between the two approaches can be reconciled by noting that the former approach to fatigue

deals primarily with the resistance to fatigue crack growth, while the latter approach based on nominally defect-free laboratory specimens focuses mainly on the resistance of fatigue initiation. Optimisation of microstructural characteristics for improved resistance to both crack initiation and crack growth would require a trade-off between the recommendations of the two approaches[22].

- 'Safe-life' and 'Fail-safe' Concepts

The safe-life and fail-safe design approaches were developed by aerospace engineers. In the safe-life approach to fatigue design, the typical cyclic load spectra, which are imposed on a structural component in service, are first determined. On the basis of this information, the components are then analysed or tested in the laboratory under load conditions which are typical of service spectra, and a useful fatigue life is estimated for the component. The estimated fatigue life, suitably modified with a factor of safety, then provides a prediction of 'safe-life' for the component. At the end of the expected safe operation life, the component is automatically retired from service, even if no failure has occurred during service (and the component has residual fatigue life). Although an estimate of life may be obtained from practical tests on the actual component, the safe-life method is intrinsically theoretical in nature. This procedure invariably has to account for several unknowns, such as unexpected changes in load conditions, errors in the estimates of typical service load spectra, scatter in the test results, variation in properties among different batches of the same material, existence of initial defects in the production process, corrosion of parts used in the component, and human errors in the operation of the component. On the other hand, if fatigue cracks are nucleated in the component during service, the component may well fail catastrophically. As noted by Gurney (1968) [cited in reference 22], the safe-life approach depends on achieving a specified life without the development of a fatigue crack so that the emphasis is on the prevention of crack initiation. The fail-safe concept, by contrast, is based on the argument that, even if an individual member of a large structure fails, there should be sufficient structural integrity in the remaining parts to enable the structure to operate safely until the crack is detected. The fail-safe approach mandates periodic inspection along with the requirement that the crack

detection techniques be capable of identifying flaws to enable prompt repairs or replacements[22].

- The Fatigue Limit

Methods for characterising the fatigue life in terms of nominal stress amplitudes using experimental data obtained from rotating bending tests on smooth specimens emerged from the work of Wohler (1860) [cited in reference 22] on fatigue of alloys used for railroad axles. In this approach, smooth (unnotched) test specimens are typically machined to plane bending, rotating bending, uniaxial compression-tension (push-pull) or tension-tension cyclic loading.

Engineering structures invariably contain stress concentrations which are principal sites for the inception of fatigue flaws. The stress and deformation fields in the immediate vicinity of the stress concentration have a strong bearing on how fatigue cracks nucleate and propagate[22].

In conclusion, fatigue crack analysis is essential in helping understanding the factors that are important for controlling the fatigue damage whilst components are in service and also for design and selection of materials that can have an increased resistance to crack growth[28].

2.4.3. Fatigue Behaviour of Titanium Alloys

Titanium and its alloys which have isotropic microstructures may display properties comparable with those obtained with ferrous materials. In general the factors which increase the tensile and yield strength of titanium alloys also raise the fatigue strength. Fatigue performance of titanium alloys is immensely influenced by microstructure and texture of components. Generally, the fatigue crack propagation in these alloys parallels fracture toughness in that conditions which favour highest toughness tend to also lower cyclic growth rates under fatigue loading. In this review particular attention is being paid to the Ti-6Al-4V, and as mentioned earlier a coarse basket-weave type microstructure is resistant to crack propagation, whereas a finer

microstructure tends to be advantageous in delaying the initiation of cracks. It should be noted that this applies to both room and elevated temperatures, and for α-β alloys the best compromise for overall fatigue strength seems to be a fine microstructure consisting of a mixture of grains of α and transformed β as in figure 2.4b[29].

The refinement of grains which leads to the strengthening of microcrystalline metals and alloys is often accompanied by a relative increase in fatigue endurance limit[30]. Due to this relationship the stress-life curves, which give an indication of the dependence of total fatigue live on cyclic stress in smooth fatigue specimens undergoing a constant amplitude cyclic load, generally point to an improvement in fatigue resistance with a decrease in grain size.

2.4.3.1. Fatigue Crack Initiation in Ductile Solids

The initiation of fatigue cracks is an event whose very definition is strongly linked to the size scale of observation. For example, materials scientists are likely to consider the nucleation of flaws along persistent slip bands (PSBs) as the initiation stage of fatigue failure, whilst a mechanical engineer may associate the resolution of crack detection with the threshold for crack nucleation.

Furthermore, the nature of the crack initiation and propagation in ductile solids like titanium containing both the α and β phases can be affected by phase balance of the two phases. This is due to the fact that the α phase is susceptible to cleavage along the (0002) basal plane. During heat treatment process such as the OBDH the observed coarsening of the microstructure coupled with the above-mentioned susceptibility to cleavage fracture may enhance initiation and propagation. Diffusion time and temperature will also play a significant role as long diffusion times and higher temperatures facilitate grain growth in the solids and greater time for oxygen to diffuse into the solid and more significantly in the (0002) basal plane. The following are a set of crack initiation mechanisms hypothesised.

- Surface roughness and fatigue crack initiation

The origin of fatigue cracks in metals and alloys of high purity is often rationalised by mechanisms of the type first proposed by Wood (1958) [cited in reference 22]. The basic premise of Wood's postulate is that repeated cyclic straining of the material leads to different amounts of net slip on different glide planes. The irreversibility of shear displacements along the slip bands then results in the 'roughening' of the surface of the material. This roughening is manifested as microscopic 'hills' and 'valleys' at sites where slip bands emerge at the free surface. The valleys so generated function as micronotches and the effect of stress concentration at the root of the valleys promotes additional slip and fatigue crack nucleation[22].

- Role of surfaces in crack initiation

In polycrystals PSBs formed within interior grains produce slip that is confined to the individual grain. The large transfer of material causing the creation of rough topography is possible at surface grains, but not in the interior ones because of constraint from the surrounding matrix.

Experiments dating back to the work of Thompson, Wadsworth and Louat (1956) [cited in reference 22] have suggested that removing the intrusions and extrusions by electropolishing the specimen surface increased fatigue life. More conclusive evidence for the argument that the surface geometry determines fatigue life is found in the study of Pascual and Basinski (1983) [cited in reference 22]. They demonstrated that, even in single crystals where coarse PSBs traverse through the bulk, elimination of surface roughness by electropolishing leads to a drastic enhancement in total fatigue life[22].

- Environmental effects on crack initiation

The fraction of fatigue life at which crack nucleation occurs can be significantly affected by the test environment. There is a wealth of experimental evidence indicating that the environment plays an important role in dictating the extent of slip

irreversibility and fatigue life. For example, it was demonstrated by Gough and Sopwith (1932) [cited in reference 22] and by Thompson, Wadsworth and Louat (1956) [cited in reference 22] that fatigue life is markedly improved in dry, oxygen-free media as compared to moist laboratory air. In inert environments, surface roughening during fatigue occurs primarily by a random process. On the other hand, when slip steps form during the tensile portion of a fatigue cycle in laboratory air or in a chemically aggressive medium, the chemisorption of the embrittling species (such as oxygen and hydrogen) or the formation of an oxide layer on the freshly formed slip step makes reverse slip difficult on the same slip plane upon load reversal. In embrittling medium, this process can provide a mechanism of enhanced surface roughening as well as easier transport of the embrittling species to the bulk of the material preferentially along the PSBs, thereby facilitating crack nucleation[22]. Figure 2.17 shows the nature of the processes that the effects lead to in nucleating cracks.

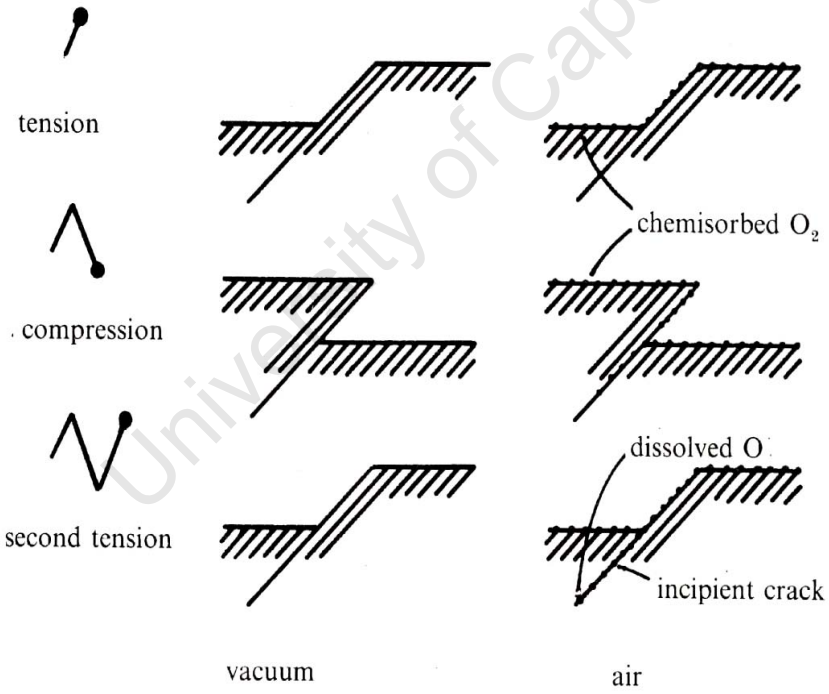

Figure 2.17: A model for fatigue crack nucleation near a free surface by the synergistic effect of single slip and environmental interactions[22]

2.4.3.2. Fatigue Crack Initiation in Titanium Alloys

Fatigue occurs because of cyclic plastic deformation that causes irreversible changes in the material's dislocation substructure. Based on these changes, it is possible for most materials to divide into partially overlapping stages in the initiation stages as follows;

(a) Cyclic hardening and/or softening, depending on the initial condition of the material and the magnitude of stress and strain amplitude. The entire volume of the material may be affected by the change in the substructure
(b) Microcrack nucleation in the subsurface layer due to stress concentration effects at micro-extrusions and micro-intrusions[15]

In most instances, fatigue cracks nucleate due to irreversible slip within the longest crystallographic slip bands available in the microstructue[23]. Fatigue cracks initiate mainly at surface defects in the short-life range which is between 10^3 and 10^5 cycles though this may shift to subsurface in the long-life range around 10^6 cycles and above or at cryogenic (very cold) temperatures. Crack initiation rather than propagation plays a more significant role in lifetime control of ultra-high cycle fatigue (UHCF) which is associated with short-life ranges.

Possible crack initiation sites in titanium alloys include α phase, α-β interface and defects such as voids or pores. Subsurface crack initiation behaviour depends on mechanical variables such as the stress level and mean stress[31]. Fatigue crack nucleation in α and α-β titanium alloys attribute the process, in part, to the occurrence of heterogeneous deformation in the form of slip bands. The slip bands interact with phase boundaries, accumulated deformation debris, and tensile stress components in the generation of a crack-like-discontinuity (CLD)[23,32]. Internal initiation of cracks may be associated with microstructural inhomogeneity if no inclusions or porosities are observed in the titanium alloy[23].

For notched fatigue tests on mill annealed Ti-6Al-4V, Benson *et al*., demonstrated that for all but the lowest stresses, the nucleation sites at room temperatures and at 315°C were slip bands in the α phase. α-β interfaces served as initiation sites only at very low stress, in room temperature tests, with no detectable slip bands[31,32]. It was also reported that at low cyclic strains, interface nucleation was observed in the absence of detectable slip lines.

Development of fatigue cracking is very much a surface-related phenomenon and also fatigue strength is dependent on surface conditions such as finish, hardness and the presence of residual stresses. Changes in surface hardness and the introduction of residual stresses introduced by fabrication processes lead to crack initiation and crack opening[33].

Some time in a fatigue-loaded component's service life there becomes a physically present, although perhaps not detectable, CLD[32]. This tends to be the crack's nucleus. These nuclei may be remnant of the material's manufacturing history. Eylon and Pierce used Ti-6Al-4V alloy to demonstrate that the portion of life attributed to crack nucleation and growth of a detectable flaw size is greater than 85% of the fatigue life in their study of low cycle fatigue (LCF) crack nucleation in lean α-β alloys.

There is some crack transition from the crack initiation site at the surface of a specimen to the subsurface when the crack is propagating. The shift of the initiation site in Ti-6Al-4V alloy is due to compressive residual stresses in the surface region which results from plastic deformation. These stresses would be a maximum at the surface and decrease gradually with increasing distance from the specimen surface to the interior[31].

High cycle fatigue (HCF) can result in essentially unpredictable failures of engine components in aircrafts due to premature initiation of fatigue cracks at small defects and their rapid propagation under high-frequency vibratory loading[26]. Reduction in fatigue strength, which is primarily due to early fatigue initiation, can be considered

to be due to four prominent factors: (1) FOD-induced microcracking, (2) stress concentration, (3) residual stress and (4) damaged microstructure[34].

Fatigue crack initiation and development tests help bring out any faults in the design of the components. Such aspects of the fault in design include;

- The presence of severe stress concentrations in the component. The shape of the components in this case would have to be analysed with respect to loads encountered to determine any possible fatalities.
- Improper selection of material properties and surface treatments.
- Inadequate or inaccurate stress analysis to identify stress fields in the component
- Improper attention to important load and environmental conditions as they relate to material performance[35].

2.4.4. General S-N Behaviour of Titanium Alloys

Two typical schematic S-N (Stress-Number of cycles) curves with trendlines obtained under axial load conditions with smooth specimens are shown in figure 2.18. In this figure S is the applied nominal stress and N_f is the number of cycles or life to failure, where failure is defined as fracture. S-N curves can be in different forms as depicted by the curves in figure 2.18. Figure 2.18a shows a continuously sloping curve, while figure 2.18b shows a discontinuity or "knee" in the S-N curve[25]. Data was obtained from medium strength steel in order to show the difference in curves. The knee has been found in these steels between 10^6 and 10^7 cycles under non-corrosive conditions. Most materials do not contain a knee even under controlled environmental conditions. In corrosive environments all S-N data invariably have a continuously sloping curve.

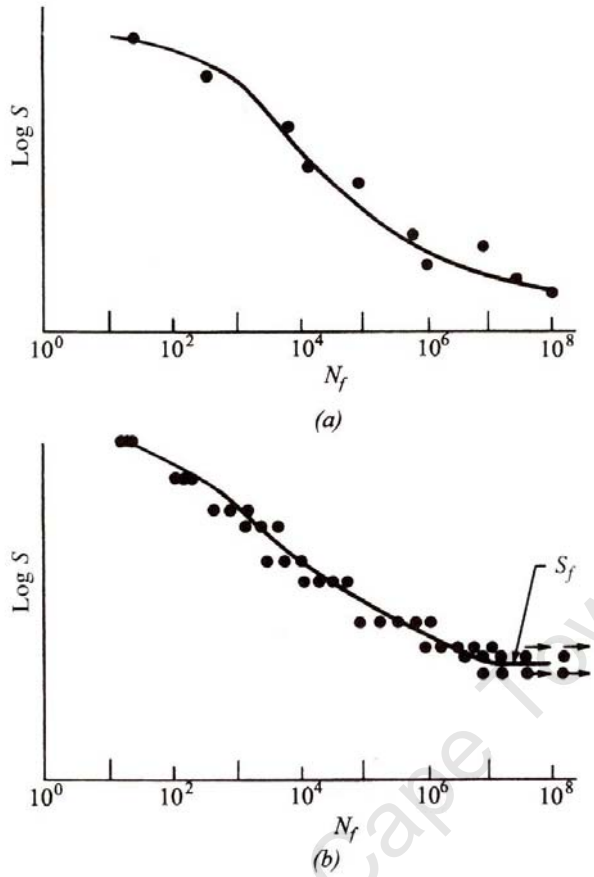

Figure 2.18: Characteristic shape of S-N curves with a (a) continuously slope and (b) "knee" [25]

The results in figure 2.19 from the work of Leinenbach and Eifler shows that corundum grit blasting leads to a pronounced decrease in fatigue life of Ti-6Al-4V alloy. The S-N_f analysis of the graphs shows that cracks are likely to have initiated mainly in the vicinity of entrained corundum (a very hard mineral that consists of aluminium oxide occurring in massive and crystalline forms which can be used as an abrasive) where a pronounced stress concentration occurs[2]. Furthermore, particle impact induces a local residual stress field, which further enhances the crack formation and the initial crack growth. This graph clearly indicates that surface topography has a large influence on fatigue life and when making comparisons a similar texture and surface roughness must be obtained.

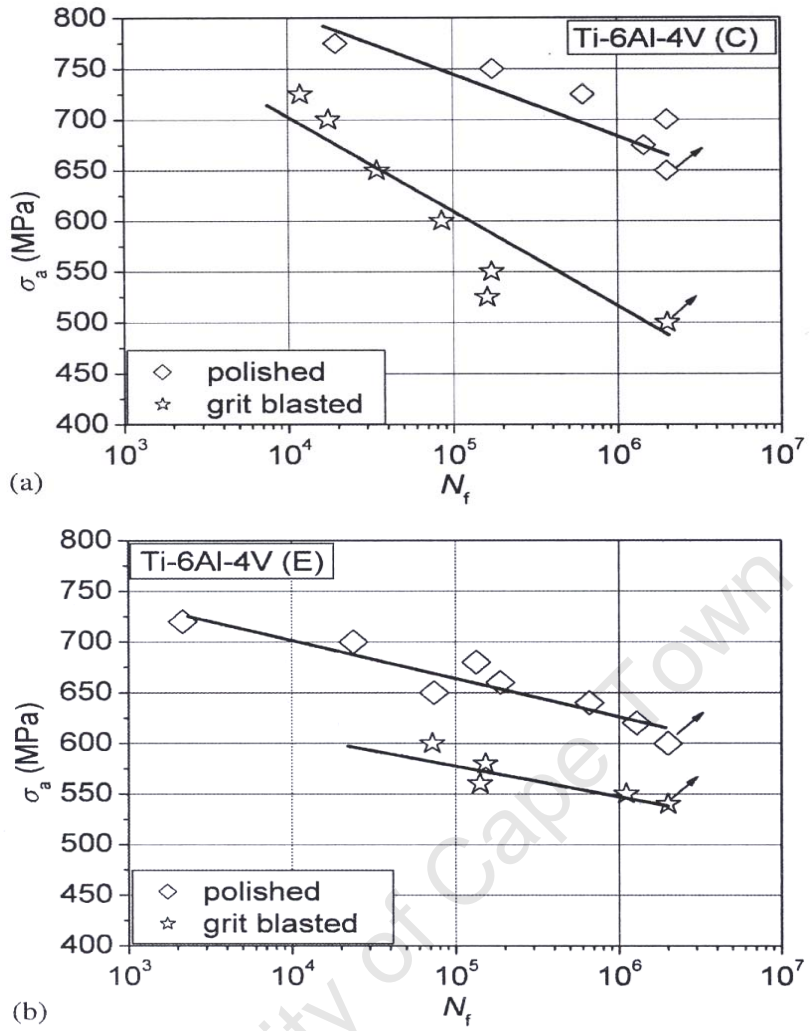

Figure 2.19: S-N curves for polished and grit blasted Ti-6Al-4V in oxygen-saturated Ringer's solution, (a) axial loading, and (b) rotating bending[2]

2.5. MICROSTRUCTURES AND THEIR EFFECT ON FATIGUE

The microstructure of an alloy is an important factor that determines its hardness, tensile properties, fracture toughness and fatigue strength[36]. Studies have revealed that fatigue crack initiation and growth is strongly influenced by microstructure, for instance grain size, grain orientation and grain boundary geometry, precipitates and other particles of the second phase[37]. The α precipitate distribution exerts a much larger influence on the fatigue strength in titanium alloys than grain size effect[36]. In two-phase materials such as Ti-6Al-4V, the nature of the crack nucleation site does not depend on microstructure factors only, but also on the respective response of each

phase with respect to cyclic straining. In Ti-6Al-4V alloy, the hcp α phase is more brittle than the bcc β phase, hence slip starts initially in the β phase, and dislocation arrays are piled up at α/β interfaces or primary α grain boundaries. Cracks are found to initiate preferentially at either slip bands or grain boundaries during cyclic loading[16, 29, 32, 31, 37, 38].

Characteristic microstructures after particular heat treatments are shown in figures 2.20-2.22. Water-quenching from all annealing temperatures leads to the formation of the ά martensite structure whereby the volume fraction of this ά structure decreases with decreasing annealing temperature. After quenching from 1100°C ά martensite prevails in the microstructure as depicted in figure 2.20a. When water-quenching takes place from 950°C a mixture of α and β structures with α plates formed inside and at prior grain boundaries is produced. Some ά martensite is present inside the β as shown in 2.20b. Figure 2.20c shows a similar microstructure to the latter except the volume of the α phase is higher and water-quenching had taken place from 900°C.

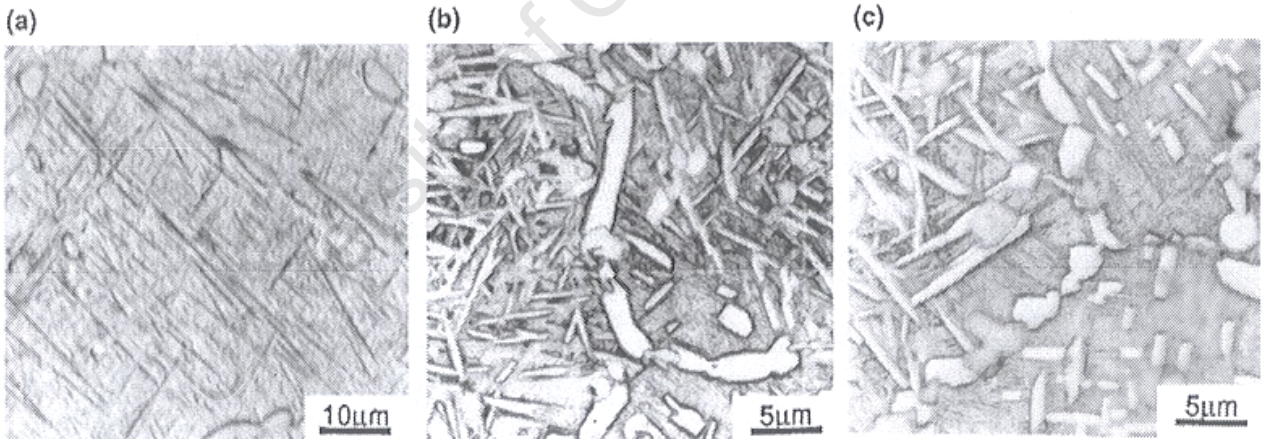

Figure 2.20: Microstructure upon water-quenching from: (a) 1100°C; (b) 950°C; (c) 900°C[14]

Air-cooling which has a much slower cooling rate leads to the formation a different morphology of microstructure compared to water-quenching. Upon air-cooling from 1100°C transformed β with rectangular-like patterns appears in the β matrix as shown in figure 2.21a. The same rectangular-like particles are visible in figure 2.21b and it is also visible that some β (dark matrix) is incorporated into a finer transformed β structure upon air-cooling from 950°C. Air-cooling from 900°C produces a structure

with more of the α phase at the expense of the transformed β and β mixture as shown in figure 2.21c. Primary α plates at boundaries of prior β grains may also be seen.

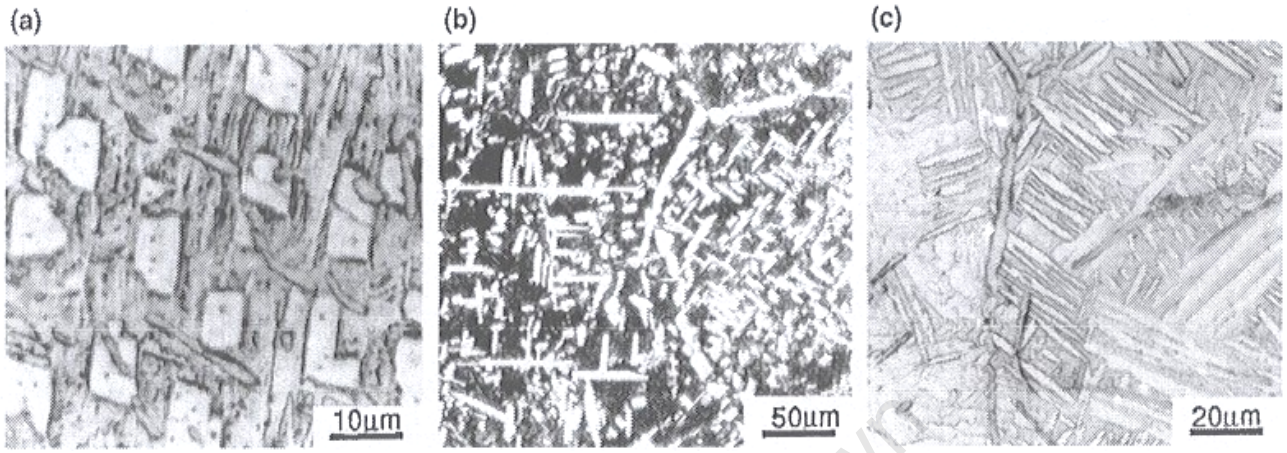

Figure 2.21: Microstructure upon air cooling from: (a) 1100°C; (b) 950°C; (c) 900°C[14]

Samples that were furnace-cooled from annealing temperatures selected show plates of the primary α phase with some retained intergranular β as depicted in figures 2.22a-2.22c. The thickness of the α plates is higher as annealing temperature is higher.

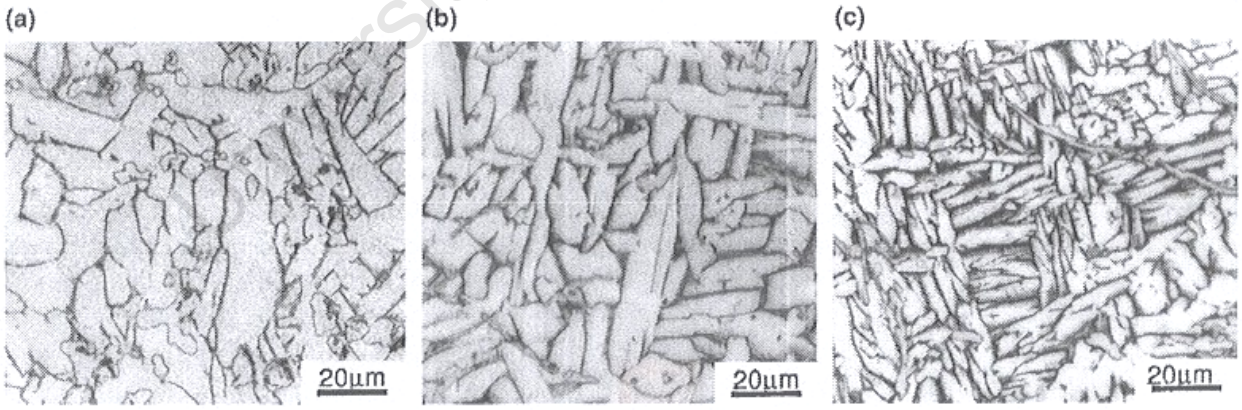

Figure 2.22: Microstructure upon furnace cooling from: (a) 1100°C; (b) 950°C; (c) 800°C[14]

The mechanical properties of the samples that have the microstructure in figures 2.20-2.22 are modified with respect to the annealing temperatures they encounter as well as the different cooling rates[14]. Generally, the hardness increases with an increase in

annealing temperature being highest upon water quenching. Furnace-cooling results in the lowest hardness of the samples. The manner in which the tensile strength changes is similar to the hardness behaviour for all three sets of microstructures shown. On the contrary, elongation and fatigue strength decrease with both annealing temperature and cooling rate. The fatigue strength drops due to the increase in grain size with increased temperature. The presence of less refined, large grains lowers the fatigue strength of the Ti-6Al-4V alloy.

To conclude on the grain size effect, it has been shown that a strong improvement is achieved in both the tensile and fatigue resistance by grain refinement. Grain refinement is a material strengthening mechanism that relies on the fact that it is difficult for dislocations to move across grain boundaries thereby making it an effective way to increase yield strength without impairing good ductility. It also causes an inhibition to crack propagation with a consequent improvement on fatigue behaviour[39, 40].

2.6. FRACTURE SURFACE ANALYSIS

An underlying feature of the fracture mechanics analysis is that they are based on macroscopic aspects of crack growth. Fracture surfaces are often smooth to the naked eye but are found to be irregular when subjected to microscopic examination. Hence the morphology of grains and grain boundaries in a material could have a significant effect on the fracture parameters[17,27]. An attempt to identify whether there are one or more crack origins, since this may provide an indication of the magnitude of stress in the critical region, should be the initial step. Generally, the number of crack nuclei increases with increasing applied stress and magnitude of an existing stress concentration factor. The fracture surface often reveals contour lines that point back to the origin of the crack, that is in instances were cracks are present. These features are referred to as chevron markings and are very common in engineering solids. They aid the investigation of locating the region where crack has formed or pre-existed. With such information, the focus can now be shifted to the micromorphological features of the origin and gain insight into the cause of failure[17,27].

Reliable fracture analysis work can be obtained from scanning electron microscopy (SEM) work. Fractures surfaces from failed test samples are observed under this advanced microscope and fractographs are obtained at different magnifications to determine the fracture modes whether macroscopic or microscopic. The macroscopic nature of failure refers to the overall nature of failure while the microscopic mechanisms relate to the local failure processes such as microscopic void formation, microscopic void growth and eventual coalescence and finally the nature, intensity, and severity of both the microscopic and macroscopic cracks[36].

The usefulness of a fractograph depends directly on the knowledge that can be gained from the study of it. Fractographs should enable one to tell something about the conditions of stress, effect of temperature and chemical environment and how the crack progressed to final rupture. When interpreting SEM fractographs the fracture features to look for include: (i) cleavage features(tongues, microtwins and location of cleavage-crack origins), (ii) quasicleavage features, (iii) dimples from microvoid coalescence, (iv) tear ridges, (v) fatigue striations, (vi) separated grain facets, (vii) mixed fracture surfaces incorporating i to vi, and (viii) features of fractures resulting from chemical and thermal environments[41].

Titanium alloy scanning electron micrographs with some of the mentioned descriptions are shown in figures 2.23 and 2.24. Both the longitudinally and transversely orientated test specimens were prepared and their micrographs are figures 2.23 and 2.24 respectively. The descriptions mentioned along with others are associated with certain types of fracture. The fractures are a result of tensile tests carried out on Ti-4Al-2.5V-1.5Fe-0.25O_2 alloy. Tensile overload occurs on the specimens and the fracture surfaces are thus examined. At the macroscopic level, the overall morphology of the tensile fracture surface appears rough as shown in figure 2.23a. Observation of the fracture surface at higher magnifications as in figure 2.23b and 2.23c revealed a healthy population of dimples of varying size and shape covering the transgranular fracture surface. Figure 2.23d shows a high magnification micrograph of the SEM revealing fine microscopic voids and shallow dimples covering a region of tensile overload[36].

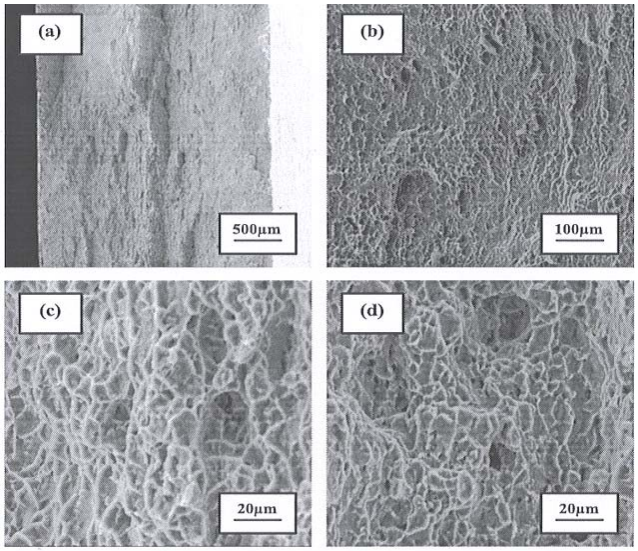

Figure 2.23: Scanning electron micrographs (longitudinal orientation) of titanium alloy showing (a) overall morphology, (b) high magnification of (a) showing the transgranular fracture region, (c) high magnification of (b) showing a healthy population of dimples covering the transgranular fracture surface and (d) fine microscopic voids and shallow dimples covering a region of tensile overload[36]

Figure 2.24a shows a rough overall morphology whilst 2.24b shows fine microscopic cracks surrounded by a healthy population of dimples and voids. At regular intervals deep-seated macroscopic cracks were evident on the fracture surface as depicted by figure 2.24c. A section of the overload region shown in 2.24d revealed a population of dimples of varying size and shape and fine microscopic voids. There were also isolated cracks in deep pockets, surrounded by dimples[36]. Transgranular surface regions revealing fine microscopic cracks surrounded by a population of microscopic voids and dimples are reminiscent of locally brittle and ductile failure mechanisms. Dimples of varying size coupled with fatigue striations are associated with ductile fracture of specimens.

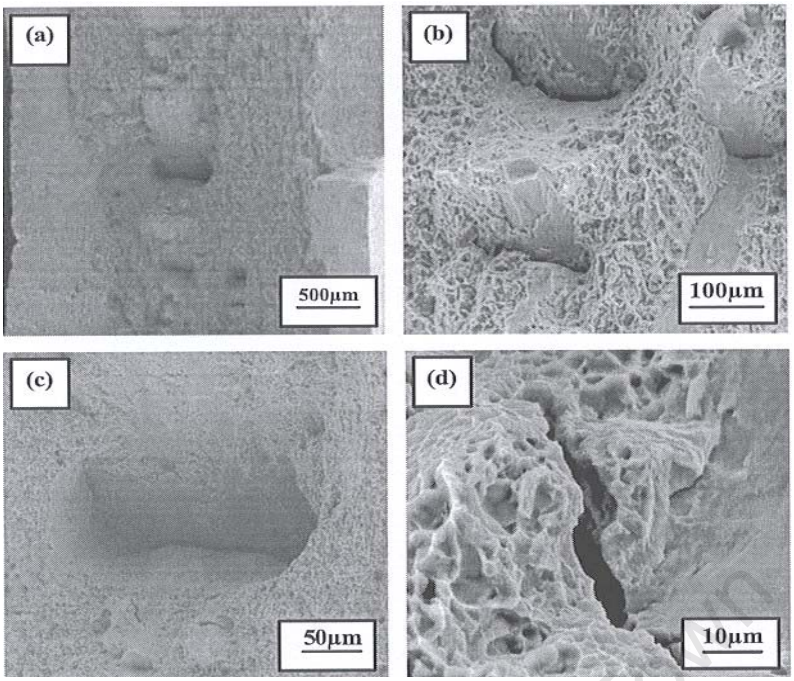

Figure 2.24: Scanning electron micrographs (transverse orientation) of titanium alloy showing (a) overall morphology, (b) high magnification of (a) showing an array of microscopic cracks, (c) macroscopic cracks surrounded by a healthy population of dimples and voids and (d) macroscopic crack surrounded by voids and dimples[36]

3. EXPERIMENTAL DETAILS

This chapter details the experimental methods and testing used in accordance to the laid out plan of development. The procedure was carried out in a sequential process in order to determine the fatigue performance and supporting experimental data of the surface treated titanium alloy.

3.1. MATERIAL USED

The alloy used for testing is the Ti-6Al-4V as per project proposal supplied by Goodfellow, Cambridge Limited, Huntington. In its as received state it was cylindrical bar stock with 12.7 mm diameter. Ti-6Al-4V has wide usage in the aerospace industry and artificial biomedical implants and this justifies why experiments are being carried out to determine its fatigue endurance. The chemical composition of the alloy is shown in table 3.1.

Table 3.1: Chemical Composition of Ti-6Al-4V alloy

Element	Content (weight %)
Carbon	< 0.08
Iron	< 0.25
Nitrogen	< 0.05
Oxygen	< 0.2
Aluminum	5.5 – 6.76
Vanadium	3.5 – 4.5
Hydrogen	< 0.0375
Titanium	Balance

3.2. FATIGUE TESTING

The fatigue performance testing follows after the specimens are heat treated. A single phase rotating bending machine modified and used by Rambocus *et al.* is used for the fatigue tests. The machine consists of components of the rotational bending machine illustrated in figure 3.1a.

It should be noted that the motor does not switch on unless a minimum force of 50N is provided. This is designed for a safety reason, whereby if the specimen happens to break during testing the motor will switch off automatically.

With the specimen intact as shown in figure 3.1a, the machine was switched on and the bending force applied. Rotational bending due to the force applied and transferred through the hydraulic cylinder and motor is experienced by the specimen until fatigue failure is encountered. The point of failure is marked as the point of interest in figure 3.1a or facture point in the schematic layout in figure 3.1b and that is the point that experiences the largest bending moment in the test. The number of cycles to cracking will then be recorded using the revolution counter.

3.2.1. Bending Stress Theory and Application

The formula for bending stress in a beam when the load is applied uni-axially is used to determine the specimen dimensions and force limit on the specimens during the fatigue testing using the rotational bending machine shown in figure 3.1a. Section 2.4.1 in chapter 2 reflects on different machinery available for different types of test pieces. The cantilever rotating bending machine was readily available and with minimum modifications it sufficed. This ensured a cut in costs and the use of rods for testing was enabled due to the operation of the machine. The rod lengths along with the fatigue limits reviewed and co-relationships with the formulae helped the application process. From the previous chapter it was concluded by Dong and Li[1] that a fatigue limit of approximately 500 MPa applied from a bending force is obtained. With knowledge of the force limit of the machine and the test specimen dimensions, design calculations of the second moment of area (I), bending moment (M), stress concentration factor (K_t) and maximum bending stress (σ) were made using the following equations;

$$I = \frac{\pi d^4}{64}$$

$$M = Force \times L$$

$$\sigma = K_t \times \frac{\left(M \times \frac{d}{2}\right)}{I}, \text{ where } K_t = 1.3 \text{ as obtained from Juvinall and Marshek[42].}$$

The tests can be carried out with a range of bending stresses selected from approximately 380 MPa to 970 MPa to ensure that the specimens do get fatigued in the low cycle fatigue region. The 970 MPa stress was chosen after considering the ultimate tensile strength of Ti-6Al-4V alloy which falls in that range.

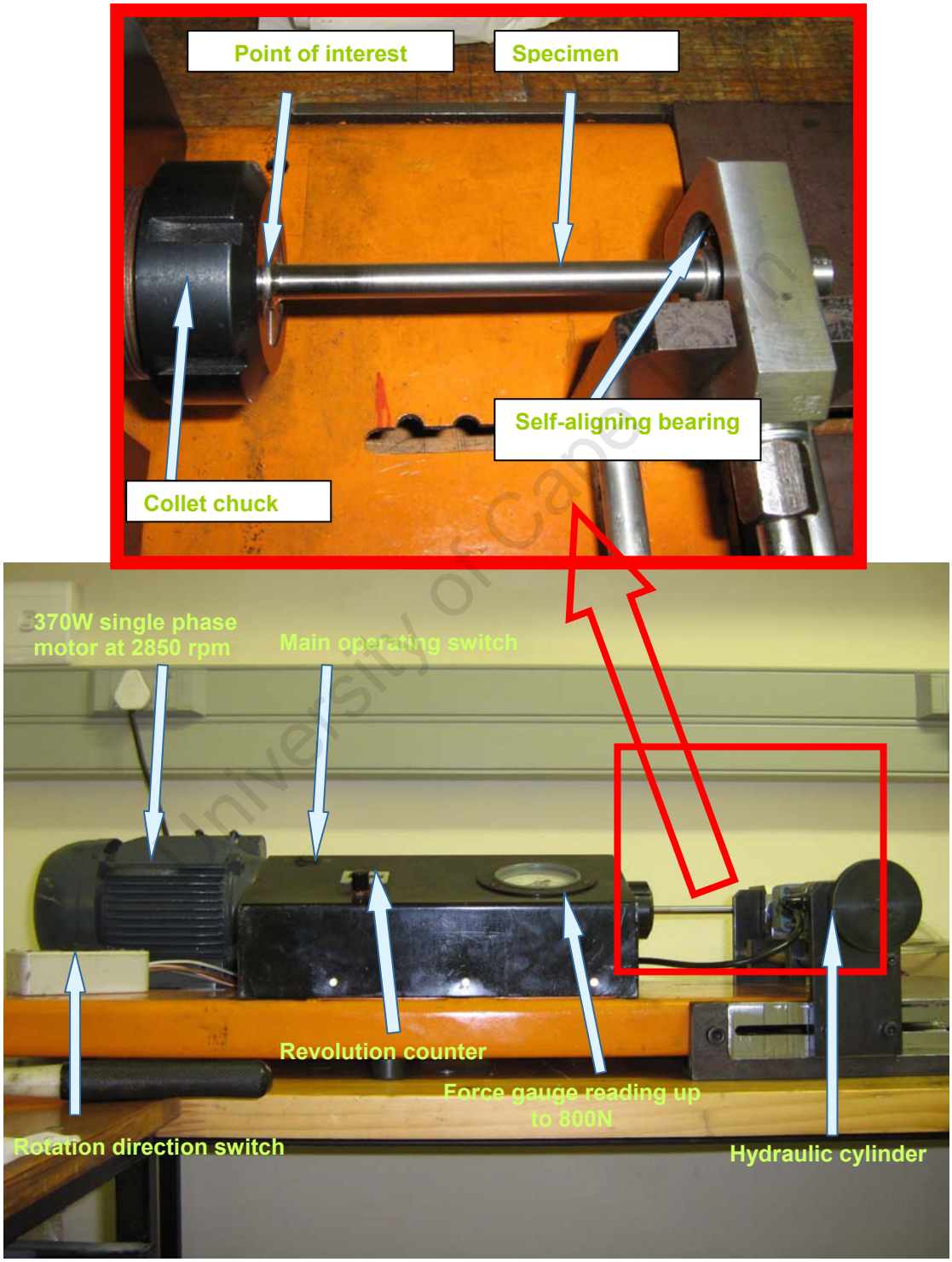

Figure 3.1a: Rotational Bending machine

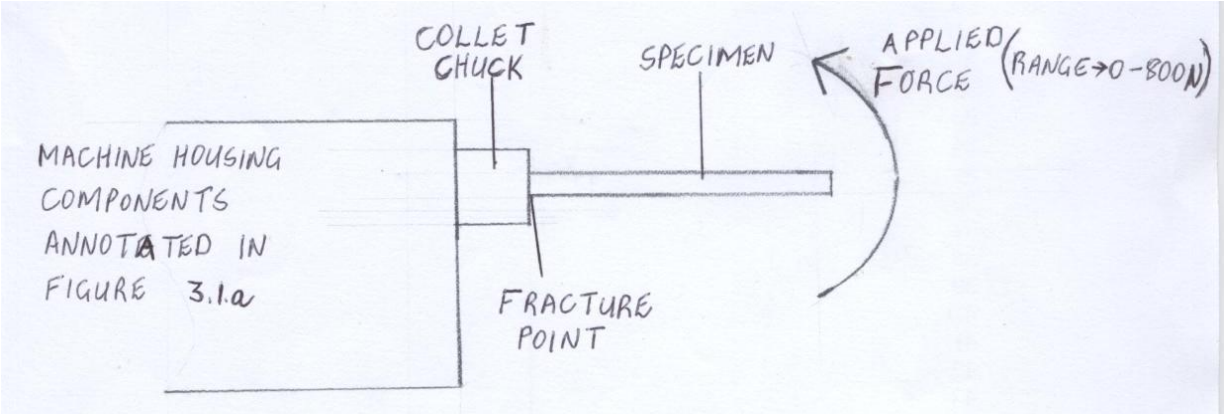

Figure 3.1b: Schematic Layout of the Rotational Bending machine

3.2.2. Specimen Dimensions

In order to facilitate justifiable results in this research the cylindrical bar stock was dimensioned and prepared using a particular criterion. Due to cost, the dimensions of the material had to be reasonably analysed and selected, taking note of the rotational bending machine in which they were going to be inserted for fatigue testing. A 'ballpark' figure for the length (L) of the section of the specimen which is to be tested was selected as 75 mm. This was after taking into account the literature review of the length of cylindrical specimens used in fatigue crack initiation testing. Calculations made to determine this length were also dependent on the bending stress formula, design calculations related to the mechanical properties of the Ti-6Al-4V alloy and the rotational bending machine specifications. A cross sectional drawing of the specimen dimensions is shown in figure 3.2. The diameter (d) of this section was hence calculated to be 8 mm and it is illustrated in figure 3.2. The machine has a chuck collet and part of this specimen is gripped in this collet. The diameter (D) of the gripped section is 12.7 mm. The diameter was a standard value from the material suppliers and hence it was used as is so as to minimise the wastage of the metal. It then tapered down at the beginning of the critical section of the specimen with a fillet radius (r) of 2 mm, thereby creating a stress concentration into the 8 mm section.

Machining of the alloy in accordance with the drawing was done so as to produce well over 30 specimens of the above mentioned dimensions.

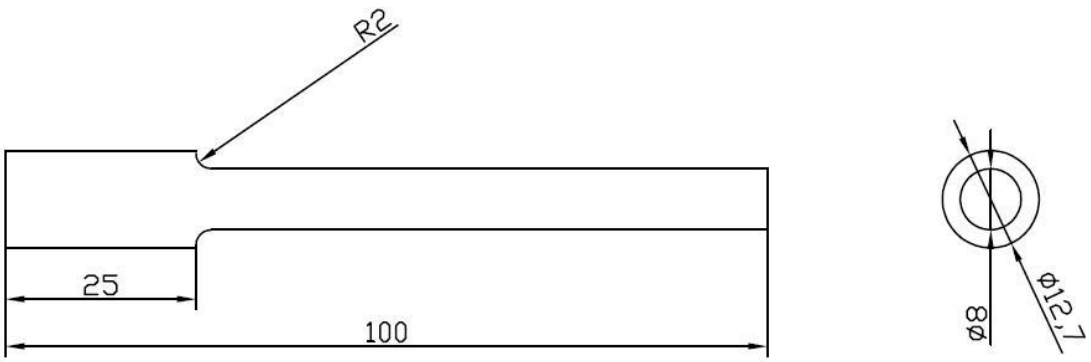

Figure 3.2: Cross-sectional drawing of specimen making out the dimensions

3.2.3. Polishing Technique

The machined specimens were polished after machining with the aim of obtaining a similar surface roughness for the components before they were exposed to the different heat treatments that needed comparison. Silicon carbide paper in 5 different grit sizes were used in ascending order to obtain a shiny and much smoother surface for the surface treatment. A 200, 400, 600, 800 and 1200 grit pad is used for each sample polish.

Due to the difficulty in polishing the region of interest where the fillet is located (marked as R2 in figure 3.2), a buffer is used to ensure that the region is smooth and ready for treatment and fatigue testing.

3.3. HEAT TREATMENTS

The test specimens were then subjected to heat treatment processes in order to diffuse oxygen in them. As highlighted in section 1.1 there are 2 steps taken in the oxygen diffusion hardening. Firstly, oxidation takes place in the air at elevated temperatures and secondly the diffusion treatment is carried out in a furnace that has either a vacuum or an argon environment. There are processes that excluded one of the 2 steps. It should be noted that all the oxidation treatments took place for 30 minutes in air inside the oxidation furnace. The diffusion step took place at 850 ºC for 20 hours in a controlled atmosphere furnace. The furnace may either have a vacuum atmosphere or an argon atmosphere. Of all the possible temperatures and

environments the following processes were selected in order to ascertain the most desirable one as well as analyse which are the contributing factors to the fatigue and hardness behaviour. The processes are detailed in table 3.2 and are also summarised in figures 3.3-3.7.

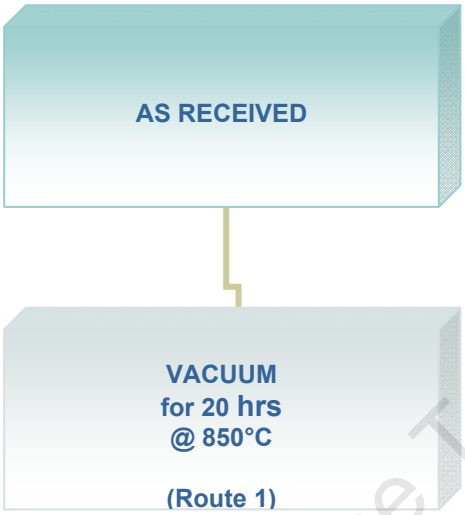

Figure 3.3: Chart showing steps taken in Route 1 of heat treatments

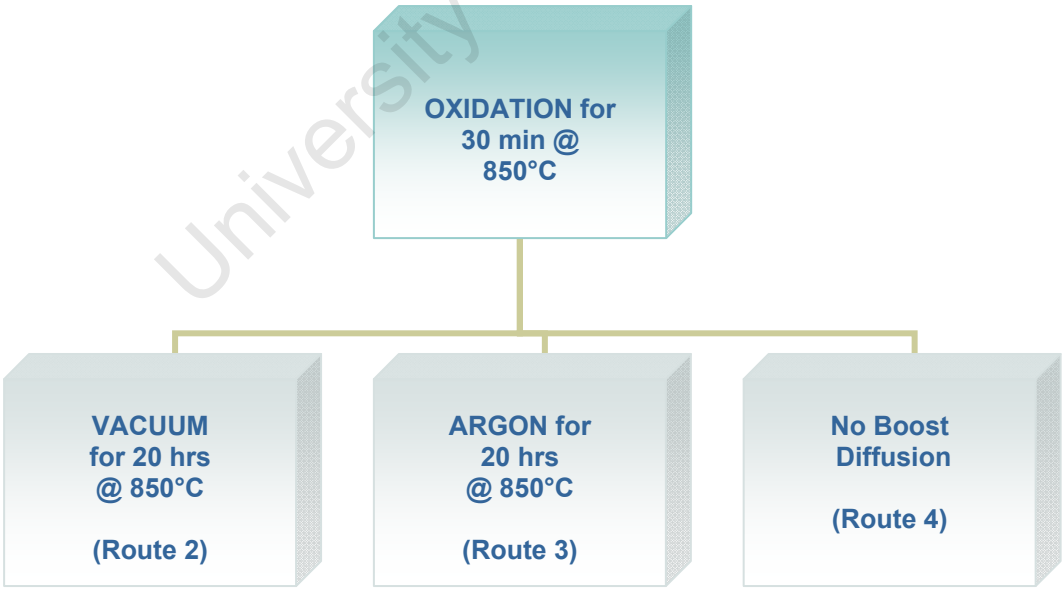

Figure 3.4: Chart showing steps taken in Routes 3, 4 and 5 of heat treatments

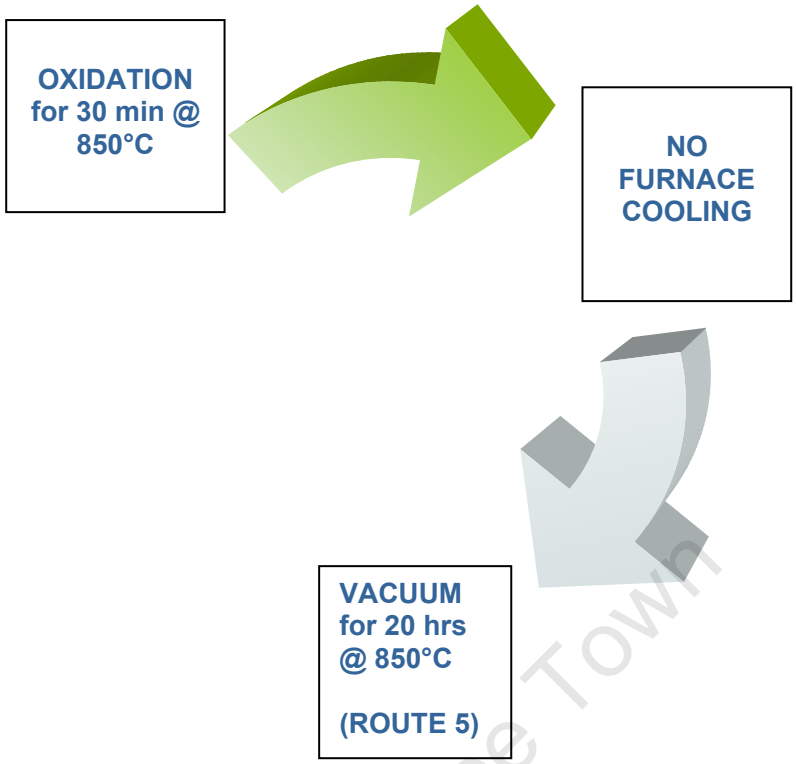

Figure 3.5: Chart showing steps taken in Route 5 of heat treatments

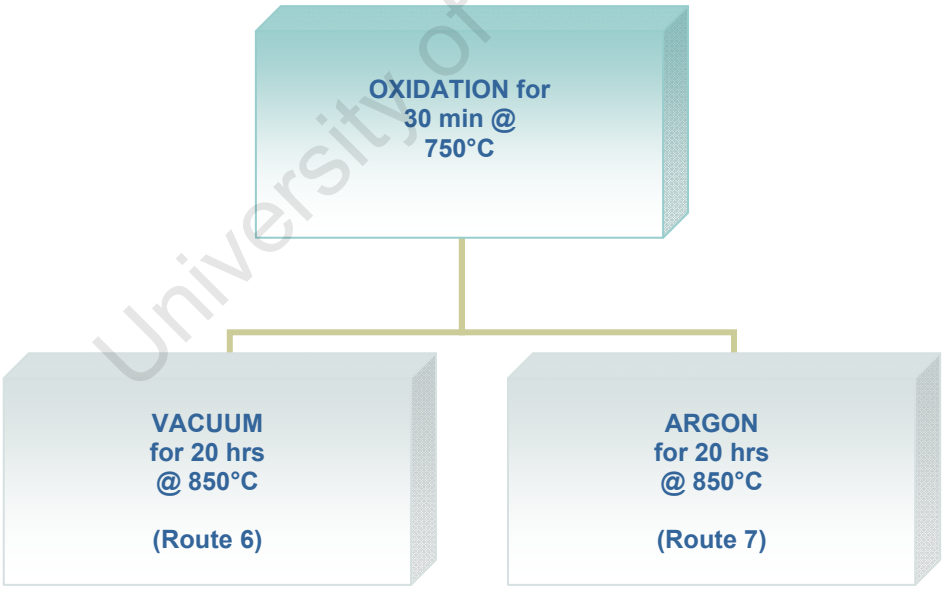

Figure 3.6: Chart showing steps taken in Routes 6 and 7 of heat treatments

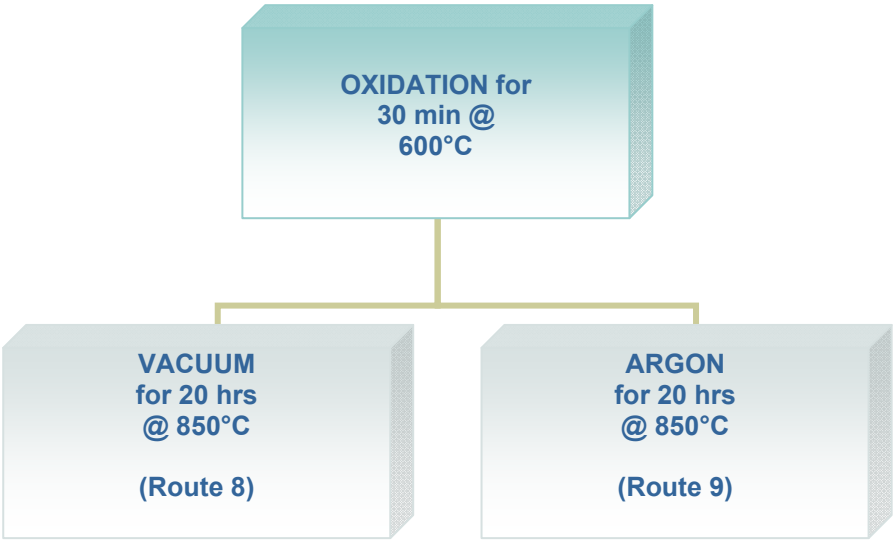

Figure 3.7: Chart showing steps taken in Route 8 and 9 of heat treatments

An extra route which involves no heat treatment of the specimen was used as the yardstick for comparison of the effectiveness of the OBDH was undertaken. The controlled atmosphere furnace in which the diffusion step of the OBDH takes place is shown in figure 3.8a. The schematic layout of the furnace is shown in figure 3.8b and components within the furnace and the means of heating are depicted.

Figure 3.8a: Controlled atmosphere furnace set-up

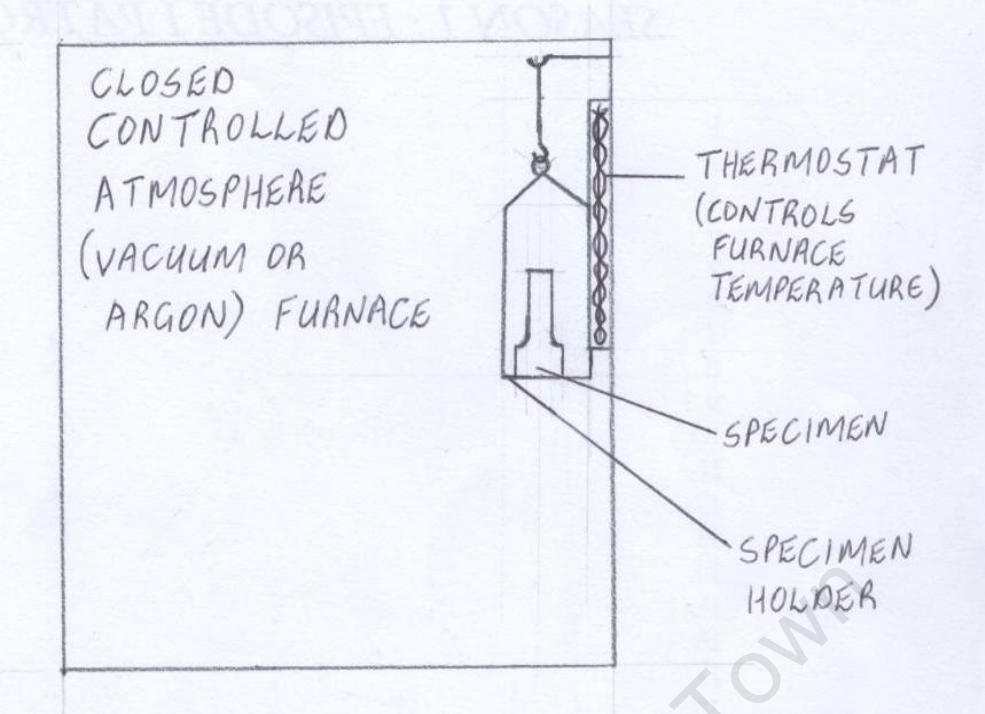

Figure 3.8b: Schematic Layout of the Controlled atmosphere furnace set-up

On completion of the various OBDH treatments the specimens were not further polished. This was due to the fact that polishing the layer would effectively remove the layer that has formed on the surface thereby rendering the OBDH treatment unreliable with regards to the study objectives.

Table 3.2: Process identifications in relation to heat treatment steps performed

Route	Process Identification	Process Description
1	850Va	Furnace treatment straight from the as received state at 850ºC for 20 hours under vacuum at about $1x10^{-4}$ torr and furnace cooling to room temperature afterwards.
2	Ox850/850Va	Oxidation at 850ºC and furnace cooled to room temperature. Diffusion treatment under vacuum follows at about $1x10^{-4}$ torr at 850ºC for 20 hours and thereafter furnace cooling to room temperature.

3	Ox850/850Ar	Oxidation at 850ºC and furnace cooled to room temperature. Diffusion treatment carried out in an argon environment. Vacuum is pumped until a pressure of about $1x10^{-4}$ Pa is reached for the furnace. Argon is purged into the furnace at room temperature until the pressure gauge reads 620 torr. As the furnace heats up argon will expand until 760 torr at 850ºC. Diffusion treatment is carried out at 850ºC for 20 hours after which furnace cooling takes place until room temperature.
4	Ox850	Oxidation at 850ºC and furnace cooled to room temperature.
5	Ox850NFC850Va	Involves the same process as in route 2 but there is no furnace cooling (NFC) in between the oxidation and diffusion, that is, straight after 30 minutes of oxidation the specimen is diffusion treated in vacuum at 850ºC for 20 hours. Furnace cooling to room temperature takes place afterwards.
6	Ox750/850Va	Oxidation at 750ºC and furnace cooled to room temperature. Diffusion treatment under vacuum follows at about $1x10^{-4}$ torr at 850ºC for 20 hours and furnace cooling to room temperature follows.
7	Ox750/850Ar	Oxidation at 750ºC and furnace cooled to room temperature. Diffusion is carried out in an argon environment. Vacuum is pumped until a pressure of about $1x10^{-4}$ Pa is reached for the furnace. Argon is purged into the furnace at room temperature until the pressure gauge reads 620 torr. As the furnace heats up argon will expand until 760 torr at 850ºC. Diffusion treatment is carried out at 850ºC for 20 hours after which furnace cooling takes place until room temperature.
8	Ox600/850Va	Oxidation at 600ºC and furnace-cooled to room temperature. Diffusion treatment under vacuum follows at about $1x10^{-4}$ torr at 850ºC for 20 hours after which furnace cooling to room temperature occurs.
9	Ox600/850Ar	Oxidation at 600ºC and furnace-cooled to room temperature. Diffusion is carried out in an argon environment. Vacuum will be pumped until a pressure of about $1x10^{-4}$ torr is reached for the

		furnace. Argon is purged into the furnace at room temperature until the pressure gauge reads 620 torr. As the furnace heats up argon will expand until 760 torr at 850ºC. Diffusion treatment is carried out at 850ºC for 20 hours after which furnace cooling takes place until room temperature.

3.4. HARDNESS AND METALLOGRAPHY

The specimens are loaded till they have fractured due to the fatigue induced by the rotational bending machine, metallographic analysis and hardness experimental work is carried out. Initially they are cut into small cylindrical cross-sections with a length of about 5 mm.

3.4.1. Hardness Measurement

Specimens undergoing all the different processes selected for heat treatment were initially cut using the precision cutter and were mounted into a resin.

The next step involved the grinding and polishing stage and it is summarised in table 3.3.

Table 3.3: Grinding and Polishing Method for the Specimens

Grinding		**Polishing**	
Stage 1	The specimen is ground using 500 grit pad with water as lubricant for 2 minutes with an applied force of 30N at a speed of 300rpm.	Stage 1	The specimen is polished using dur-pad for 10 minutes with an applied force of 30N at 150rpm. At regular intervals 9 µm diamond suspension is poured on the pad.
		Stage 2	An "attack" solution made up of 50 ml colloidal silica suspension and 10 ml hydrogen peroxide is prepared. The specimen is

			polished using a chem-pad for 10 minutes with a 30N applied force at a speed of 150rpm. Again, at regular intervals the "attack" solution is poured onto the pad.

Following the polishing process, hardness measurements were performed using the Zwick Microhardness Tester. The hardness was measured from the surface towards the centre of the specimen. For each selected distance from the surface, eight hardness readings were made. In the hardened zone illustrated in figure 3.9a, the distances selected were 15, 30, 60, 100, 130, 160, 200, 250, 300 and 350 μm from the specimen edge. For the bulk of the material tests were carried out at 400, 1000, 1500, 2000, 2500, 3000, 3500 and 4000 μm as measured from the outer circumference of the specimen cross section and this zone is illustrated in figure 3.9b. Figure 3.9 shows the hardened layer and bulk layer zones from which microhardness testing was done on the specimen cross-section.

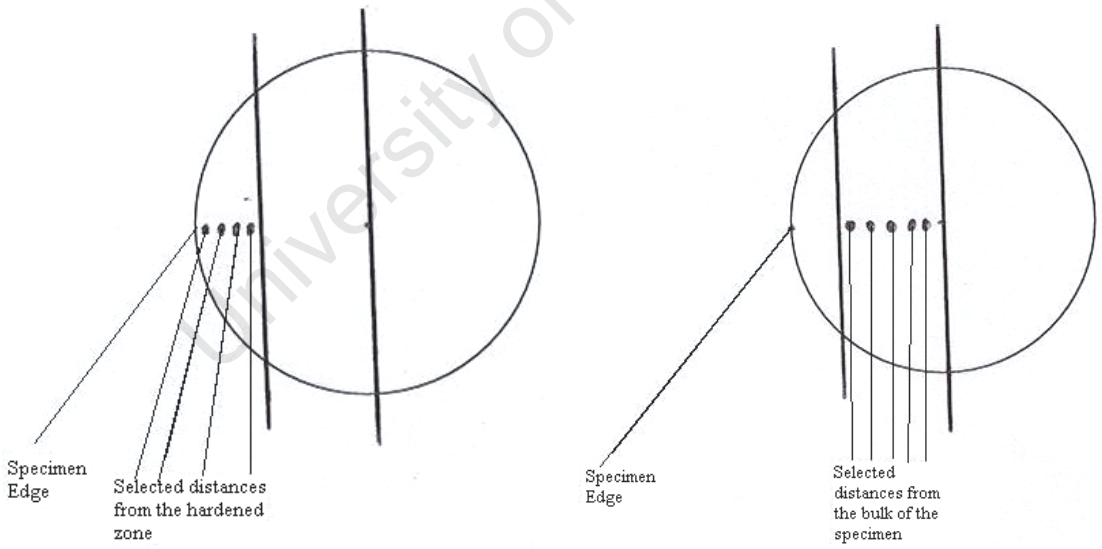

(a) **(b)**

Figure 3.9: Schematic diagram of the cross-section of the specimen illustrating the points where hardness tests were done in the (a) hardened zone and (b) bulk of the material

3.4.2. Metallographic Studies

In order to examine the different microstructures from the specimens under the light microscope etching had to take place first after polishing. The etchant was a solution of 10 ml hydrogen fluoride, 30 ml nitric acid and 50 ml of water. The samples were then dipped into the solution for 15-20 seconds and that completed the etching.

The microstructures were examined using an Inverted Light Microscope in the bright field mode.

3.4.3. Grain Size Measurement

Grain size measurement was performed using micrographs obtained from the light microscope. The Lineal Intercept Method was used for measuring grain sizes from the surface of the specimen right up to the centre. Four counts were made for each and every microstructure obtained and the data was then captured for graphical representation. The cross-sectional planar micrographs are used in the capturing of the grain size data. This is because right through the length of the specimens the grains are equi-axed.

The method involved the following steps;

1. Obtain a conversion factor by dividing the micron marker value on the microstructure by the number of millimetres it represents.
2. Counting the number of grains intercepted by four straight lines that cut across the microstructure obtained as illustrated in figure 3.10. The numbers on the figure indicate the grains.
3. Recording the length in millimetres of the straight lines that cut across the microstructures.
4. The grain sizes in millimetres are then calculated by dividing the length of the straight lines by the number of intercepts.
5. The grain size in microns is then obtained by changing the millimetre value to the micron value using the conversion factor mentioned earlier.
6. Since four straight lines were used on each micrograph an average value of grain size is then obtained.

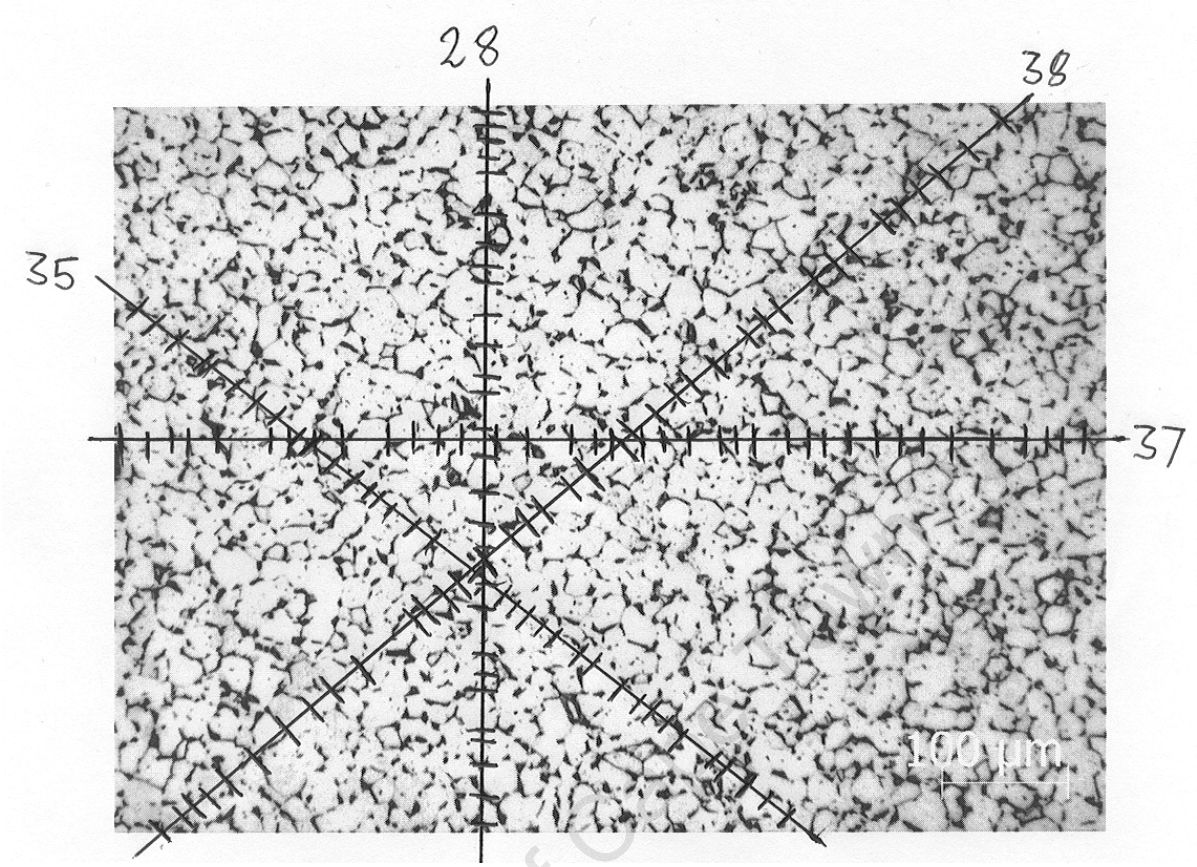

Figure 3.10: Micrograph showing the microstructure of Ti-6Al-4V alloy with lines and markings used to determine grain size

3.4.4. Fractography

Three specimens for selected treatment process are observed under a scanning electron microscope. The chosen processes were the as received specimen and the ones that underwent processes Ox850/850Va and Ox850/850Ar. Gold palladium application on the fracture surface was carried out in order to prevent charging of the electrons. The settings used on the microscope enabled the secondary detector to operate and pick up secondary electrons which give a picture based on topography (valleys, hills and ridges) of the fracture surface of the specimen. This occurs after the electron beam hits the specimen. The filament current helps in achieving the best possible resolution for the fractographs needed and it was kept at a constant. Fractographs were obtained in such a way that the cross-sectional face of the fractured specimen was captured from end to end in sequence. Figure 3.11 shows two fractographs of adjacent portions of the fracture, as pictures are captured across the

cross section. These fractographs enabled the measurement of the crack initiation region, the crack size and the fast fracture region. Added to that, the fracture surface is also analysed in order for a possible mode of failure to be concluded.

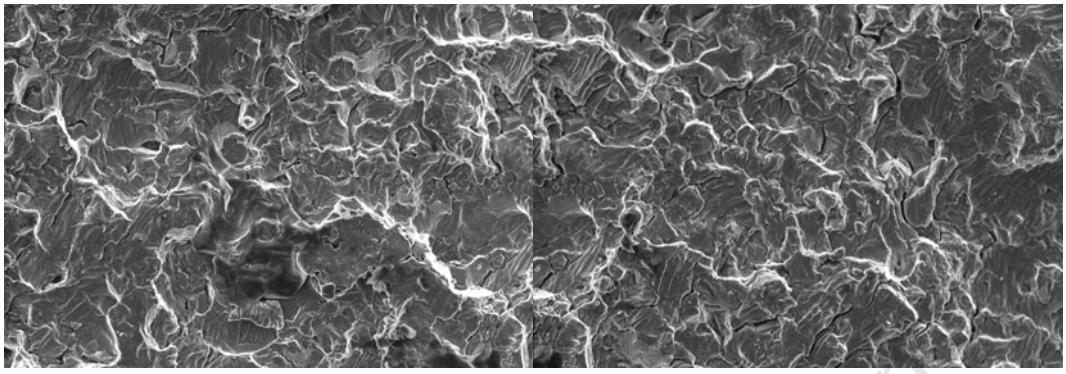

Figure 3.11: Adjacent fractographs of the fractured Ti-6Al-4V specimen used to analyse the fracture

3.5. DIFFICULTIES AND SOLUTIONS

There was an experimental complication that was encountered in conducting this research and this sub-section will cover it. The difficulty and solution was experienced in the crack detection under fatigue loading of the specimen.

The initiation of the cracks on the specimens as the rotational bending machine was in use was supposed to be detected. A die penetrant set was used in conjunction with a light microscope for crack detection. Crack detector is sprayed on the specimen at the point of interest shown in figure 3.1 and when a crack appears the liquid sprayed should flow in the direction of the crack. The difficulty was due to the fact that the machine had to be run and stopped and thereafter the detector is sprayed. When there is no crack detection the spray is cleaned of and the machine run again. With this stop and start procedure of the machine there is a point at which the crack will initiate and due to the machines rotational speed, identifying this stage is difficult. The proof that a crack was obtained was when the crack detector was sprayed and it flowed in the direction of the crack. Therefore, at some point during the starting and stopping of the machine there would have been crack initiation but the exact number of cycles can not be ascertained. Moreover soon after the crack, the specimens break in some instances and this also makes it more difficult. The above reasons would render the crack

initiation experiments unreliable so it was proposed that loading the specimens to failure be adopted.

4. RESULTS AND DISCUSSIONS

INTRODUCTION

This chapter covers the results and discussion of various techniques that were applied during the experimental stages of the investigation of the fatigue behaviour of the surface treated Ti-6Al-4V alloy. Firstly, the characterisation of the surface hardening and the microstructural analysis of the different heat treatment processes are discussed. The microstructural analysis will also encompass the grain size measurement. Having grasped the first stage, a presentation of the stress-life curves of selected treatments will take place in order to understand the life span variations of the treatments. Thereafter, a study and analysis on the influence of different treatments on failure at a fixed stress will take place. Lastly, the fracture analysis is presented to sum up the investigation of the fatigue behaviour of the alloy paying attention to the main processes of treatment.

4.1. SURFACE HARDENING

Microhardness measurements and profiles were carried out as explained in the previous chapter. The specimens that underwent different heat treatment processes were sliced on the 75mm long test section shown in figure 3.1 into approximately 5mm long slices maintaining their cylindrical cross-section. The metal surface is supposed to be hardened by the treatment process and therefore characterisation of its hardness profile is important. Equally important is the characterisation of the hardness of the bulk of the metal as it makes it easier to conclude the hardness effect on the depth of the material from the metal surface. If the difference of the microhardness profiles are quantified and analysed from surface into the bulk material it would possibly be able to give an explanation of the fatigue performance of the treated specimens.

4.1.1. Microhardness Profile Transition in the Hardened and Bulk Layers

The hardness profile changes from higher magnitudes at depths that are closer to the metal surface, to lower magnitudes at the bulk of the specimen as shown in figure 4.1. This behaviour concurs with work done in the previous research done by Camagu[11]. Microhardness measurements towards the edge of the specimen showed a marked increase for 850Va where the specimen went through the simulated diffusion step at 850°C in a vacuum environment and Ox850 which involved oxidation at 850°C only. The as received specimen has relatively uniform values throughout. As expected the treatments have an effect on the hardness of the specimens. In the case of the 850Va the simulated diffusion step occurs at a high temperature and long duration that is sufficient to induce a hardened case which is skin deep in comparison to the full OBDH treated specimens. The Ox850 process displays a higher hardness profile than the 850Va which shows that the oxidation temperature has more effect on hardness than the oxygen diffusion cycle duration. This characterisation of the transition of hardness profile from higher to lower values from the surface to the bulk was carried out in order to cement the previous work done as well as for reproducibility purposes so that the present study is assured of following the right course.

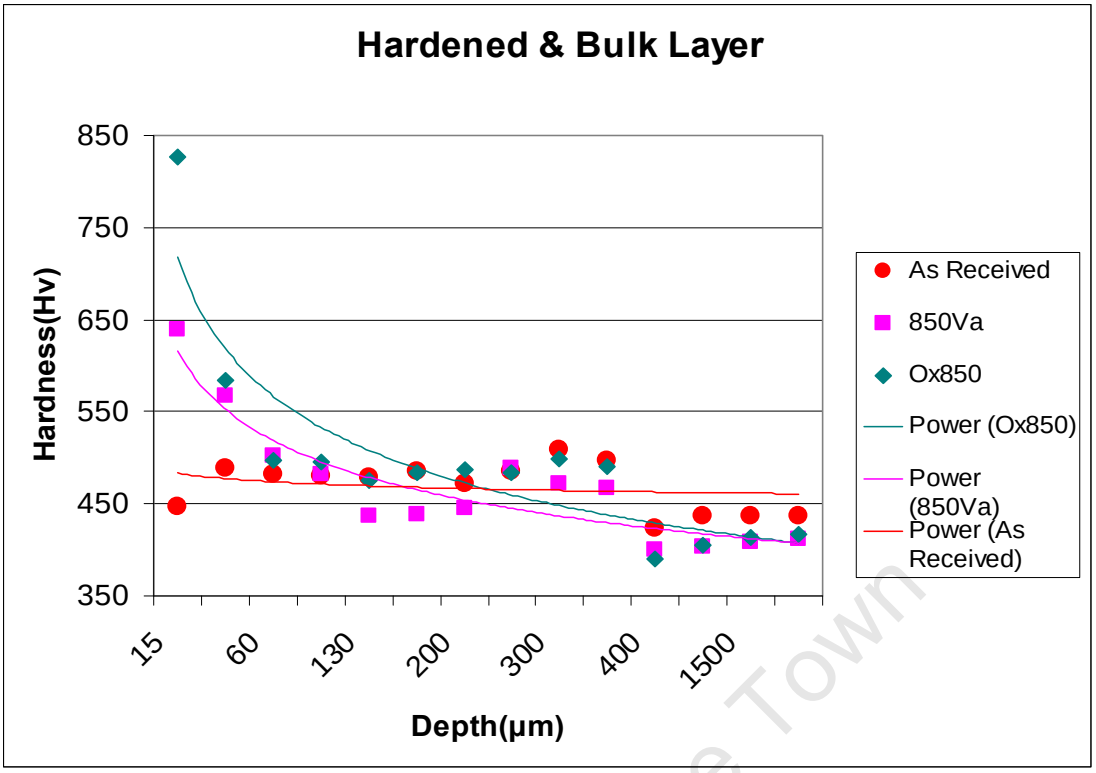

Figure 4.1: Microhardness data for Ti-6Al-4V alloy in the hardened layer and bulk of the material for the as-received specimen and the specimens undergoing 850Va and Ox850

4.1.1.1. Microhardness of the Hardened Layer

Microhardness profiles of selected processes are shown in figure 4.2. The values of the hardness show steady values from a depth of approximately 400µm to the centre of the specimen. At a depth less than 350µm the values increase differentially depending on the treatment except that of the as received specimen. When ranked in decreasing order, the hardness of the specimens was as follows; Ox850NFC850Va, Ox750/850Va, Ox850/850Ar, Ox850/850Va, Ox850, 850Va and finally the as received. The specimen designated Ox850NFC850Va where there was no furnace-cooling between the two-step process had the most desirable hardening. This brings out the role boost diffusion plays on an oxidised specimen. All samples that went through the two steps of OBDH show higher hardness values than those that went through one step or no step. As indicated by Camagu[11] the conditions that are used to conduct these heat treatments in this research encourage more diffusion of oxygen into the Ti-6Al-4V alloy as more time and higher temperature are used.

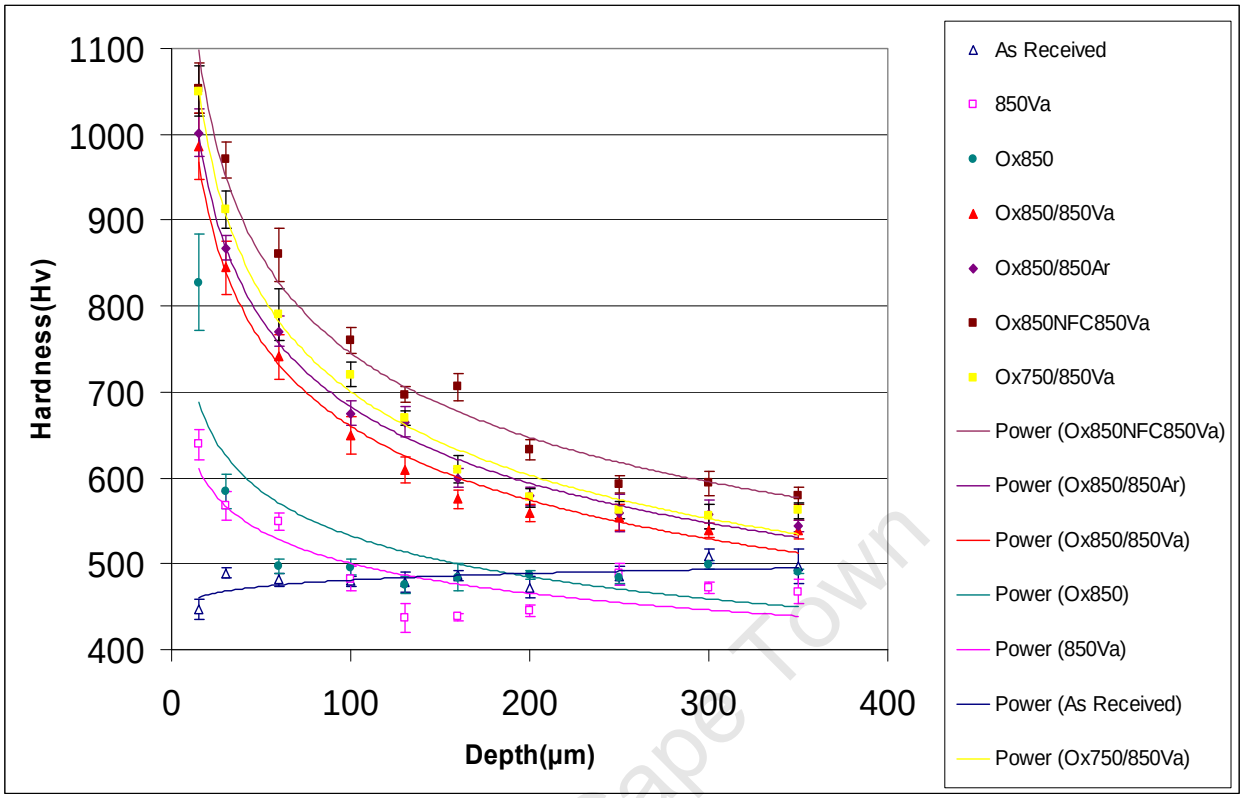

Figure 4.2: Microhardness profiles for Ti-6Al-4V alloy for the as-received specimen and the specimens that undergo selected processes

4.1.1.2. Microhardness of the Bulk Layer

The graph in figure 4.3 shows that the bulk of the material has a steady value of hardness ranging between 400 and 450 Hv for the as received and heat treated specimens. The processes picked were those that did not undergo the full OBDH process, which are the as received, 850Va and Ox850. The values also confirm that in the bulk of the material the hardness is relatively similar for all conditions.

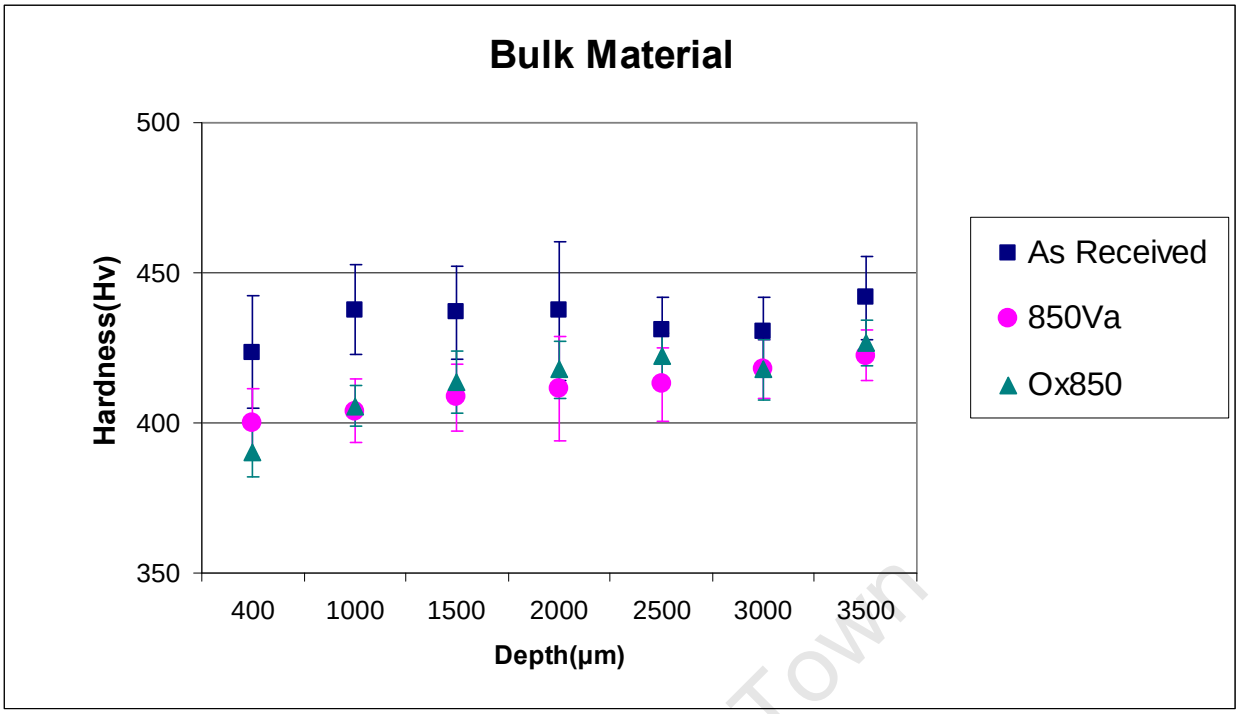

Figure 4.3: Microhardness data for Ti-6Al-4V alloy in the bulk of the material for the as-received specimen and the specimens undergoing 850Va and Ox850

4.1.2. Comparison of Selected Treatment Processes

The microhardness testing on the specimens was done on selected heat treatment processes. This was done in order to make comparison of OBDH treated, oxidised, diffusion-treated and as received specimen data. The selection therefore encompassed the different variables that can be incorporated regarding the treatment of the specimens.

4.1.2.1. Surface Hardening During Oxidation Only

Figures 4.2 and 4.4 show microhardness profiles for the process Ox850 where oxidation at 850°C is carried out is discussed in this section. In figure 4.2 the hardness profile lies third from bottom. The effect of not carrying out the diffusion step is shown. Had diffusion been carried out, the hardness values would have been raised to the values in the same domain as the profiles above Ox850 results. In figure 4.4 the Ox850 profile has higher hardness values than the 850Va (simulated diffusion process). This effect indicates that there is a thick oxide formation after the 850°C for

30 minutes oxidation step. The oxidation time of 30 minutes corresponds to the optimum values indicated in the study of Dong and Li[1]. With regards to surface hardening and this oxidation step, the attained results will be sufficient to yield desirable hardness values after the subsequent diffusion step.

4.1.2.2. Surface Hardening During Simulated Diffusion Step

The omission of the oxidation step was carried out in order to investigate the influence of undertaking the diffusion step without an oxygen-rich oxide layer obtained from the oxidation step on the hardness of the specimen. The effect of omitting the oxidation step in the OBDH process results in less hardening as compared to omitting the diffusion step as depicted by figure 4.4. As explained earlier the oxidation process creates an oxygen reservoir in a thick oxide layer for which the diffusion step can utilise. With no oxidation taking place the oxygen reservoir is non existent and therefore the "diffusion" occurs on an as received specimen, meaning that there is no medium for diffusion to increase the hardness of the specimen. The absence of the oxidation step exempts solid solution strengthening of the specimen that occurs due to the interstitial oxygen introduced during the oxidation step. Therefore, whether or not temperature is changed in the diffusion step, the presence of the pre-oxidised layer is extremely essential that the magnitude of the hardness will not be improved. The hardness values slightly rises just below the metal surface due the annealing effect on the alloy during the diffusion step which occurs at 850°C for a long duration.

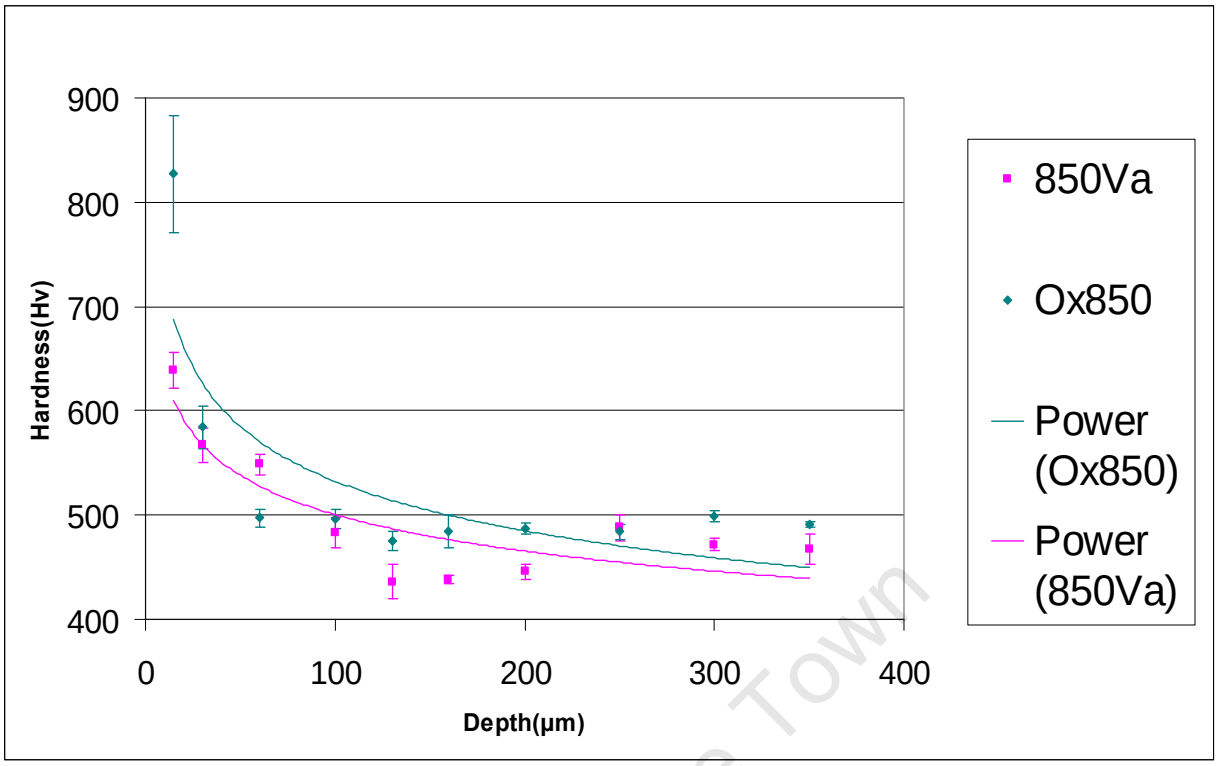

Figure 4.4: Microhardness profiles for Ti-6Al-4V alloy specimens that undergo 850Va and Ox850

4.1.2.3. Effect of Carrying Out Process Ox850NFC850Va as Opposed to Carrying Out Ox850/850Va on Surface Hardness

Carrying out the process Ox850NFC850Va exhibits the microhardness profile with the highest curve, which has the largest values as shown in figure 4.2. The titanium oxide or rutile that forms in the oxidation step experiences the diffusion step without cooling and this should accelerate diffusion as temperature is still high and there is no furnace cooling taking place. The specimen is not removed from the position it was during the switching of steps as the same furnace is used. Solid solution strengthening due to the interstitial oxygen occurs and this phenomenon is immediately transformed to diffusion cycle conditions which are the same temperature and this increases the effect of the depth and hardness of the boost diffusion layer. Therefore, when this transition occurs, the already thick oxygen-rich oxide layer with its oxygen reservoir obtains a thicker layer than the specimen undergoing process Ox850/850Va (both oxidation and diffusion steps are done at 850°C temperatures with furnace-cooling in between steps) when diffusion takes place. The cooling that takes place in the

specimen that goes through process Ox850/850Va results in the atoms and molecules inside that specimen being less active than the ones in the specimen going through Ox850NFC850Va. The diffusion is therefore less effective in the Ox850/850Va than Ox850NFC850Va specimen thereby resulting in a less thicker hardened zone. The extra thickness of the hardened zone of the Ox850NFC850Va contributes to the high hardness profile.

4.1.2.4. Effect of the Diffusion Step Environment on Surface Hardness

Figure 4.5 shows the microhardness profiles of the specimens that go through the OBDH process with the diffusion step environment being the only difference. The two profiles are fairly similar with that of process Ox850/850Ar with diffusion occurring in an argon environment having slightly higher values. This phenomenon can be explored by investigating the effect of argon on the titanium oxide whilst in the vacuum at high temperatures such as the 850°C used. It is known that the oxygen diffusion hardening process depends on three parameters namely solute dissolved in the titanium, the temperature at which the diffusion process is carried out and the partial pressure of the oxygen in the system[11]. The temperature used for both environments is the same and the same alloy is used throughout the different heat treatment processes. An analysis using the ideal gas equation which states that;

$$PV = nRT$$

where P is the pressure of the system, V is the volume within the system, n is the number of moles of the gases in the system, R is the gas constant and T is the absolute temperature of the system. In both the argon and vacuum environments the temperature, gas constant and volume are the same therefore the pressure is directly proportional to the number of moles of gases in the systems. Therefore, for the argon environment system there is an increase in the total pressure due to the addition of argon into the furnace. There is no difference in the partial pressures of the oxygen for both environments system and hence there is no difference in the amount of oxygen in the different environments[11].

It should be noted that argon does not form compounds with the titanium alloy specimens and this is due to the fact that argon is inert. The interaction of argon with titanium surfaces at high temperatures could be a possible reason for higher hardness values than in vacuum environments. These high temperatures can facilitate oxygen diffusion and speed it up resulting in the slightly higher hardness values. Furthermore, in the argon atmosphere, the argon could 'unpack' the titanium specimen surface creating a passage for the oxygen to diffuse into the titanium matrix. This process is often referred to as the exchange reaction.

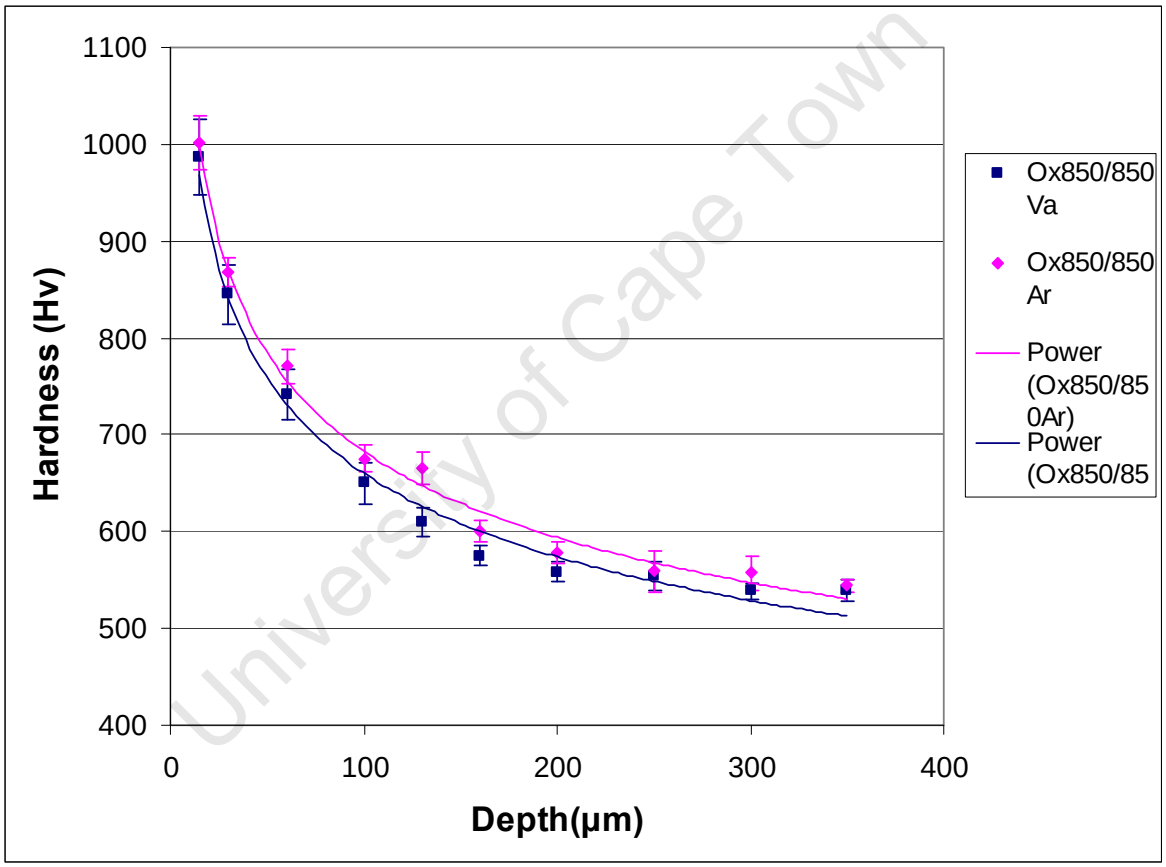

Figure 4.5: Microhardness profiles for Ti-6Al-4V alloy specimens that undergo Ox850/850Va and Ox850/850Ar showing the effect of the diffusion step environment

4.2. MICROSTRUCTURAL AND GRAIN SIZE ANALYSIS

Optical micrographs of the Ti-6Al-4V alloy were captured in order to understand the effect of the heat treatments on the underlying microstructure of the alloy as well as to suggest the relation of this microstructure to fatigue performance of the alloy. The micrographs were captured at 20 x objective lens magnifications.

The microstructural analysis (including the grain size effect) was investigated. The grain sizes were measured from the surface of the specimen to a depth of 3500μm. The relationship of the measured grain sizes and the fatigue response may help understand the fatigue behaviour of the different heat treatment routes used on this alloy.

4.2.1. Effect of the Heat Treatment Processes on the Microstructure

In chapter 2 it was mentioned that the microstructure of the Ti-6Al-4V alloy consists of a combination α-β grain structure. The stabilisers of both the α and β phase are aluminium and vanadium respectively. The density of the phases should change with respect to the different heat treatments the alloy undergoes. Five heat treatment processes were selected for the analysis of the microstructure in addition to the as-received condition. Furthermore the same processes were selected for the grain size analysis, save for the as received condition whose microstructure proved difficult to do grain measurement with the selected method.

The as received specimen has the microstructure shown in figure 4.6 which shows small grains of the HCP α (light) and BCC β (dark) phase. Grain structure in this specimen is dispersed with a dominance of the the light α phase.

The alloys that undergo heat treatment processes have a general sequence of microstructural change that they go through. Before the final microstructure, upon cooling, the alloy undergoes numerous metastable phase transformations during thermal treatment.

The difference in grain sizes of the samples that were selected were ranked in the following order from biggest grains to smallest; 850Va, Ox850NFC850Va, Ox850/850Va and Ox850/850Ar, Ox850 and finally the as-received sample. The graph in figure 4.7 shows the distribution and the as received sample is not shown as it had a very small dispersed grains shown in figure 4.6 which could not be measured using the Lineal Intercept Method. As expected the grain size in titanium alloys increases as heat treatment is applied on them due to grain growth relationship with elevating temperatures. The extent to which the grains differ in growth per treatment is to be analysed.

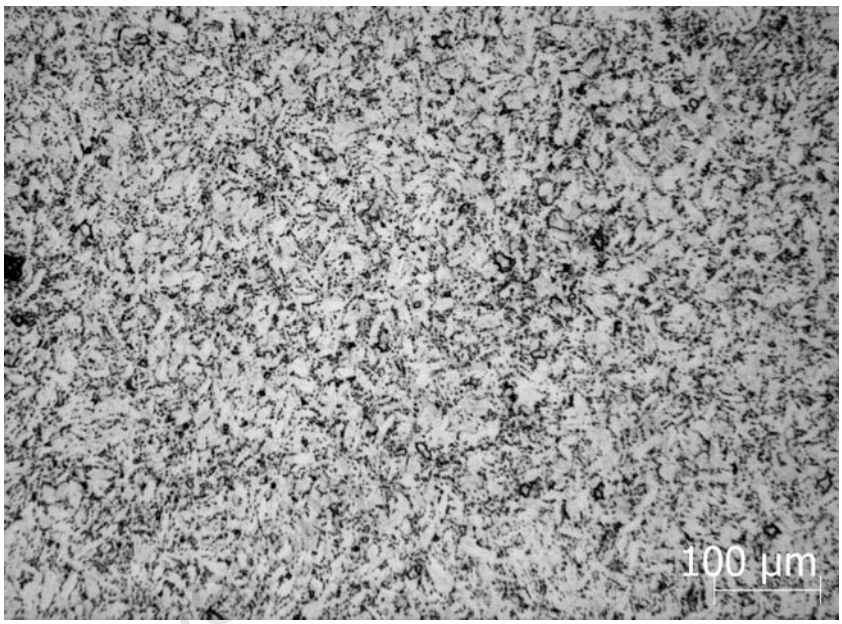

Figure 4.6: Optical micrograph outlining the underlying microstructure of the as received Ti-6Al-4V alloy

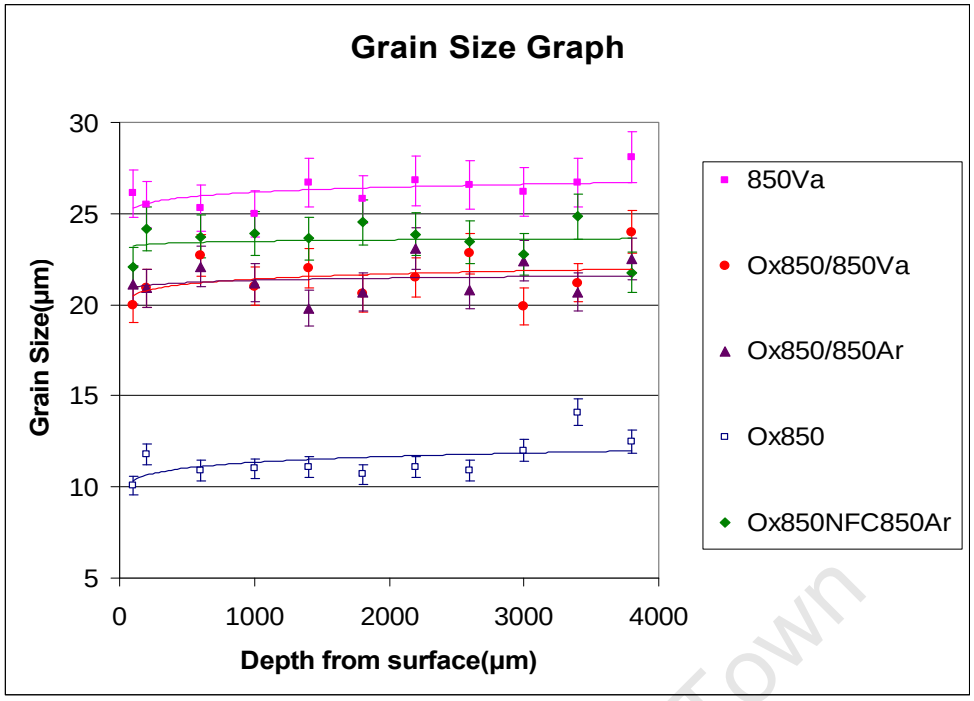

Figure 4.7: Graph showing the grain sizes of selected heat-treated specimens

4.2.1.1. Effect of Oxidation Step on the Microstructure

After going through the oxidation step only at 850°C the grain structure of the Ti-6Al-4V alloy appearance is shown in figure 4.8. There is evidence of the formation of an equi-axed grain structure in comparison with the dispersed grains shown in the as received specimen shown in the figure 4.6. The grains are still forming and hence their size is classified small as depicted by process Ox850 in the graph in figure 4.7. This formation and growth of grains is made possible by the heat treatment that takes place for 30 minutes. The short time experienced in this oxidation process results in less growth as compared to treatment processes that are done with the specimen exposed to the heat for a longer time. The growth in grain size results in a lower fatigue endurance as compared to the as received specimen. The larger the grain size the more the fatigue crack growth rate is increased. With the Ox850 specimen the grains did not grow to a large size as heat treatment was short and hence amongst the treated specimens it produced the best fatigue endurance.

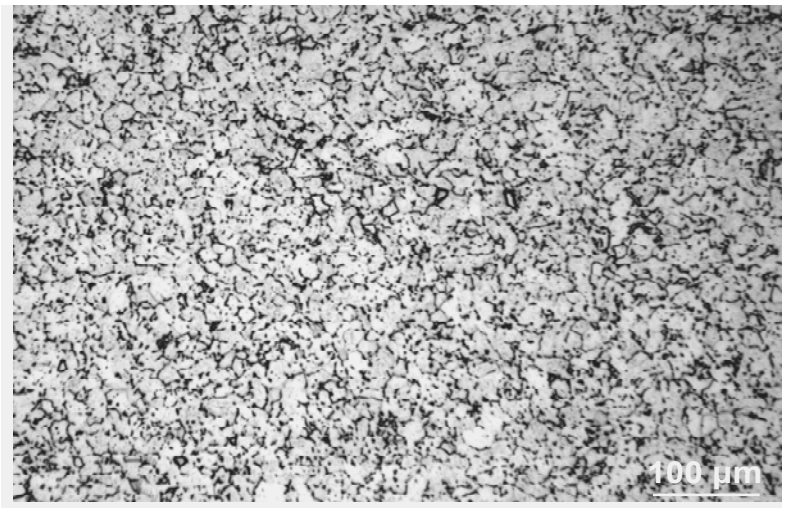

Figure 4.8: Optical micrograph showing the microstructure of the specimen that was treated using process Ox850

4.2.1.2. Effect of Simulated Diffusion Step on the Microstructure

The micrograph in figure 4.9 shows the microstructure of the specimen that did not go through the oxidation step of the OBDH process. It has large grains and this could be attributed to the time it was exposed to the vacuum furnace undergoing diffusion treatment. This process took 20 hours at a high temperature of 850°C and this may have accelerated grain growth. The dominance of the α phase is somewhat not conforming to the fact that the specimen did not go through the oxidation phase, where the oxygen in the oxide layer formed is usually diffused into the bulk of the specimen resulting in the volume fraction dominance of the α phase. This may then have been due to the fact that the titanium had some oxygen present on its surface as it is kept in free air and this small amount of oxygen may have diffused into the specimen during the diffusion step.

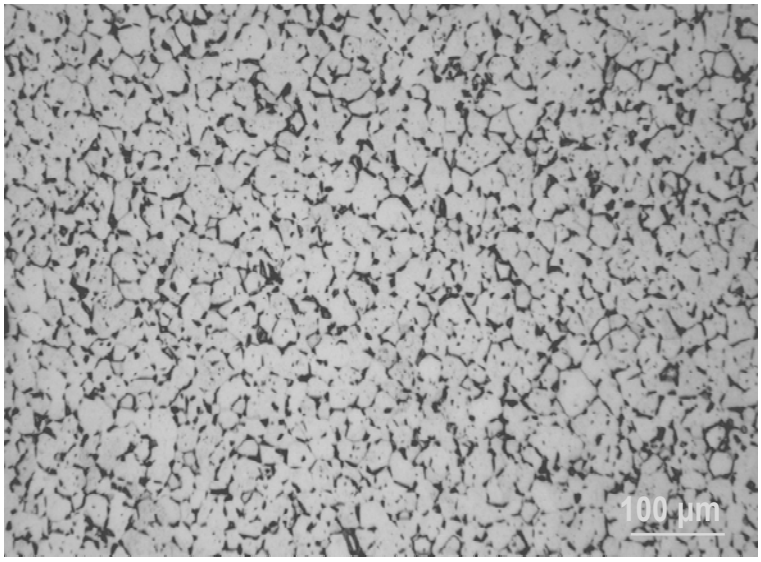

Figure 4.9: Optical micrograph showing the microstructure of the specimen that was treated using process 850Va

Grain size measurement of this sample resulted in the largest grains of the treated specimens as shown in figure 4.7. This grain size is a result of the time and temperature the specimen spent in the vacuum furnace. The simulated diffusion took place for 20 hours at 850°C which is ideal to inflict grain growth. The graph shown in figure 4.10 illustrates how the grain size can differ by omitting either of the two steps. 850Va, where oxidation is omitted, shows greater grain size than Ox850, where diffusion is omitted, and this is attributed to the fact that the time spent in a heated environment for 850Va is more than Ox850. The large grains facilitate fatigue crack growth and therefore the fatigue endurance of the specimen undergoing Ox850 is better than that of the 850Va as shown in section 4.3.

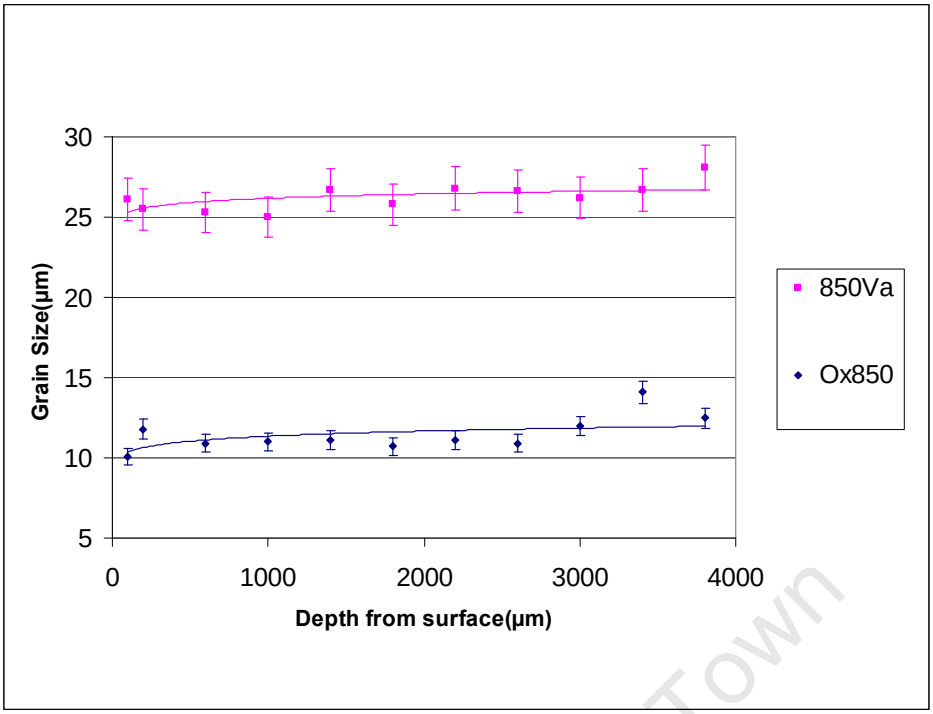

Figure 4.10: Graph showing the grain sizes of the heat-treated specimens that underwent 850Va and Ox850

4.2.1.3. Effect of Carrying Out Process Ox850NFC850Va as Opposed to Carrying Out Ox850/850Va on the Microstructure

There is no difference in the micrographs of the bulk microstructure for the two processes Ox850/850Va which involves furnace-cooling in between the two OBDH steps and Ox850NFC850Va. Ox850NFC850Va which does not encounter furnace-cooling in between the two OBDH steps has a grain structure in which there is equivalent α and β phase contents quantity as in Ox850/850Va as depicted in figure 4.11. The equi-axed grains are larger than those from process 850Va with α phase being more dominant than the β phase.

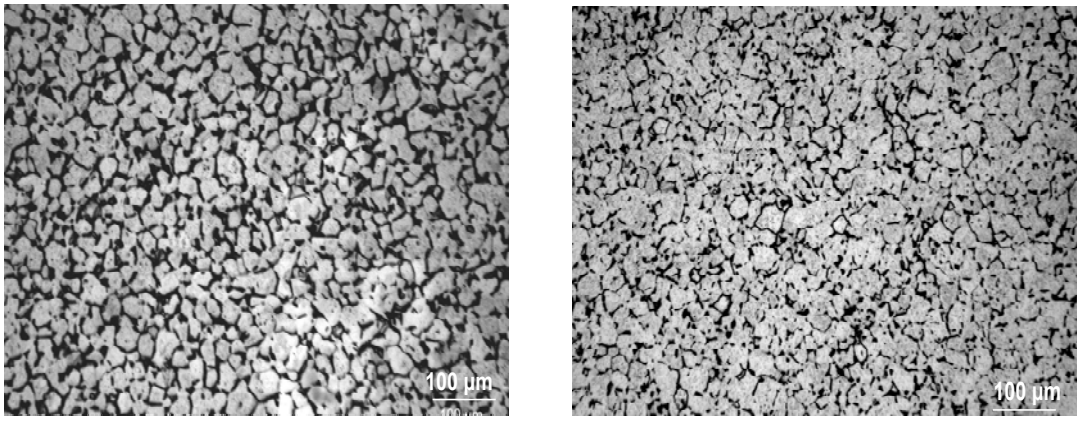

(a) **(b)**

Figure 4.11: Micrographs showing the grain sizes of the heat-treated specimens that underwent (a) Ox850NFC850Va and (b) Ox850/850Va

Figure 4.12 shows that the grain sizes of the two processes are also not different although the grain size of the Ox850NFC850Va sample is slightly larger than those of the Ox850/850Va sample. This slightly larger grain size maybe attributed to the fact that in the process Ox850NFC850Va there is no furnace-cooling and therefore the continuous heat treatment facilitates grain growth as temperature is maintained at 850°C rather then when cooling is involved between the OBDH process. Cooling in between the steps slows down atomic and molecular activity due to the temperature drop which impedes grain growth. The relatively large grains in these samples provide an acceleration of fatigue crack growth in during cyclic loading and the Ox850NFC850Va sample fractures earlier than the Ox850/850Va sample due to the slightly larger grains and the embrittled layer that is thicker as well.

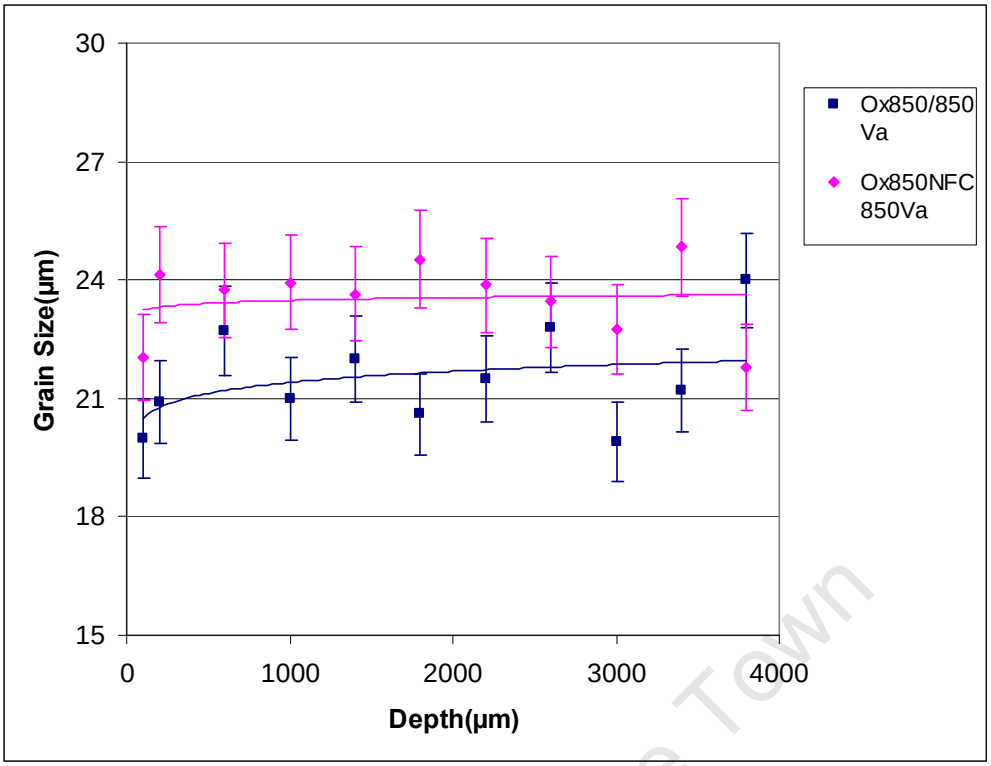

Figure 4.12: Graph showing the grain sizes of the heat-treated specimens that underwent Ox850/850Va and Ox850NFC850Va

4.2.1.4. Effect of the Diffusion Step Environment on the Microstructure

Observation of the bulk microstructure micrographs that had different diffusion environments shows that there is no difference in their appearance as illustrated by figure 4.13. The volume fractions of the α and β phases of both specimens undergoing processes Ox850/850Va (diffusion in vacuum) and Ox850/850Ar (diffusion in argon) are the same. Such an occurrence should lie in the fact that the two routes follow the same procedure with respect to time for oxidation and diffusion steps. These times are 30 minutes and 20 hours respectively and both are furnace-cooled in between the steps.

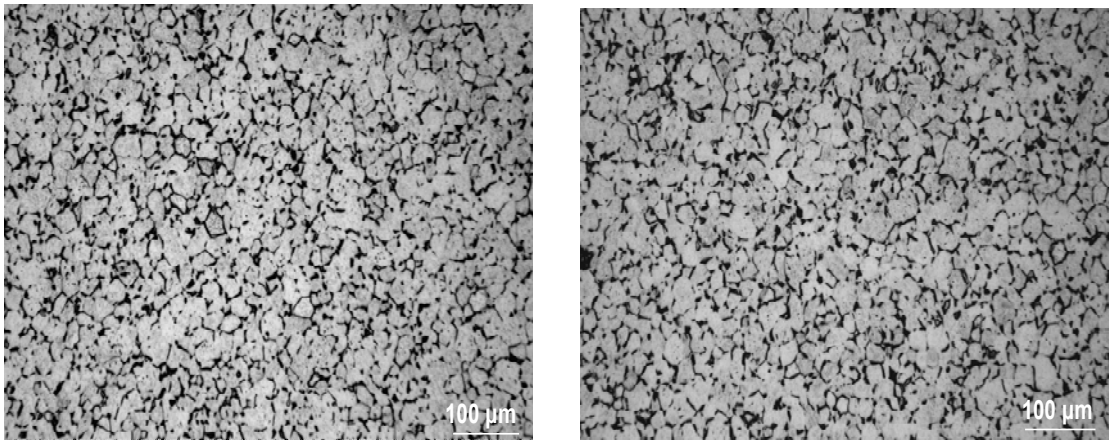

(a) **(b)**

Figure 4.13: Micrographs showing the grain sizes of the heat-treated specimens that underwent (a) Ox850/850Va and (b) Ox850/850Ar

The grain sizes of the two routes are similar too. It should be noted that their hardness profiles are also similar. Another shortfall experienced with specimen that underwent process Ox850/850Va is that there was spalling off of the oxide layer which suggested that there may have been less oxygen content made available for the diffusion step[11]. These characteristics show that the amount of time spent undergoing OBDH or a different comparative process is essential, and for optimal results regarding to fatigue response these should be carefully considered.

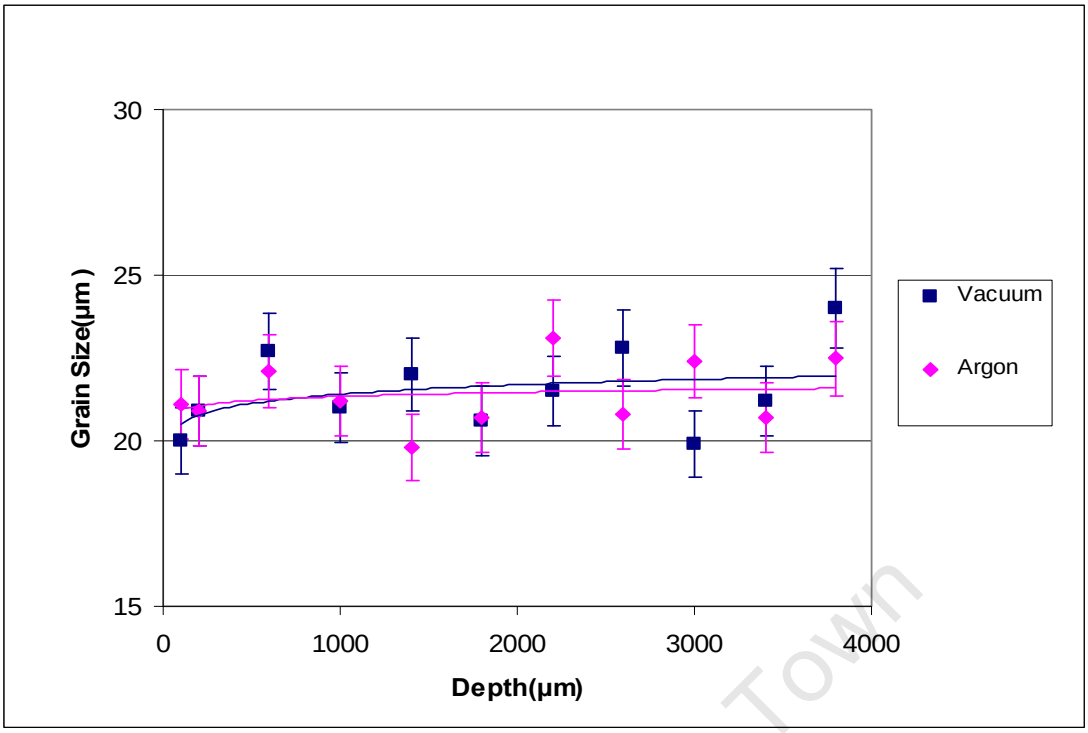

Figure 4.14: Graph showing the grain sizes of the heat-treated specimens that underwent Ox850/850Va and Ox850/850Ar

4.3. FATIGUE BEHAVIOUR

Fatigue tests carried out on the rotational bending machine generated data that would yield stress-life curves as well as fatigue cycles of specimens treatment by all the different processes mentioned in chapter 3. Initially the cycles were aimed at obtaining the point of crack initiation on the specimens but due to difficulty in the detection of cracks the testing was altered to measure the number of cycles to failure at a fixed stress level.

4.3.1. Stress - Life Curves of Selected Heat Treatments

The stress-life curves in figure 4.15 show the general behaviour of the Ti-6Al-4V alloy undergoing fatigue loading at different stress levels of various selected heat treatments. As demonstrated by the graph the as received specimens have the most fatigue resistance followed by the specimen that undergoes 850Va. The specimens that go through both steps under vacuum environment (Ox850/850Va and

Ox750/850Va) have similar curves, which cement the fact that their fatigue performance is relatively similar too. The latter were chosen but the effect of the oxidation temperature with respect to the stress-life curves generated was investigated. The result shows that at 850°C the fatigue cycles to failure are slightly more than those at 750°C. The as received specimen with the most desirable fatigue limit was loaded with stresses ranging from 530 to 480 MPa and failure occurred at 1.5 to 3.5 million cycles (not appearing in figure 4.15) respectively. For the same stress range (not appearing figure 4.15) the specimen that undergoes 850Va fails after 1.2 million cycles for a corresponding stress of 390 MPa which tends to show its fatigue limit as the curve becomes flat resembling an asymptote. The log stress-life graph in figure 4.16 shows the values that are not appearing in the figure 4.15.

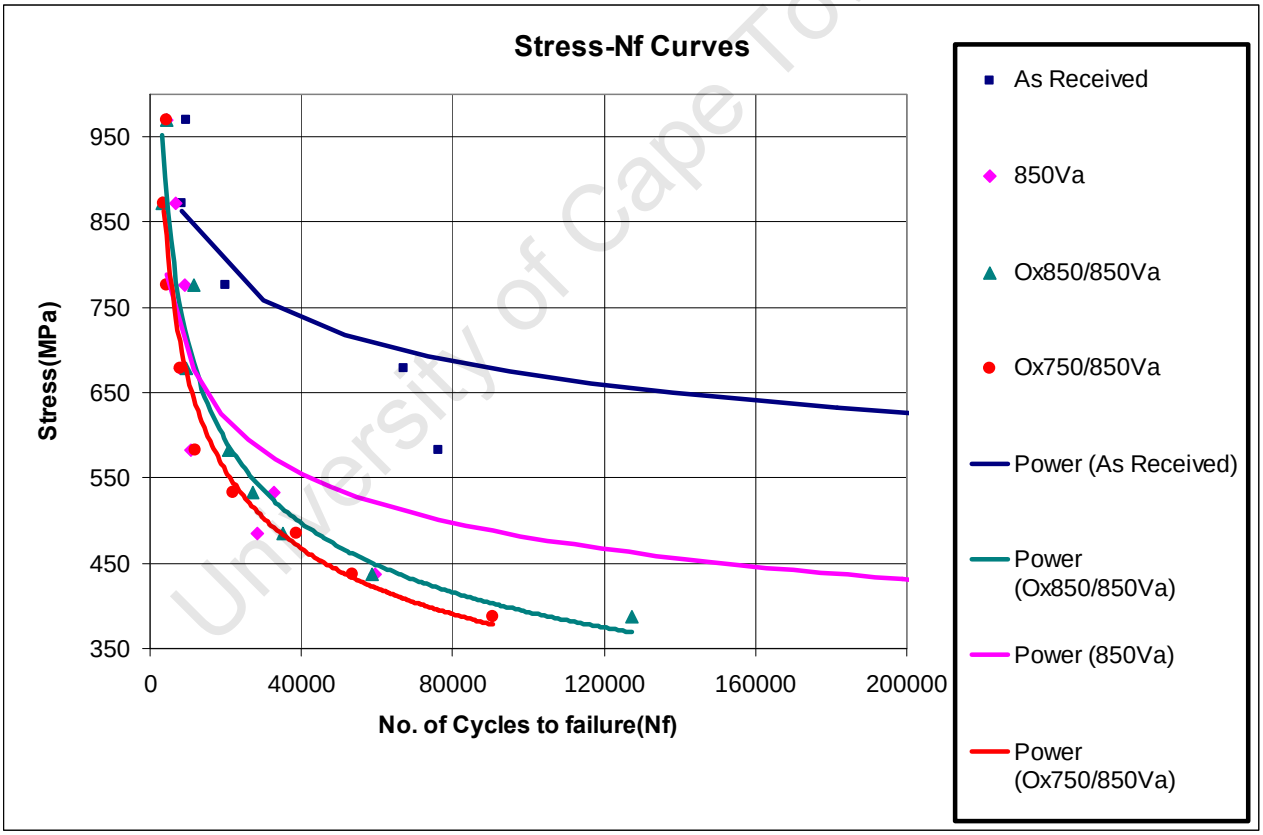

Figure 4.15: Stress-Life curves for the as-received specimen and specimens undergoing 850Va, Ox850/850Va and Ox750/850Va

In figure 4.16, as noted in the stress-life curves in figure 4.15, the fatigue performance is mostly favourable with the as received specimen followed by the 850Va specimen

and lastly the specimens undergoing Ox850/850Va and Ox750/850Va. There is evidence of the difference in treatment procedures undertaken as the gradients of the log stress-life curves show. The gradient is steeper for the specimens that undergo the whole OBDH process (Ox850/850Va and Ox750/850Va) and these gradients are fairly similar. It gets less steep when the two step OBDH process is lessened to one or none of the steps as shown by the difference in gradient from the specimen undergoing 850Va and finally the as received condition. These gradients do explain why the fatigue resistance of the specimens decreases with more time exposure to heat treatment. The fatigue limit and life cycle range for a selected domain of stresses is reduced with longer heat treatment and this is due to embrittlement of the specimen surface during heat treatment and cooling. There is a loss of ductility within the surface and more significantly at the specimen surface where diffusion hardening occurs resulting in a brittle case being formed. Residual stresses which arise mainly from the combination of the heat treatment and the bending stress applied whilst loading the specimen contribute to such fatigue behaviour. The heat treatment results in stresses within the specimen being created and even with the heat gradient upon cooling the stresses remain across the cross section of the specimen. The 850Va specimen did not go through the oxidation step where an oxygen reservoir would have been created for diffusion to occur resulting in similar curves as that of specimens identified by Ox850/850Va and Ox750/850Va.

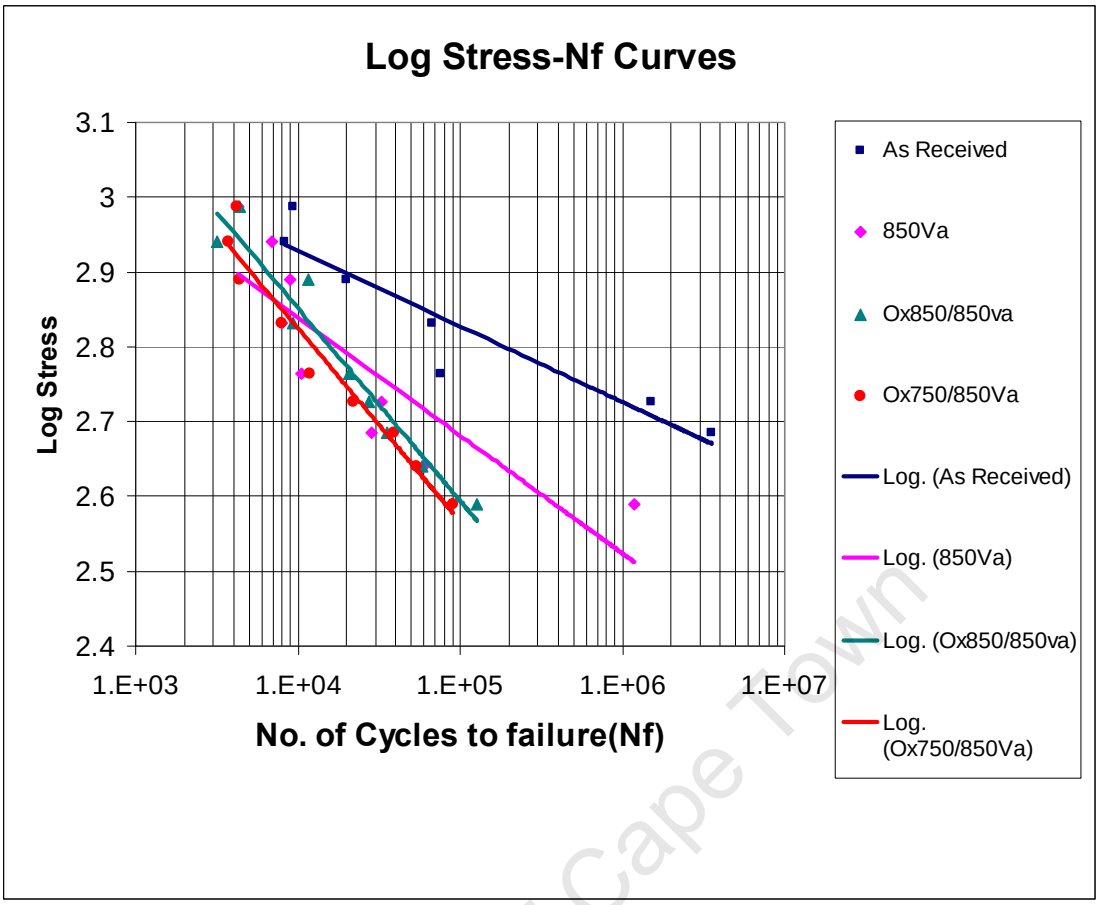

Figure 4.16: Log stress-life curves for the as-received specimen and specimens undergoing 850Va, Ox850/850Va and Ox750/850Va

4.3.2. Influence of Heat Treatments on Failure at a Fixed Bending Stress

The specimens were loaded at an applied bending stress of 678MPa which was obtained from exerting a 350N force. The chosen force was selected after a literature survey of the work done by Dong and Li[1]. They obtained a fatigue limit of 490MPa in their study and their limit was obtained in the high-cycle fatigue range. Application of the 678MPa bending stress ensured that the heat treated specimens would fail within the low-cycle fatigue range. Failing in the high-cycle fatigue range would make it difficult and unreliable to compare the different heat treated specimens' performances as the cycles to failure would lie anywhere on the horizontal line shown in figure 2.11. The horizontal line depicts the fatigue limit and therefore a specimen randomly breaks at any number of cycles on this line.

The design of the specimens used in the study ensures that the point of interest shown in figure 3.1 is the point where the specimen breaks. This is due to the stress concentration induced by the change in specimen diameters at that point as well as the gripping force applied by the collet when it holds the specimen in position. The stress concentration and gripping force in conjunction with the applied bending force ensure the braking point to be the point of interest. The bending stress was applied on the ten different heat treated specimens twice and thereafter an average value was obtained. Repetitive fatigue tests per heat treated specimen were reduced to two tests due the availability of the material.

As mentioned in the previous chapter heat treatments are varying in terms of oxidation temperature, diffusion environment and whether oxidation only or simulated diffusion steps are taken or not. There is a marked reduction in the fatigue resistance of the treated specimens as depicted by the results in figure 4.17. This reduction falls between 60 and 90% depending on which of the nine treatments is considered. The effect of the heat treatment is thus confirmed as substantially high. The specimen that undergoes the heat treatment which is identified as Ox850 (oxidation only at 850°C) has the best resistance whilst the least resistant is that designated Ox850NFC850Va (both oxidation and diffusion steps without furnace-cooling in between the steps) and it is shown in figure 4.18. The number of cycles to failure for the specimen undergoing 850Va (simulated diffusion step only) and Ox750/850Va (oxidation at 750°C and diffusion at 850°C) was the same after taking average values hence the number of data points on the figures 4.17 and 4.18 is off the mark by a single data point as the similar values have overridden each other. These results provide the basis for one to investigate which treatment process is most ideal in terms of fatigue behaviour.

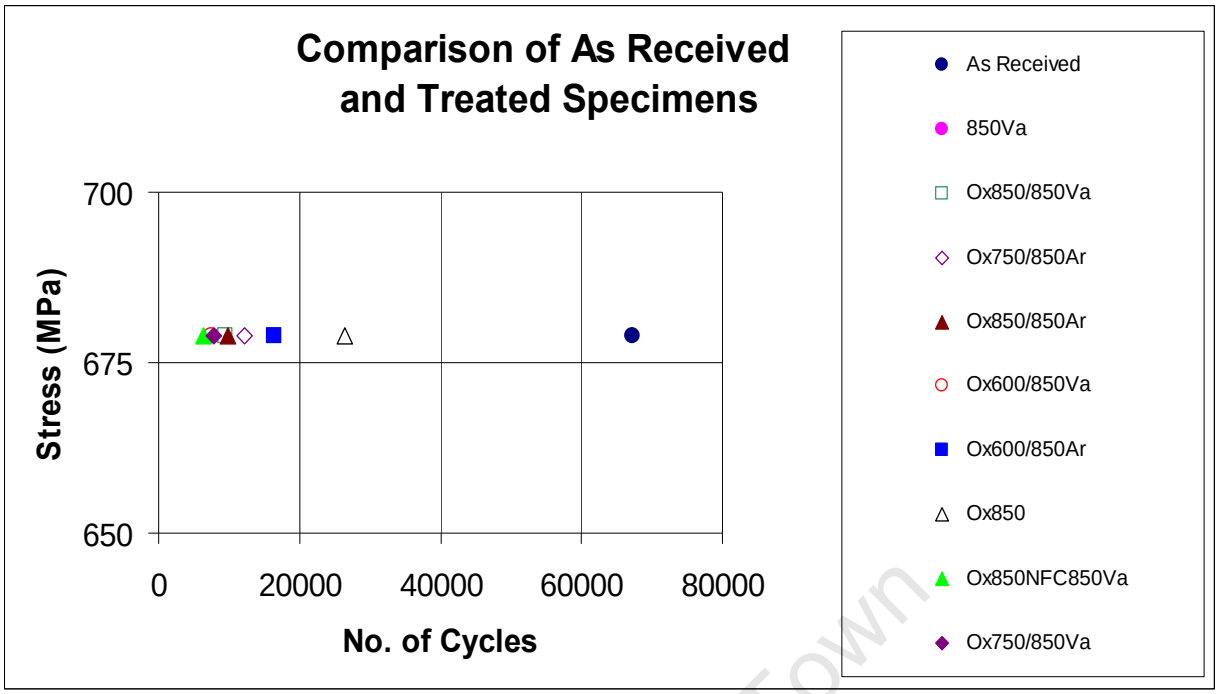

Figure 4.17: Comparison of the fatigue performance of as-received specimens and the heat-treated specimens at an applied stress of 678MPa

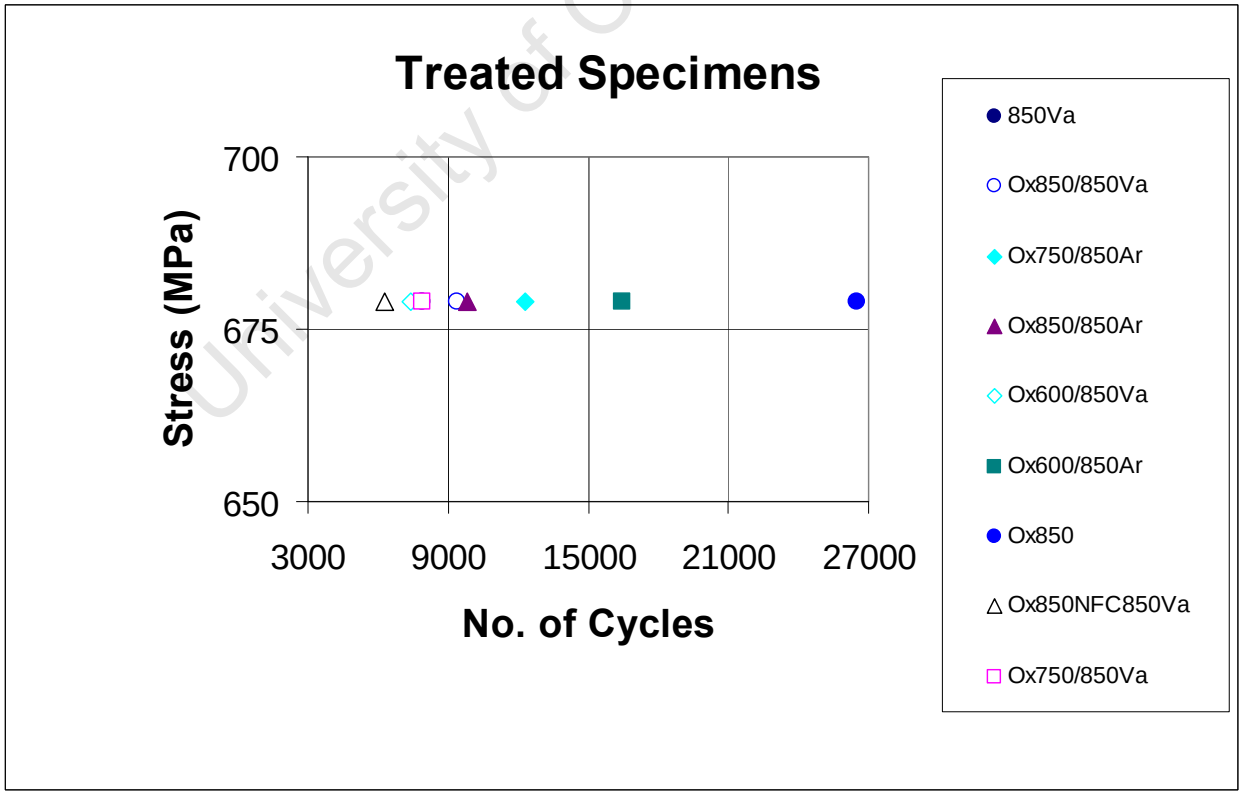

Figure 4.18: Fatigue response of all the heat treated specimens at 678MPa

4.3.2.1. Effect of Oxidation Step on Fatigue Behaviour

The oxidation step is the initial step in the heat treatment process. Fatigue resistance of the specimen that undergoes oxidation with no further treatment gives the best resistance as compared to the other treatments as shown in figure 4.18. The average number of cycles to failure at a 350N applied force is equal to 26500 and the closest value to it is that of a specimen undergoing Ox600/850Ar (oxidation at 600°C and diffusion at 850°C) with 16450 cycles. Omitting the diffusion stage of the heat treatment exposes the specimen to less time in the 850°C hot environment as opposed to the rest of the specimens that have to go for 20 hour diffusion step. The long hours encountered during the diffusion stage at 850°C result in residual stresses being formed within the specimen especially in the hardened zones which have been pre-oxidised. The stresses then enhance the process of fatigue hence the shorter fatigue life as compared to the specimen that undergoes Ox850.

It should be noted that section 4.1.2 shows that hardness does not have a direct effect on the fatigue performance of the treated alloy. The same specimen that went through Ox850 had the best fatigue resistance relative to other heat treated specimens whereas the hardness profile proved to be less desirable than those depicted by specimens that underwent the two-step OBDH process.

4.3.2.2. Effect of Simulated Diffusion Step on Fatigue Behaviour

In order to ascertain the role played by the oxidation step prior to the diffusion, specimens where placed in the controlled atmosphere furnace for a simulated diffusion step without carrying out the oxidation step. Comparison of the effect of oxidation followed by diffusion against simulated diffusion can then be analysed.

The average number of cycles to failure for the specimen that undergoes 850Va (simulated diffusion step at 850°C only) is similar to that of the specimen that undergoes Ox750/850Va and the magnitude is 7900 cycles as shown in figure 4.19. Fatigue resistance of all the samples that underwent the diffusion stage for the stipulated 20 hours should be in the same range considering that the time taken for the

diffusion stage is the same and immensely higher than the oxidation time. However, this is not the case due to the different oxidation temperatures and diffusion environments proposed in the project hence the fatigue life cycle data for the specimen that undergoes 850Va lies in between the data for specimens treated using different routes as depicted in figure 4.19. It should be noted that without oxidation the specimen is going to be less hard than the other heat treated specimens that undergo oxidation. This specimen was only treated in a vacuum environment which will be proven later in this section that it is a less desirable environment compared to argon environment in terms of fatigue response. Furthermore the role of residual stresses, due to the high temperature experienced during the simulated diffusion and furnace-cooling, plays a significant role in lowering the fatigue performance of the specimen.

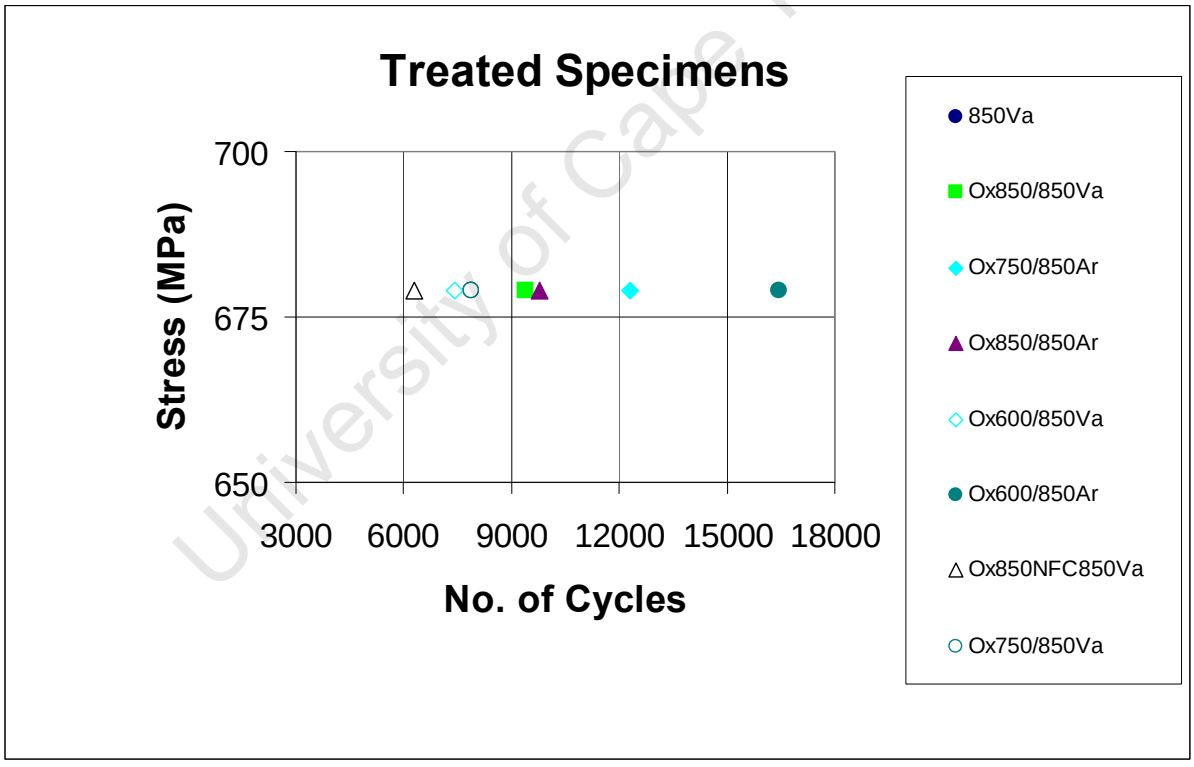

Figure 4.19: Fatigue response of heat treated specimens at 678MPa excluding Ox850

4.3.2.3. Effect of Carrying out Process Ox850NFC850Va as Opposed to Carrying out Ox850/850Va on Fatigue Behaviour

Figure 4.18 shows that the fatigue resistance behaviour of a specimen that undergoes Ox850/850Va (furnace-cooling between the two steps) is much better than that which undergoes Ox850NFC850Va (no furnace-cooling between the two steps) with the average number of cycles being 9400 and 6295 respectively. In essence this shows that the immediate transition from the oxidation to diffusion is ineffective when fatigue life has to be maximised. This is mainly due to the fact that as the oxidation takes place and the rutile forms there is simultaneous stresses that are exerted on the specimen due to the high oxidation temperatures. The diffusion stage follows and the exposure to the high temperature is further increased. This occurs with no break between the two steps further increasing the effective stresses exerted on the specimen. Furthermore, when diffusion takes place the oxygen diffuses significantly in the specimen's interior and the stress within the specimen increases. This is as a result of the high temperature associated with the diffusion step. Upon cooling the specimen after the OBDH process the stress exerted on the specimen is not removed and it creates high residual stress component. The specimen that undergoes Ox850NFC850Va has the lowest fatigue resistance as mentioned earlier. The fact that there was no point at which the specimen was cooled in between both cycles as well as the time spent in the furnace results in the diminished fatigue resistance, although it is advantageous with regards to the hardness of the specimen as explained in section 4.1.2.

4.3.2.4. Effect of Oxidation Temperature on Fatigue Behaviour

In order to compare the effect of oxidation temperatures on fatigue resistance, three temperatures were chosen; these were 600°C, 750°C and 850°C. The results that are depicted by figure 4.20 illustrate this effect. There are two different data points for each temperature as one represents diffusion in vacuum environment and the other represents diffusion in argon environment. At 600°C the average number of cycles to failure for the two different heat treatment routes chosen shows a huge difference in magnitude with one having a value of 16450 cycles to failure and the other having

7400 cycles. There is also a difference for the specimens that had an oxidation step temperature of 750°C with the higher value being 12300 cycles and the lower being 7900 cycles. For the 850°C oxidation temperature the two routes show relatively similar values for the average number of cycles to failure which are 9400 and 9800 cycles. The similarity in the number of cycles to failure when the specimen undergoes the 850°C oxidation temperature proves the reliability of this particular oxidation temperature. The small difference in cycles to failure can then be attributed to the diffusion stage environment. This may also be enhanced by the fact that after oxidation, the diffusion steps are all carried out at 850°C which exposes the latter specimens to temperatures they have already been oxidised with. The specimens that undergo oxidation step at 600°C and 750°C experience a different temperature (850°C) in the diffusion step as well as difference in environment (vacuum or argon). The resultant effect will be a differential response of the rate and amount of oxygen diffusing into the specimen during the diffusion step. This differential response then results in a relative scatter in the average number of cycles to failure.

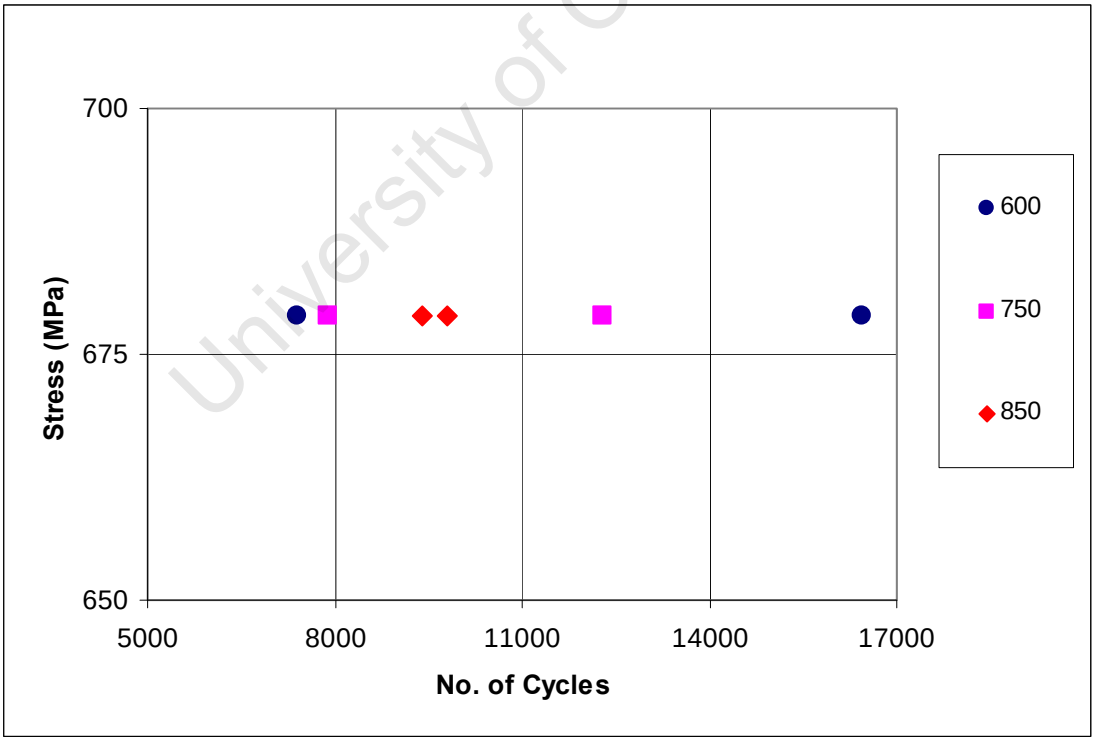

Figure 4.20: Fatigue response comparison of specimens at 600°C, 750°C and 850°C

The co-relation between oxidation temperature and fatigue endurance should resemble the one shown in figure 4.21. This is due to the fact that at a higher oxidation temperature (850°C) the grain growth is greater and with the subsequent prolonged diffusion the specimen is more susceptible to fatigue failure under cyclic loading than when at lower temperature (600°C).

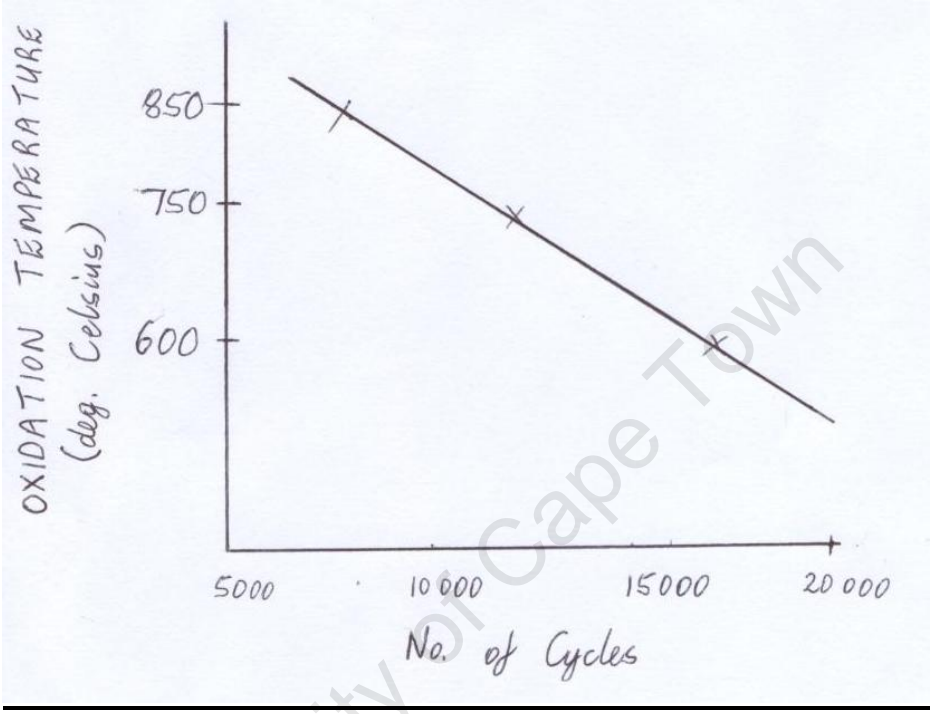

Figure 4.21: Expected fatigue response and oxidation temperature co-relation

The results obtained from the graph in figure 4.22 do not fully correspond to the expected co-relation of oxidation temperature and fatigue endurance. The specimens that were diffusion treated in argon correspond to the expected phenomenon whereas the specimens that underwent diffusion treatment in vacuum show an opposite relationship. The relatively large difference of the number of cycles to failure at 600°C is a cause for concern. With the available literature and in depth analysis of the cause of the discrepancy, it is unfortunate that no conclusion has been drawn to explain it. It has thus been recommended that in future the role of the oxidation temperature during the OBDH process be investigated with respect to fatigue endurance.

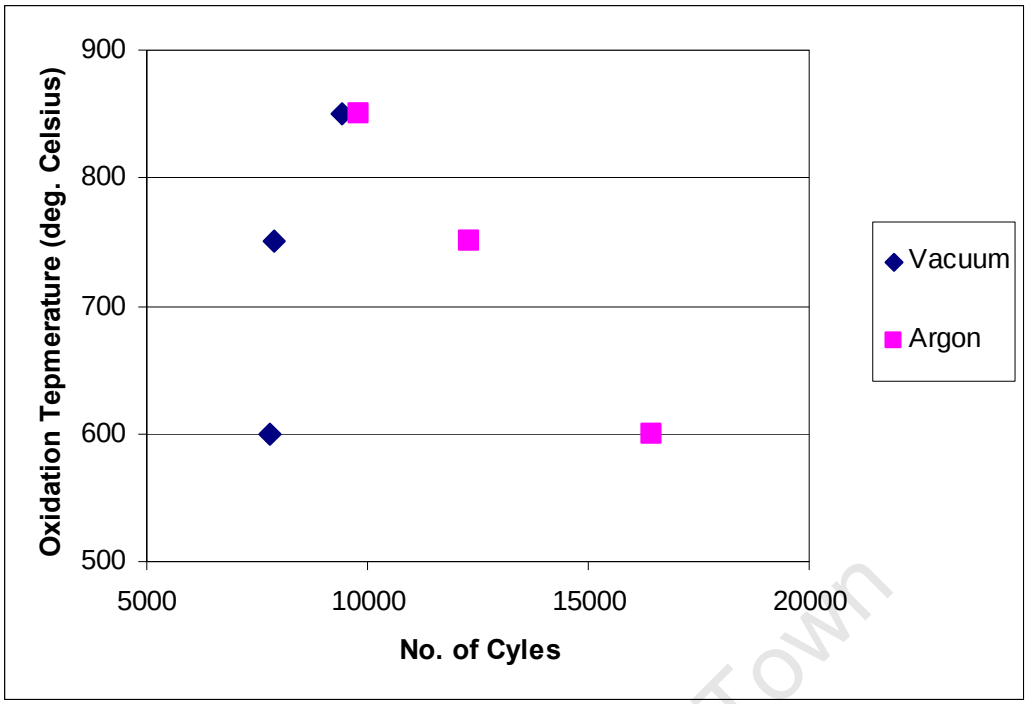

Figure 4.22: Fatigue response and oxidation temperature co-relation

4.3.2.5. Effect of the Diffusion Step Environment on Fatigue Behaviour

The figure 4.23 shows the effect that the diffusion step environment has on the fatigue behaviour of the specimens. The numbers of cycles to failure of the specimens that underwent diffusion in the argon environment are higher than those that went through the vacuum environment in all 3 different temperatures (600°C, 750°C and 850°C) for the oxidation stage. At this stage it should be noted that from the study of Camagu[11] the total pressure increase in the argon environment is due to the addition of argon into the furnace and the partial pressure of oxygen is the same for both systems.

The argon environment which enhances the diffusion of oxygen during the diffusion step of the OBDH thereby yielding specimens that are more fatigue resistant than the specimens that undergo diffusion in the vacuum environment. The microhardness data and the microstructures of the specimens at the relative temperatures and environments are similar and therefore the response to the applied bending stress is attributed to the enhanced oxygen diffusion in the argon environment which results in a β depleted zone on the specimen surface. The stronger α phase that remains at the

specimen edge facilitates the better fatigue resistance in the specimens experiencing diffusion in the argon environment.

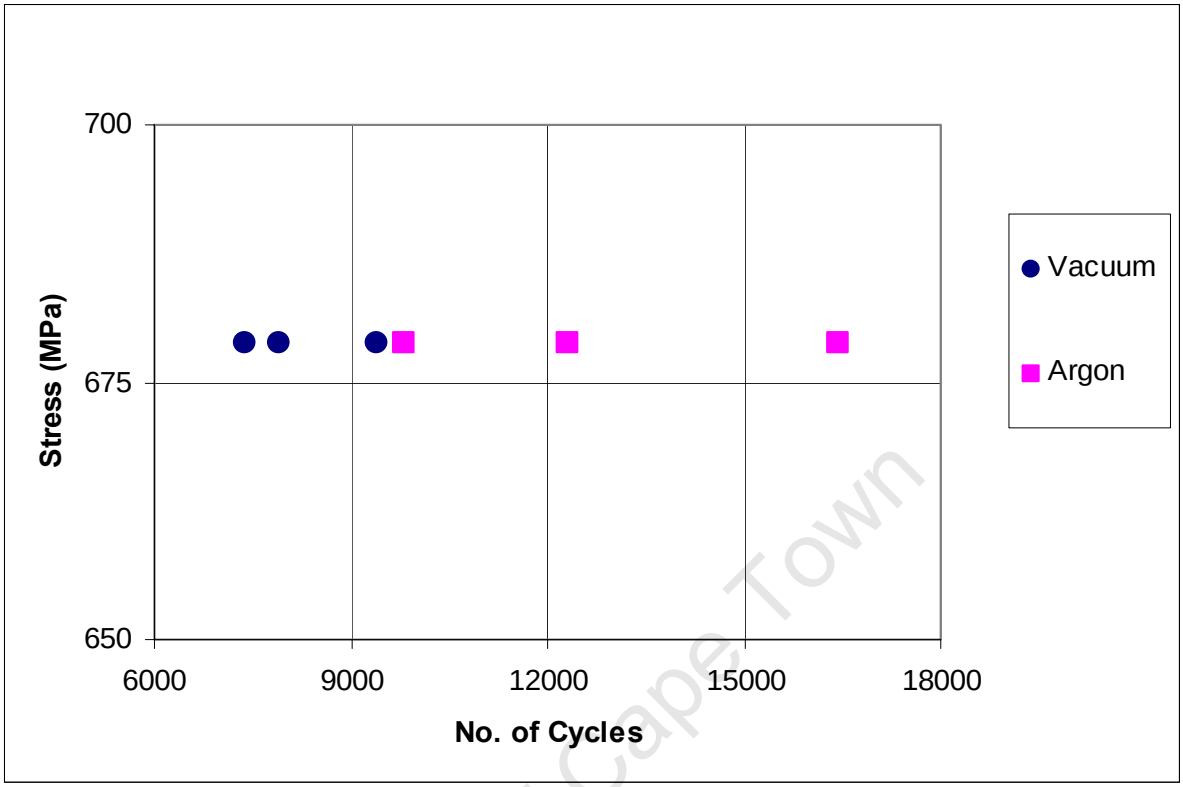

Figure 4.23: Fatigue response comparison of the vacuum or argon environment during the diffusion step

4.4. FRACTOGRAPHIC ANALYSIS

The morphology of the fractured surfaces of the failed specimens are analysed and discussed in this section. Fractographs across the whole cross-section of the specimen on the fractured face were captured. Figure 4.24 shows selected fractographs of the specimen in the as received condition. In figure 4.24a the overall fracture surface is shown with ratchet marks at the edges. Figure 4.24b shows the edge of the fractured surface which coincidentally is the crack initiation zone. There is a significant amount of dimples and also a region showing the presence of secondary cracks. In the crack propagation zone (figure 4.24c) fatigue striations can be observed within the grains of the microstructure. Most of the striations are intragranular. Finally in figure 4.24d which is the final fracture zone there is an abundance of dimples which are uniformly dispersed. The observations made on this section of the specimen suggest that the

specimen underwent ductile fracture. The presence of dimples in abundance supports this fact. The secondary cracks also enhance the ductile fracture.

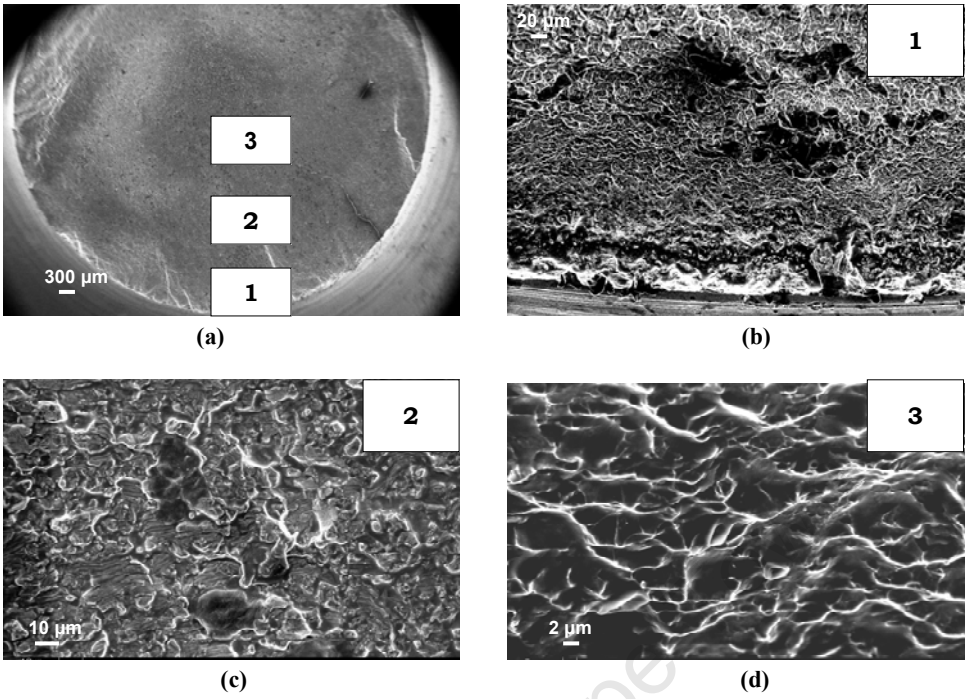

Figure 4.24: Fatigue fracture morphology of Ti-6Al-4V in the as received condition. (a) overall fracture surface; (b) crack initiation zone; (c) crack propagation zone and (d) fast fracture zone

The specimen that underwent the heat treatment designated Ox850/850Va (two steps carried out at 850°C with no furnace cooling in between) has its fractographs shown in figure 4.25. Ratchet marks are more conspicuous as compared with the as received specimen. They are well defined at the periphery of the specimen and they are shown in figure 4.25a. They also have a stepped appearance which is characteristic whenever fatigue cracks emanate from several origins and subsequently meet to form a principal crack front. Their occurrence requires virtually simultaneous initiation of several fatigue cracks, a situation that is favoured by high stress and to a lesser extent by the presence of high stress concentration factors[41]. The edge of the specimen has some fatigue striations which are not densely populated. There is a big intergranular crack which in essence facilitates cleavage fracture as shown in figure 4.25b although it should be noted that fracture could have occurred along the (0002) basal plane of the α-grain of the α-β microstructure. Furthermore, the nature of the crack initiation and propagation in titanium containing both the α and β phases can be affected by phase

balance of the two phases. This is due to the fact that the α phase is susceptible to cleavage along the (0002) basal plane. During heat treatment process such as the OBDH the observed coarsening of the α-grain coupled with the above-mentioned susceptibility to cleavage fracture may enhance initiation and propagation. Diffusion time and temperature will also play a significant role as long diffusion times and higher temperatures facilitate grain growth in the solids and greater time for oxygen as an interstitial solid solution element to diffuse into the solid and more significantly in the (0002) basal plane. This also increases brittleness of the α-phase. The crack propagation zone which is shown in figure 4.25c is similar in structure to that of the as received specimen having fatigue striations as the dominant feature. Figure 4.25d shows the fast fracture zone and there are a lot of dimples in this zone. Therefore to sum it up the fracture mode of this specimen was brittle in nature and at the onset of facture. The dimples suggest that some ductile fracture was experienced within the specimen and this is due to the fact that the region in the centre of the specimen was not hardened and there it closely resembled the as received specimen.

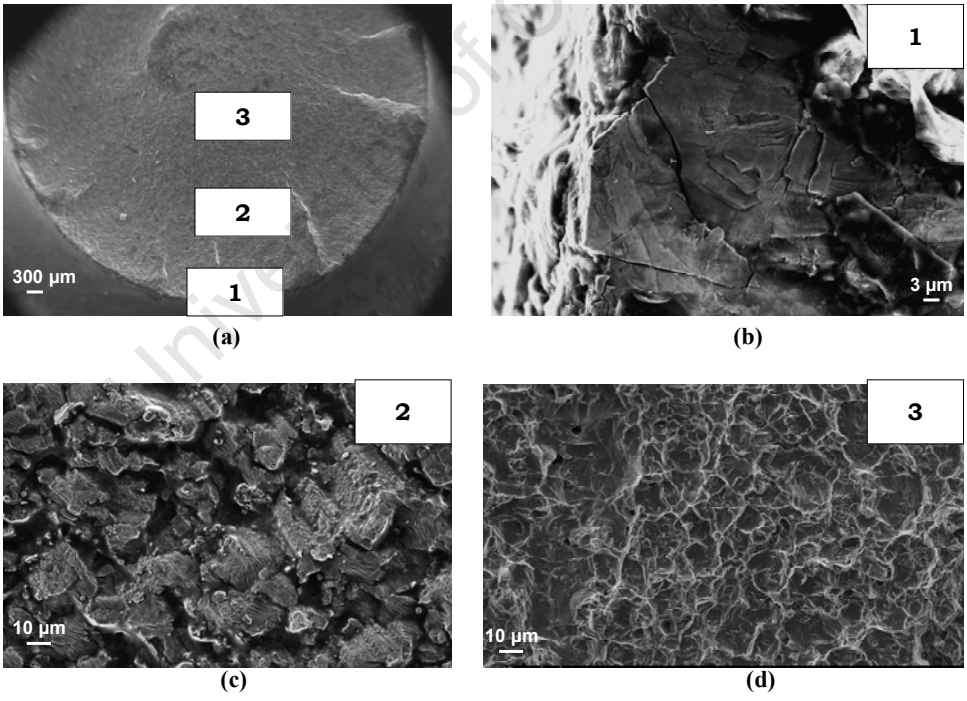

Figure 4.25: Fatigue fracture morphology of Ti-6Al-4V specimen that underwent Ox850/850Va. (a) overall fracture surface; (b) crack initiation zone; (c) crack propagation zone and (d) fast fracture zone

Figure 4.26 has the fractographs of the specimen that underwent Ox750/850Va (oxidation at 750°C and diffusion at 850°C without furnace-cooling) treatment process. This specimen was analysed in order to compare its morphology with that of the specimen undergoing Ox850/850Va. The two differ in the oxidation step temperatures only. Figure 4.26a shows the overall structure and there are ratchet marks just similar in length to those observed in the specimen that underwent the treatment designated Ox850/850Va. In figure 4.26b the edge of the specimen is shown and there is a stepped appearance of river-pattern cleavage facets. The subsequent diagrams figure 4.26c and 4.26d had evidence of striations and dimples just like the Ox850/850Va specimen. Failure was also brittle in nature and this justified that the two different oxidation temperatures had no influence on the fracture morphology of the specimens.

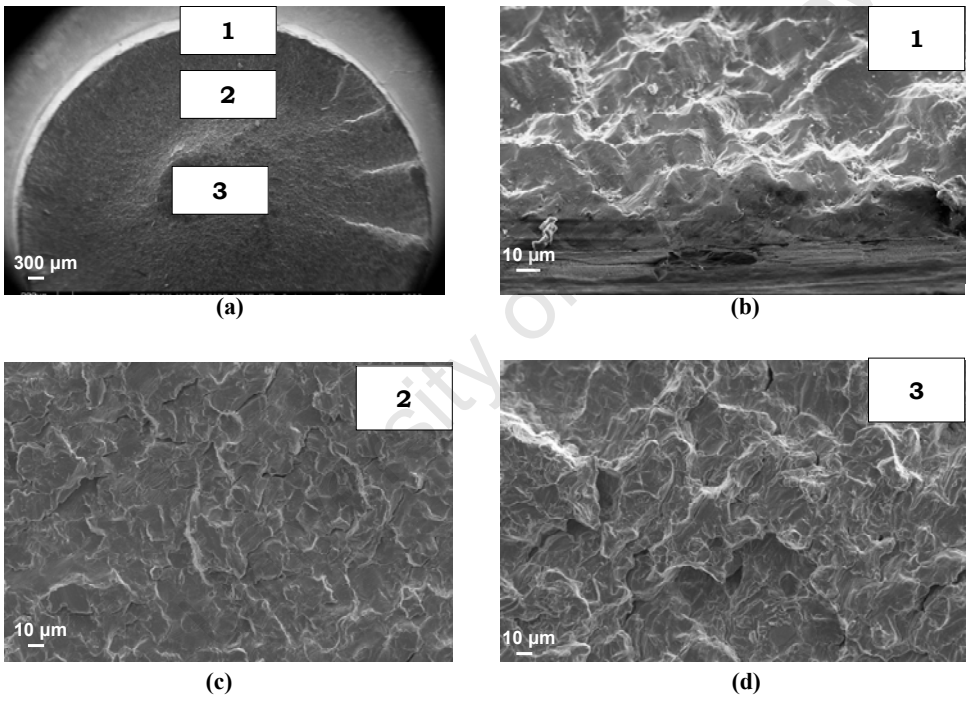

Figure 4.26: Fatigue fracture morphology of Ti-6Al-4V specimen that underwent Ox750/850Va. (a) overall fracture surface; (b) crack initiation zone; (c) crack propagation zone and (d) fast fracture zone

4.4.1. Crack Lengths and Fracture Toughness

The specimens selected for fractographic analysis were then analysed for the crack lengths, fast facture zone lengths and fracture toughness. The procedure involved

taking fractographs along the whole diameter of the specimens sequentially at the same magnification. The fractographs are then lined up one against another in order to observe the crack initiation, crack propagation and final fractures zones enabling the measurement of these zones to be calculated as illustrated in figure 4.27.

The crack initiation and propagation zones as well as the final fracture zone were measured according to the scale and magnifications that are marked on the fractographs. The results obtained are tabulated in table 4.1 and include the fracture toughness values. The fracture toughness was also measured using the equation;

$$K_{IC} = \sigma\sqrt{(\prod a)}$$

Where $\mathbf{K_{IC}}$ = Fracture Toughness

$\boldsymbol{\sigma}$ = Applied Stress

a = Crack Length.

Ideally the fracture toughness is a mechanical property that should never change even if different stresses are applied on the specimen. An increase in the stress applied should correlate with a decrease in the crack length. At high stress level, fatigue cracks occur on the surface of the specimen whereas at low stress amplitude fatigue cracks are difficult to detect. Fracture toughness values are bound to depict a difference for the applied stresses chosen as the crack length determination is not the most accurate method to use when quantifying this mechanical property.

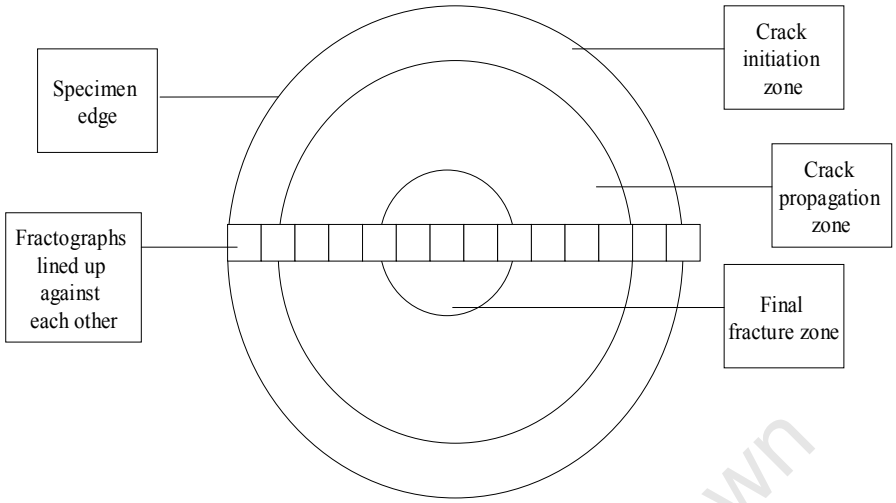

(a)

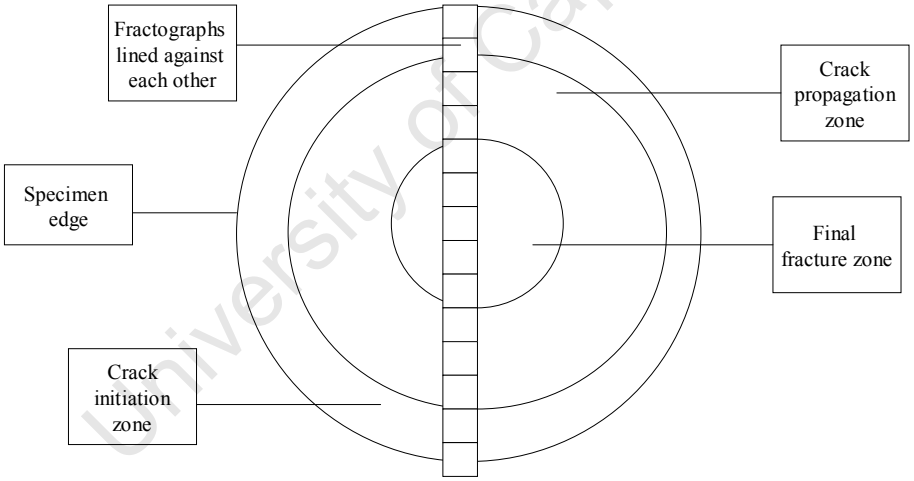

(b)

Figure 4.27: Schematic diagram of the cross-section of the specimen illustrating the points where fractographs were captured in order to evaluate fracture zones using two different orientations

Table 4.1: Fracture Toughness Values at Two Different Applied Stress Values

Heat Treatment	Applied Stress(MPa)	Crack Length(mm)	Fast Fracture Zone (mm)	Fracture Toughness(MPa√m)
Ox850/850Va	679	6.9	1.1	100
	872	4.2	3.8	100
As Received	679	7	1	100.7
	872	6.62	1.38	125.8
Ox750/850Va	679	5.91	2.09	92.5
	872	4.09	3.91	98.8

For each of the specimens used to determine the fracture toughness values, applied stresses of 679 MPa and 872 MPa were implored. Fracture toughness values of 100 MPa√m were obtained for the specimens that were treated using process Ox850/850Va for both the above-mentioned values of applied stress. The as-received specimens had a difference in the fracture toughness values of 100.7 MPa√m and 125.8 MPa√m for applied stresses of 679 MPa and 872 MPa respectively. Process Ox750/850Va had minor differences in the fracture toughness values of 92.5 MPa√m and 98.8 MPa√m for the applied stresses of 679 MPa and 872 MPa.

The fatigue crack length of the as received specimen is larger than that of the treated specimens. This is attributed to the mode of failure that is experienced by the specimen. The ductile fracture is bound to take longer than brittle fracture hence resulting in a crack length that is longer than that of the specimens undergoing Ox850/850Va (both steps carried out with oxidation done at 850°C) and Ox750/850Va (both steps carried out with oxidation done at 750°C). This is enhanced by the fact that the closely-packed grains in the as received specimens help decelerate the fatigue crack growth as opposed to the larger grains in the treated specimens. Consequently, the fatigue life of the treated specimens is lower than that of the as received specimens due to the lower fracture toughness.

Previous studies have shown that sub-surface crack initiation is highly encountered in titanium alloys. It results from the presence of processing-induced, surface compressive residual stresses due to heat treatment case-hardening or shot-peening

procedures. These residual stresses can also be due to preferential plastic deformation at the surface under tension-tension loading or inhomogeneity in phase particles (in the titanium alloy) in the bulk of the material compared to the surface[26]. In this research sub surface crack initiation is not present in the treated specimens. The cracking occurs in the hardened zone of the specimens which is located on the specimen surface. The fractographs show any form of cracks being mostly experienced in the zone very close to the surface. This goes against the studies that have revealed that any crack formation is difficult to detect after initiation. It should be noted that SEM observation of fracture surfaces shows that the crack initiation sites abruptly shift from surface to interior with decreasing stress amplitude.

It has been hypothesised that oxide formation and oxygen diffusion are enhanced at grain boundaries and phase interfaces, therefore cracks initiated will occur at α/β interfaces[17]. The nature and thickness of the hardness zone should also be a factor as to how the cracks are aligned and their occurrence. Furthermore, results show that there is a difference in the way the specimens failed, as it was noticed that the treated specimens failed due to brittle failure whereas the as received specimen failed due to ductile fracture as observed in the fractographic analysis in section 4.4.

5. CONCLUSIONS

The main objectives of the research were to investigate the effect of surface modification on the fatigue performance of Ti-6Al-4V alloys. This was to be carried out taking note of the number of cycles obtained to the failure of the specimens as well as observing properties such as hardness, grain size and microstructure and fracture morphology. With this information decisions on the surface modification processes to select for the development of products in industry can be made with the fatigue endurance being core to the decision-making. The surface treatment process used in the research known as the OBDH process involves heat treatments.

This research has led to the cementing of previously obtained results and new findings have been unearthed. The main conclusions drawn from these findings are as follows:

- The fatigue life of the heat treated samples was reduced in comparison to that of the as received specimen. The extent of the low life cycle values of the treated specimens were of huge concern considering that they could be used to make products of the alloys for use in the aerospace industry. The specimen that underwent the full OBDH treatment without cooling in between oxidation and diffusion steps (Ox850NFC850Va) had the lowest value of fatigue life and this alone results in it being discarded as an option for being selected as this research looks to select a process that yields good fatigue properties.

- Microhardness, grain size, heat treatment time and diffusion environment all play a role in determining the fatigue behaviour of the Ti-6Al-4V alloy. The major factors though are heat treatment time and the grain size. They have a more direct relationship with the fatigue behaviour as observed in the results section.

- The OBDH process can be successfully operated yielding a hardened layer that has high hardness values. The hardened layer is embrittled and upon fatigue loading the fatigue endurance is low. This brittle layer accelerates crack initiation and hence the specimen undergoing the OBDH process

fractures at lower fatigue life cycles as compared to untreated specimens. The instant at which the initiation of fatigue in the test specimens occurs proved difficult due to the nature of the crack detection equipment.

- The grain size effect has a direct relationship with the fatigue life. The specimens with the smaller grains are the ones that had the best fatigue performance and the ones with large grains had the worst. This is a result of the bulk microstructure of the specimens having an effect on the fatigue crack propagation which finally leads to the fast fracture. With the smaller grains the cracks do not propagate as fast as they would with the large grains.

- Fractographic analysis shows that the specimens failed due to brittle fracture in the heat treated specimens. The as received specimen used as a comparison failed in a ductile manner.

- The fatigue crack length of the as received specimen is larger than that of the heat treated specimens. This is attributed to the mode of failure that is experienced by the specimen. The increase in grain size that occurs during the OBDH process leads to decrease in fracture toughness and hence the critical crack length for eventual fast fracture is reduced.

Furthermore the following important findings are observed:

- The fatigue behaviour of the samples is affected by the furnace environment as well. The study shows that the fatigue resistance when the diffusion step is carried out in an argon environment is much better than using a vacuum environment. The argon environment enhances the diffusion of oxygen during the diffusion step of the OBDH thereby yielding specimens that are more fatigue resistant than the specimens that undergo diffusion in the vacuum environment.

- Stress – Number of cycles to failure curves for selected samples were constructed. The different gradients of the curves showed how crucial it is in

changing parameters like diffusion temperatures or number of steps in the heat treatments. The gradient gets less steep when the two step OBDH process is lessened to one step or better still to the as received condition. These gradients do explain why the fatigue performance of the specimens decreases with more time exposure to heat treatment and the associated grain growth.

- The long diffusion time and temperature will also play a significant role as long diffusion times and higher temperatures facilitate grain growth in the solids and greater time for oxygen to diffuse into the solid and more significantly in the (0002) basal plane whose α phase is susceptible to cleavage.

6. RECOMMENDATIONS

OBDH is not necessarily effective in improving fatigue strength in Ti-6Al-4V alloys even though the hardness may increase. The improvement of the fatigue property of surface modified Ti-6Al 4V alloy as in this study may be through a more quantitative process on the heat treatments. My recommendations would include the following:

- The introduction of shot-peening after the OBDH process as this increases the samples' ability to resist the initiation of fatigue. Essentially this would then improve the fatigue performance.

- Since argon is a better option when considering fatigue performance, the study of the effect of other inert gases as an environment for diffusion is an option. These inert gases would be the ones higher on the periodic table like krypton and xenon.

- The oxidation time looks set to be the best utilised as 30 minutes. There could be an alteration in the diffusion step so that information can be obtained as to whether the 20 hours is ideal or not. Less time may result in thinner diffusion layer but an increase in fatigue strength. This could lead to compromising situation where decisions can be made on the extent of time reduction.

- The OBDH process that does not have cooling in between the oxidation step and the diffusion step can be re-done using a lower temperature. This may bring a whole new dimension to the investigation as the non-cooling effect may be neutralised by the lower temperature thereby resulting in a different outcome of results.

- Detection of the crack initiation points proved difficult in this research. The use of much more sophisticated equipment such as high-speed resolute cameras and digital image processors for the detection of cracks can be done to solve the problem.

REFERENCES

[1] Dong, H., and Li, X.Y., "Oxygen boost diffusion for the deep-case hardening of titanium alloys", *Materials Science and Engineering A280*, 2000, pp. 303-310.

[2] Leinenbach, Christian, and Eifler, Dietmar, "Fatigue and cyclic deformation behaviour of surface-modified titanium alloys in simulated physiological media", *Biomaterials 27*, 2006, pp. 1200-1208.

[3] Titanium Industries Website, 2008, [Online], Available: http://www.titanium.com/titanium/aerospac.cfm, [2008, April 25]

[4] Key2BTEC National Engineering Website, 2007, [Online], Available: www.key2study.com/btecnat, [2007, September 20]

[5] Akahori, T., Niinomi, M., Fukui, H., and Suzuki, A., "Fatigue Performance of Low Rigidity Titanium Alloy for Biomedical Applications", *Materials Science Forum Vols. 449-452*, 2004, pp. 1265-1268.

[6] Boyer, R.R., "An overview on the use of titanium in the aerospace industry", *Materials Science and Engineering A213*, 1996, pp. 103-114.

[7] Khan, Akhtar S., Kazmi, Rehan., Farrokh, Babak., and Zupan, Marc., "Effect of oxygen content and microstructure on the thermo-mechanical response of three Ti-6Al-4V alloys: Experiments and modelling over a wide range of strain-rates and temperatures", *International Journal of Plasticity,* 2007, pp. 1105-1125.

[8] Lovrich, N.R., and Neu, R.W., "Effect of mean stress on fretting fatigue of Ti-6Al-4V on Ti-6Al-4V", *Fatigue Fracture Engineering Structure Vol. 29,* 2006, pp. 41-55.

[9] Komano, K., Ishihara, S., McEvily, A.J., and Shibata, H., "Effect of microstructure on small fatigue crack initiation and propagation behaviour of Ti-6Al-4V alloy", *Key Engineering Materials Vols. 353-358,* 2007, pp. 1215-1218.

[10] Polmear, I.J., *Light Alloys: From Traditional Alloys to Nanocrystals*, Australia, 2006, pp. 300-364.

[11] Camagu, S.T, "Surface modification of titanium based alloys", MSc (Applied Science), University of Cape Town, 2007

[12] Bache, M.R., Evans, W.J., Suddell, B., and Herrouin, F.R.M., "The effects of texture in titanium alloys for engineering components under fatigue", *International Journal of Fatigue 23,* 2001, pp. S153-S159

[13] University of Cambridge Materials Science and Metallurgy Website, 2008, [Online], Available: http://www.msm.cam.ac.uk/phase-trans/2004/titanium/titanium.html [2008, March 19]

[14] Jovanovic, M.T., Tadic, S., Zec, S., Miskovic, Z., and Bobic, I., "The effect of annealing temperatures and cooling rates on microstructure and mechanical properties of investment cast Ti-6Al-4V alloy", *Materials and Design 27*, 2006, pp. 192-199.

[15] Rice, R., *SAE Fatigue Design Handbook*, United States, 1997, pp. 17-18

[16] Zuo, J.H., Wang, Z.G., and Han, E.H., "Effect of microstructure on ultra-high cycle fatigue behaviour of Ti-6Al-4V", *Materials Science and Engineering A473,* 2008, pp. 147-152.

[17] Jayatilaka, A.D.S, *Fracture of Engineering Brittle Materials*, 1979, pp. 51-53,77, Chap. 3.

[18] Azom Website, 2008, [Online], Available: http://www.azom.com/details.asp?ArticleID=1547 [2006, July 10]

[19] Asaoka, Kenzo., and Maejima, Kunimitsu., "Effect of surface oxide films on degradation of titanium", *Materials Science Forum Vols. 539-543,* 2007, pp. 3649-3654.

[20] Altenberger, I., "Alternative mechanical surface treatments for fatigue strength enhancement", *Materials Science Forum Vols. 490-491,* 2005, pp. 328-333.

[21] Son, S.Y., Nishida, S., Hattori, N., Jang, H.D., and Son,Y.J., "The effect of surface treatment of Ti-6Al-4V alloy specimens", *Key Engineering Materials Vols. 297-300,* 2005, pp. 2429-2434.

[22] Suresh, S., *Fatigue of Materials*, United Kingdom, 1998, pp. 1, 12-15, 132-158, 221-224, 228-230

[23] Lin, Chia-Wei., Ju, Chien-Ping., and Lin, Jiin-Huey Chern., "A comparison of the fatigue behaviour of cast Ti-7.5Mo with commercially pure titanium, Ti-6Al-4V and Ti-13Nb-13Zr alloys", *Biomaterials 26,* 2005, pp. 2899-2907.

[24] Akahori, T., Niinomi, M., Fukui, H., and Ogawa, M., "Mechanical Properties and Microstructures of Beta-Type Titanium Alloy for Biomedical Applications", *Materials Science Forum Vols. 539-543*, 2007, pp. 557-562.

[25] Stephens, R., Fatemi, A., Stephens, R.R., and Fuchs, H.O., *Metal Fatigue in Engineering*, Canada, 2001, pp. 59-68

[26] Nalla, R.K., Boyce, B.L., Campbell, J.P., Peters, J.O., and Ritchie, R.O., "Influence of microstructure on high-cycle fatigue of Ti-6Al-4V: Bimodal vs.

lamellar structures", *Metallurgical and materials transactions A,* 2002, pp. 899-918.

[27] Tait, R.B, *Fracture Mechanics Notes,* 2005, pp. L1, L9

[28] Sadananda, K., and Vasudevan, A.K., "Fatigue crack growth behaviour of titanium alloys", *International Journal of Fatigue Vol. 27,* 2005, pp. 1255-1266.

[29] Lei, J.F., Wang, Z.G., Li, D., and Hu, Z.Q., "Fatigue crack initiation in Ti-5Al-4Sn-2Zr-1Mo-0.7Nd-0.25Si high temperature titanium alloy", *International Journal of Fatigue Vol. 19*, 1997, pp. S95-S98.

[30] Hanlon, T., Tabachnikova, E.D., and Suresh, S., "Fatigue behaviour of nanocrystalline metals and alloys", *International Journal of Fatigue Vol. 27,* 2005, pp. 1147-1158.

[31] Tokaji, K., Ohya, K., and Kariya, H., "Subsurface fatigue crack initiation in beta titanium alloys", *Fatigue Fracture Engineering Materials Structure Vol. 23,* 2000, pp. 759-766.

[32] Hall, J.A., "Fatigue crack initiation in alpha-beta titanium alloys", *International Journal of Fatigue Vol. 19,* 1997, pp. S23-S37.

[33] Garrett, G.G., *Failure by Fatigue- Failure Analysis Notes,* 1980, pp. 86.

[34] Ritchie, R.O., and Peters, J.O., "Foreign-object damage and high-cycle fatigue of Ti-6Al-4V", *Materials Science and Engineering A319-321,* 2001, pp. 597-601.

[35] Hertzberg, R.W., *Deformation and Fracture Mechanics of Engineering Materials,* 1983, pp. 426-427, 621-623.

[36] Kuruvilla, M., Srivatsan, T.S., Petraroli, M., and Park, L., "An investigation of microstructure, hardness, tensile behaviour of a titanium alloy: Role of orientation", *Sadhana Vol. 33 Part 3*, 2008, pp. 235-250.

[37] Hu, Y.M., Floer, W., Krupp, U., and Christ, H.J., "Microstructurally short fatigue crack initiation and growth in Ti-6.8Mo-4.5Fe-1.5Al", *Materials Science and Engineering A278,* 2000, pp. 170-180.

[38] Cao, Jingxia., Bai, Fang., and Li, Zhenxi., "High temperature low cycle fatigue behaviour of titanium aluminide Ti-24Al-15Nb-1Mo alloy", *Materials Science and Engineering A424,* 2006, pp. 47-52.

[39] Moosbrugger, J.C., and Morrison, D.J., "Effects of grain size on cyclic plasticity and fatigue crack initiation in nickel", *International Journal of Fatigue Vol. 19,* 1997, pp. S51-S59.

[40] Di Schino, A., and Kenny, J.M., "Grain size dependence of the fatigue behaviour of ultrafine-grained AISI 304 stainless steel", *Materials Letters 57,* 2003, pp. 3182-3185.

[41] Boyer, H.E. *et. al.*, Metals Handbook Volume 9 Fractography and Atlas of Fractographs, *American Society of Metals*, United States, pp. 64-78, 273-278.

[42] Juvinall, R.C., and Marshek, K.M., *Fundamentals of Machine Component Design*, 1999, pp. 144-148, Chap. 4.

APPENDICES

Appendix A: Spreadsheet Data Containing the Calculations to Determine the Stress Range and the Fatigue Loading Applied

Determination of Stress Amplitudes on the Rotational Bending Machine

Ti-6Al-4V Specimens

Uses 370W single-phase motor with a rotational speed of 2850rpm

Specimen length(focused portion) = 0.075 m y = 0.004

Gauge Force	The second moment of area	Bending Moment	r (fillet radius)	d (smaller diameter)	D (larger diameter)	Stress	Kt	Max Stress
N	m^4	Nm	m	m	m	MPa		MPa
0	2.01062E-10	0	0.002	0.008	0.0127	0	1.3	0
50	2.01062E-10	3.75	0.002	0.008	0.0127	74.60388	1.3	96.98504345
100	2.01062E-10	7.5	0.002	0.008	0.0127	149.20776	1.3	193.9700869
150	2.01062E-10	11.25	0.002	0.008	0.0127	223.81164	1.3	290.9551303
200	2.01062E-10	15	0.002	0.008	0.0127	298.41552	1.3	387.9401738
225	2.01062E-10	16.875	0.002	0.008	0.0127	335.71746	1.3	436.4326955
250	2.01062E-10	18.75	0.002	0.008	0.0127	373.0194	1.3	484.9252172
275	2.01062E-10	20.625	0.002	0.008	0.0127	410.32134	1.3	533.417739
300	2.01062E-10	22.5	0.002	0.008	0.0127	447.62328	1.3	581.9102607
350	2.01062E-10	26.25	0.002	0.008	0.0127	522.22716	1.3	678.8953041
400	2.01062E-10	30	0.002	0.008	0.0127	596.83104	1.3	775.8803476
450	2.01062E-10	33.75	0.002	0.008	0.0127	671.43492	1.3	872.865391
500	2.01062E-10	37.5	0.002	0.008	0.0127	746.0388	1.3	969.8504345
550	2.01062E-10	41.25	0.002	0.008	0.0127	820.64268	1.3	1066.835478
600	2.01062E-10	45	0.002	0.008	0.0127	895.24655	1.3	1163.820521
650	2.01062E-10	48.75	0.002	0.008	0.0127	969.85043	1.3	1260.805565
700	2.01062E-10	52.5	0.002	0.008	0.0127	1044.4543	1.3	1357.790608
750	2.01062E-10	56.25	0.002	0.008	0.0127	1119.0582	1.3	1454.775652
800	2.01062E-10	60	0.002	0.008	0.0127	1193.6621	1.3	1551.760695

Appendix B: Stress – Number of Cycles Data for Construction of the Stress – Life Curves

STRESS - No. OF CYCLES				
HEAT TREATMENT	Stress	**No of Cycles**	LOG(Stress)	Log(Cycles)
As-Received	484.9252172	**3581000**	2.685674769	6.554004321
	533.417739	**1510100**	2.727067454	6.179005708
	581.9102607	**76200**	2.764856015	4.881954971
	678.8953041	**67200**	2.831802805	4.827369273
	775.8803476	**20000**	2.889794752	4.301029996
	872.865391	**8350**	2.940947274	3.921686475
	969.8504345	**9400**	2.986704765	3.973127854
850Va	387.9401738	**1192500**	2.588764756	6.076458388
	436.4326955	**59550**	2.639917278	4.774881766
	484.9252172	**28400**	2.685674769	4.45331834
	533.417739	**32600**	2.727067454	4.5132176
	581.9102607	**10600**	2.764856015	4.025305865
	678.8953041	**7900**	2.831802805	3.897627091
	775.8803476	**9000**	2.889794752	3.954242509
	872.865391	**6900**	2.940947274	3.838849091
	969.8504345	**4300**	2.986704765	3.633468456
Ox850/850Va	387.9401738	**127400**	2.588764756	5.105169428
	436.4326955	**58500**	2.639917278	4.767155866
	484.9252172	**35150**	2.685674769	4.545925329
	533.417739	**27200**	2.727067454	4.434568904
	581.9102607	**20700**	2.764856015	4.315970345
	678.8953041	**9400**	2.831802805	3.973127854
	775.8803476	**11700**	2.889794752	4.068185862
	872.865391	**3200**	2.940947274	3.505149978
	969.8504345	**4400**	2.986704765	3.643452676
Ox750/850Va	387.9401738	**90500**	2.588764756	4.956648579
	436.4326955	**53500**	2.639917278	4.728353782
	484.9252172	**38900**	2.685674769	4.589949601
	533.417739	**21975**	2.727067454	4.341928884
	581.9102607	**11900**	2.764856015	4.075546961

	678.8953041	**7900**	2.831802805	3.897627091
	775.8803476	**4400**	2.889794752	3.643452676
	872.865391	**3700**	2.940947274	3.568201724
	969.8504345	**4200**	2.986704765	3.62324929
Ox850/850Ar	678.8953041	**12300**	2.831802805	4.089905111
Ox850	678.8953041	**26500**	2.831802805	4.423245874
Ox850NFC850Va	678.8953041	**6295**	2.831802805	3.798995734
Ox750/850Ar	678.8953041	**12300**	2.831802805	4.089905111
Ox600/850Va	678.8953041	**7400**	2.831802805	3.86923172
Ox600/850Ar	678.8953041	**16450**	2.831802805	4.216165902

Appendix C: Microhardness Data for the Construction of the Respective Hardness Profiles

As Received

Depth(µm)										Standard
Reading	1	2	3	4	5	6	7	8	AVERAGE	Deviation
15	450.2	444	490.4	423.3	417.6	409.3	437.9	501.2	446.7375	33.31674558
30	479.8	469.6	473	486.8	476.4	505	505	520.2	489.475	18.37791765
60	469.7	466.3	447.1	473	497.6	479.8	505	512.5	481.375	22.04254004
100	476.4	479.8	450.2	476.4	490.4	501.2	490.4	473	479.725	15.2510187
130	479.8	466.3	437.9	432	516.3	476.4	505	512.5	478.275	32.18747538
160	486.8	486.8	463	483.3	473	483.3	516.3	497.6	486.2625	15.88331897
200	486.8	494	479.8	390.9	466.3	483.3	497.6	483.3	472.75	34.39231642
250	505	501.2	524.1	497.6	463	429	497.6	469.7	485.9	30.1339391
300	501.2	494	548.6	540.2	494	490.4	516.3	483.3	508.5	24.23156147
350	505	524.1	561.5	561.5	396	501.2	434.9	490.4	496.825	57.61606299
400	338.5	406.6	393.5	423.3	429	450.2	476.4	469.7	423.4	44.8593994
1000	376.1	417.6	403.9	466.3	444	459.8	486.8	447.1	437.7	36.22595754
1500	371.4	423.3	403.9	463	440.9	453.4	494	444	436.7375	37.50100713
2000	344.7	401.3	409.3	440.9	440.9	466.3	532.1	463	437.3125	54.99247838

850Va

Depth(µm)										Standard
Reading	1	2	3	4	5	6	7	8	AVERAGE	Deviation
15	701	701	593.4	617.8	638.5	671.5	570.3	617.8	638.9125	48.46555294
30	593.4	579.4	476.4	622.9	548.6	565.9	540.2	612.8	567.45	46.80952284
60	532.1	501.2	479.8	456.6	512.5	501.2	548.6	486.8	502.35	29.2114459
100	476.4	459.8	453.4	476.4	447.1	476.4	574.8	497.6	482.7375	40.48586835
130	447.1	466.3	328.5	417.6	450.2	440.9	459.8	479.8	436.275	47.27735036
160	444	432	440.9	447.1	447.1	412	440.9	440.9	438.1125	11.58045613
200	440.9	440.9	434.9	450.2	434.9	420.4	459.8	483.3	445.6625	19.0947216
250	479.8	459.8	453.4	444	505	552.8	501.2	508.7	488.0875	36.02845849
300	476.4	440.9	456.6	494	473	494	463	476.4	471.7875	18.09786392
350	456.6	380.9	459.8	476.4	476.4	516.3	473	501.2	467.575	40.32619673
400	359.9	434.9	378.5	369	412	412	414.8	420.4	400.1875	27.18242276
1000	351.1	417.6	396	396	401.3	406.6	429	434.9	404.0625	25.92626564
1500	378.5	366.7	423.3	396	412	412	434.9	444	408.425	26.73733345
2000	414.8	322.7	403.9	414.8	414.8	473	409.3	437.9	411.4	42.18977534

Ox850/850Va

Depth(µm)										Standard
Reading	1	2	3	4	5	6	7	8	AVERAGE	Deviation
15	817.4	955.6	1107.4	1049.3	1119.6	891.1	1049.3	899.9	986.2	103.9048363

30	759.3	773.2	833	946	985.4	817.4	891.1	752.5	844.7375	82.15804795
60	643.8	732.6	773.2	745.8	873.9	649.2	780.4	732.5	741.425	69.18371828
100	561.5	565.9	665.9	649.2	713.4	660.2	732.6	649.2	649.7375	57.123724
130	603	561.5	598.1	603	677.3	570.3	665.9	593.4	609.0625	38.87572949
160	598.1	557.1	570.3	557.1	622.9	548.6	540.2	607.9	575.275	28.46211297
200	561.5	570.3	536.1	508.7	570.3	593.4	540.2	588.6	558.6375	26.75826683
250	512.5	528.1	544.4	512.5	565.9	638.5	570.3	561.5	554.2125	38.42347712
300	512.5	524.1	520.2	512.5	552.8	565.9	570.3	548.6	538.3625	22.25589458
350	508.7	512.5	516.3	524.1	528.1	561.5	584	579.4	539.325	28.80758364

Ox850/850Ar

Depth(µm)										**Standard**
Reading	1	2	3	4	5	6	7	8	**AVERAGE**	**Deviation**
15	975.3	1170.5	927.2	1027.3	995.6	1006	917.9	995.6	1001.925	72.89629192
30	825.2	873.9	891.1	891.1	825.2	825.2	873.9	936.5	867.7625	37.6233949
60	766.2	857.2	809.8	701	739.1	732.6	766.2	794.9	770.875	46.023384
100	671.5	739.1	726.1	665.9	654.7	677.3	622.9	643.8	675.1625	36.94607346
130	638.5	719.7	638.5	598.1	683.1	671.5	628	745.8	665.4	46.28501377
160	588.6	612.8	593.4	565.9	574.8	665.9	579.4	617.8	599.825	30.03950524
200	528.1	565.9	598.1	552.8	598.1	565.9	603	617.8	578.7125	28.35240014
250	557.1	612.8	574.8	528.1	434.9	633.2	552.8	579.4	559.1375	56.41741614
300	552.8	466.3	532.1	593.4	532.1	628	561.5	593.4	557.45	46.35959987
350	532.1	557.1	516.3	540.2	540.2	574.8	536.1	557.1	544.2375	16.92482921

Ox850

Depth(µm)										**Standard**
Reading	1	2	3	4	5	6	7	8	**AVERAGE**	**Deviation**
15	985.4	739.1	689	955.6	732.6	707.2	1095.4	713.4	827.2125	158.837513
30	528.1	516.3	565.9	638.5	593.4	603	683.1	544.4	584.0875	57.12671223
60	456.6	476.4	512.5	516.3	476.4	516.3	516.3	508.7	497.4375	23.82663201
100	494	536.1	505	497.6	528.1	473	476.4	459.8	496.25	26.58968651
130	469.7	544.4	486.8	505	497.6	401.3	466.3	432	475.3875	44.31966469
160	505	483.3	466.3	473	486.8	486.8	505	466.3	484.0625	15.33305836
200	479.8	483.3	479.8	490.4	494	497.6	512.5	459.8	487.15	15.4928555
250	466.3	497.6	520.2	469.7	479.8	486.8	497.8	453.4	483.95	21.26512907
300	501.2	512.5	508.7	520.2	505	486.8	479.8	476.4	498.825	16.01166985
350	501.2	490.4	505	486.8	479.8	486.8	490.4	486.8	490.9	8.272501781
400	390.9	344.7	398.6	406.6	406.6	401.3	390.3	383.4	390.3	20.17282472
1000	371.4	423.3	409.3	409.3	414.8	412	412	393.5	405.7	16.13868467
1500	378.5	426.1	417.6	432	420.4	437.9	371.4	426.1	413.75	24.83217958
2000	383.4	401.3	409.3	420.4	434.9	453.4	434.9	403.9	417.6875	22.61449835

Ox850NFC850Va

Depth(µm)										Standard
Reading	1	2	3	4	5	6	7	8	AVERAGE	Deviation
15	975.3	946	1095.4	1027.3	985.4	1157.5	1083.6	1157.5	1053.5	82.19242231
30	946	882.5	946	1060.5	946	1060.5	965.4	955.6	970.3125	60.93613607
60	865.5	719.7	975.3	955.6	780.4	917.9	840.9	825.2	860.0625	87.35165282
100	726.1	689	794.9	780.4	759.3	794.9	802.3	732.6	759.9375	40.67800169
130	671.5	649.2	701	707.2	707.2	719.7	701	719.7	697.0625	24.51156797
160	654.7	665.9	677.3	759.3	752.5	766.2	677.3	695	706.025	45.7247276
200	633.2	649.2	579.4	654.7	607.9	612.8	677.3	649.2	632.9625	31.32616148
250	593.4	552.8	584	588.6	584	607.9	584	649.2	592.9875	27.40961445
300	584	574.8	570.3	593.4	603	683.1	557.1	584	593.7125	38.75094238
350	561.5	598.1	607.9	557.1	603	544.4	548.6	607.9	578.5625	28.07357362

Appendix D: Illustrative Data for the 850Va Process to determine the Grain Size

		Depth(µm)	Length of Intercept(mm)	Number of Interceptions	Grain Size(mm)	Grain Size(µm)
Conversion Factor =	4.65					
1 Centre		3800	212	36	5.888888889	27.39018088
		3800	172	28	6.142857143	28.57142857
		3800	213	33	6.454545455	30.02114165
		3800	125	22	5.681818182	26.42706131
AVERAGE		3800			6.042027417	28.1024531
21.5	100					
Conversion Factor =	4.65					
2		3400	212	39	5.435897436	25.28324389
		3400	171	30	5.7	26.51162791
		3400	212	36	5.888888889	27.39018088
		3400	125	21	5.952380952	27.6854928
AVERAGE		3400			5.744291819	26.71763637
21.5	100					
Conversion Factor =	4.65					
3		3000	212	40	5.3	24.65116279
		3000	171	34	5.029411765	23.39261286
		3000	213	36	5.916666667	27.51937984
		3000	125	20	6.25	29.06976744
AVERAGE		3000			5.624019608	26.15823073
21.5	100					
Conversion Factor =	4.65					
4		2600	212	35	6.057142857	28.17275748
		2600	171	33	5.181818182	24.10147992
		2600	213	36	5.916666667	27.51937984
		2600	125	22	5.681818182	26.42706131

AVERAGE		2600			5.709361472	26.55516964
21.5	100					
Conversion Factor =	4.65					
5		2200	212	40	5.3	24.65116279
		2200	171	29	5.896551724	27.42582197
		2200	213	36	5.916666667	27.51937984
		2200	125	21	5.952380952	27.6854928
AVERAGE		2200			5.766399836	26.82046435
21.5	100					
Conversion Factor =	4.65					
6		1800	212	41	5.170731707	24.04991492
		1800	171	28	6.107142857	28.40531561
		1800	213	36	5.916666667	27.51937984
		1800	125	25	5	23.25581395
AVERAGE		1800			5.548635308	25.80760608
21.5	100					
Conversion Factor =	4.65					
7		1400	212	36	5.888888889	27.39018088
		1400	171	33	5.181818182	24.10147992
		1400	213	36	5.916666667	27.51937984
		1400	125	21	5.952380952	27.6854928
AVERAGE		1400			5.734938672	26.67413336
21.5	100					
Conversion Factor =	4.65					
8		1000	212	40	5.3	24.65116279
		1000	171	35	4.885714286	22.72425249
		1000	213	38	5.605263158	26.07099143
		1000	125	22	5.681818182	26.42706131
AVERAGE		1000			5.368198906	24.96836701
21.5	100					
Conversion Factor =	4.65					
9		600	212	37	5.72972973	26.64990572
		600	171	33	5.181818182	24.10147992
		600	213	38	5.605263158	26.07099143
		600	125	24	5.208333333	24.2248062
AVERAGE		600			5.431286101	25.26179582
21.5	100					
Conversion Factor =	4.65					
10		200	212	39	5.435897436	25.28324389
		200	171	33	5.181818182	24.10147992
		200	213	35	6.085714286	28.30564784
		200	125	24	5.208333333	24.2248062
AVERAGE		200			5.477940809	25.47879446
21.5	100					
Conversion Factor =	4.65					
11		100	138	22	6.272727273	29.17547569
		100	61	11	5.545454545	25.79281184
		100	133	27	4.925925926	22.91128338
		100	125	22	5.681818182	26.42706131
AVERAGE		100			5.606481481	26.07665805